Automation of Chemical Spray Pyrolysis Unit and Fabrication of Sprayed $CuInS_2/In_2S_3$ Solar Cell

Thesis submitted to
Cochin University of Science and Technology

in partial fulfillment of the requirements
for the degree of
Doctor of Philosophy

under the Faculty of Science

Tina Sebastian
Thin Film Photovoltaic Division
Department of Physics
Cochin University of Science and Technology
Cochin – 682 022, Kerala, India

August 2009

Automation of Chemical Spray Pyrolysis Unit and Fabrication of Sprayed $CuInS_2/In_2S_3$ Solar Cell

Ph.D thesis in the field of Thin Film Photovoltaics

Author
Tina Sebastian
Research Fellow
Department of Physics
Cochin University of Science and Technology
Cochin – 682 022, Kerala, India
email: tinadann@gmail.com

Research Advisors:
Dr. C.Sudha Kartha
Professor, Department of Physics
Cochin University of Science and Technology
Cochin – 682 022, Kerala, India
email: csk@cusat.ac.in

Dr. K.P.Vijayakumar
Professor, Department of Physics
Cochin University of Science and Technology
Cochin – 682 022, Kerala, India
email: kpv@cusat.ac.in

Cochin University of Science and Technology
Cochin-682022, Kerala, India
www.cusat.ac.in

August 2009

Dr.C.Sudha Kartha
Professor
Department of Physics
Cochin University of Science and Technology
Cochin – 682 022

Certificate

Certified that the work presented in this thesis entitled *"**Automation of Chemical Spray Pyrolysis Unit and Fabrication of Sprayed $CuInS_2/In_2S_3$ Solar Cell**"* is based on the authentic record of research done by Tina Sebastian under my guidance and supervision at the Department of Physics, Cochin University of Science and Technology, Cochin – 682 022 and has not been included in any other thesis submitted for the award of any degree.

Cochin-22 Prof. C.Sudha Kartha

Date: 3rd August 2009 (Supervising Guide)

Phone: +91 4842577404. **Fax:**. +91 484 2577595. **Email:** csk@cusat.ac.in

Declaration

I hereby declare that the work presented in this thesis entitled *"**Automation of Chemical Spray Pyrolysis Unit and Fabrication of Sprayed $CuInS_2/In_2S_3$ Solar Cell**"* is based on the original research work done by me under the supervision and guidance of ***Dr. C. Sudha Kartha,*** Professor, Department of Physics, Cochin University of Science and Technology, Cochin-682022 and has not been included in any other thesis submitted previously for the award of any degree.

Cochin – 22

Date: 3rd August 2009 Tina Sebastian

Acknowledgements

First and foremost I bow in reverence before the Lord Almighty for helping me complete this endeavor.

I express my heartfelt gratitude to my supervising guide, Prof. C. Sudha Kartha and co-guide Prof. K.P.Vijayakumar for their venerable guidance during the course of this work. I was lucky to benefit from the frequent discussions, valuable suggestions and insight gained from experience that they gracefully offered. I am indebted to them for their love and concern during the past years and also their confidence in me which helped me surmount difficult times.

I express my sincere gratitude to Prof. M.R.Anantharaman, Head, Department of Physics, Prof. Godfrey Louis, Prof. Ramesh Babu T, Prof. V.C.Kuriakose and Prof. K.P.Vijayakumar, former heads of the department for providing the necessary facilities of the department.

I am indebted to the teaching faculty of Department of Physics for their motivation and support. I remember with gratitude the office and library staff of Department of Physics, for their help and encouragement.

I also thank Dr.Y.Kashiwaba and Ms.T.Abe of Department of Electrical and Electronics Engineering, Iwate University, Japan, for their invaluable help in the XPS analysis of my samples.

I want to specially mention the technical support from the management and engineers of M/s Holmarc Opto-Mechatronics Pvt. Ltd., Kalamassery, Kochi in the design, fabrication and maintenence of the chemical spray pyrolysis unit.

The financial assistance from KSCSTE and DRDO during the course of my work is gratefully acknowledged.

I remember with appreciation my seniors Dr.Teny Theresa John, Dr.Ram Kumar Dr.S.B.Shyamala, Dr. Saravanan, Dr.Ratheesh Kumar.P.M, Dr.Beena Mary John, Mr.Wilson K.C, Dr.Paulraj Mani, and Dr.Sreekumar.A who has helped and

encouraged me in my work. In particular, I would like to thank Dr.Teny Theresa John for her patient endurance of my myriad doubts at the begining of my work.

I also thank my colleagues Ms. Meril Mathew, Ms. Deepa K.G., Dr. R. Jayakrishnan, Mr.R.Sreekumar, and Mr.V.C.Kishore, for the pleasant times filled with fun and feeling of togetherness. I fondly remember the active deliberations during lab meetings and all the joys and sorrows that we shared.

I express my thanks to my dear juniors Mr.Vimal Kumar.T.V., Ms. Pramitha V., Ms. Anita R. Warrier, Mr. Rajesh Menon M., Mr. Sajeesh T.H., Ms. Angel Susan Cherian, Mr. Subramanyan Namboodiri V., Mr. S.S. Sreeroop, Mr. Rajesh C.S., Mr. Rajeshmon V.G., Ms. Poornima Naganathan and Mr. Jaffer for the love and care they showered upon me. I have greatly benefited from their creative ideas, genuine doubts and thought provoking arguments.

I thank the M.Phil. and M.Sc. students who have done their projects in our lab. In particular, I remember with affection Ms. Manju Gopinath, Mr. Subin Thomas, Ms.Seena Xavier, Ms. Deepa Raj, Mr. Shihabuddin Mohammed, Ms.Anuradha and Ms.Sreeshma.

I remember with gratitude the research community of CUSAT and of Department of Physics in particular, for their support. I specially thank V. Subramanyan Namboodiri, research student of Department of Physics, for designing the cover page of the thesis.

I express my eternal gratitude to my dear husband Dann, who has helped me in more ways than he realizes. Without his patient understanding and loving persuasion, I would never have completed this venture. I also acknowledge with love, the support and guidance of our parents. I remember with affection my brother and sister for being there for me always.

I remember with gratefulness my teachers, friends and well wishers for their blessings and prayers.

Cochin.22
August 2009 *Tina Sebastian*

Preface

The power of the sun is almost unlimited and it provides nearly as much energy in one hour at earth's surface as the total amount of energy consumed in a year. But solar power remains relatively untapped, a niche technology even in the most photon drenched areas of the world. Harnessing photons efficiently and converting them economically into energy remains a technological challenge. Today, photovoltaic technologies are dominated by wafer based crystalline silicon (monocrystalline, polycrystalline and ribbon silicon). The major drive for research and development on PV cells during last three decades has been to reduce the cost of PV generated electricity. Cost of a solar cell or a module is primarily influenced by the interplay between its operational lifetime, its manufacturing cost per unit area and power conversion efficiency. Therefore, ongoing research efforts are focused on further increasing the efficiency of silicon-based solar cells with different grades of silicon, which can be manufactured at lower cost. Despite the constant improvement in bulk crystalline technologies, alternative photovoltaic approaches have been developed simultaneously during the past few decades. In an effort to reduce manufacturing costs, thin film technologies that require lesser materials and can be processed onto thin and lower cost substrates using high throughput fabrication processes have been subject to active research and development.

Chemical spray pyrolysis (CSP) is a versatile method of thin film deposition by which uniform polycrystalline thin films can be deposited over large area, which is specifically important for thin film photovoltaic device fabrication. But so far there have been not much works in developing this technique, so as to make it a full-fledged thin film deposition technique like sputtering or vacuum evaporation. In the present work, we have attempted to standardize the process of film deposition by automating the technique and the films deposited were characterized and used for photovoltaic device fabrication. The thesis is divided into six chapters and a brief description of each is given below.

Chapter 1 is a general introduction on photovoltaics. Basic principles of solar cells and its important parameters are discussed here. Various types of solar cells and current technology trends are detailed. The chapter concludes with an overview on thin film solar cells and describes the significance of the present work.

Chapter 2 is about fabrication of automated spray pyrolysis unit. This chapter begins with a brief review on chemical spray pyrolysis and moves on to details of fabrication of a CSP unit. Different models of mechanism of spray deposition and film formation has been discussed. Literature survey on effect of different spray parameters like substrate temperature, nature and type of spray, influence of precursors, spray rate etc. were done and documented. Details of the CSP unit fabricated by us are then described. Using the fabricated system, films of binary, ternary and quaternary compounds could be deposited successfully.

Chapter 3 focuses on deposition and characterization of Copper Indium Sulfide ($CuInS_2$) absorber layers. Effect of different preparation conditions and post deposition treatments on the properties of sprayed $CuInS_2$ films was investigated. Characterization tools used in the present work includes x-ray diffraction (XRD), atomic force microscopy (AFM), x-ray photoelectron spectroscopy (XPS), energy dispersive x-ray analysis (EDAX), I-V measurement, optical absorption and transmission study, temperature dependent conductivity measurement, thermally stimulated current measurement (TSC) and photoluminescence (PL) studies. Study on the effect of Cu/In ratio variation and S/Cu ratio variation was carried out. It was observed that, though S-rich starting solution was required for obtaining stoichiometric films, increasing S beyond a limit did not result in its incorporation in the film and hence had no effect on the properties. Cu rich films were good in terms of crystallinity and low resistivity, but these films had low photosensitivity and non-uniform composition over the surface. High resistivity and low crystallinity put limits on the use of In-rich films as absorber layer, inspite of their good photosensitivity. The near stoichiometric sample which showed intermediate value of photosensitivity, crystallinity and resistivity, were better suited for device

applications. It was also seen that very thick $CuInS_2$ films could not be prepared by continuous spray. Multiple sprays resulted in thick films, but their transport properties showed detrimental nature. Smaller spray rates gave films with better crystallinity and good opto-electonic properties. From the study of the effect of substrate temperature on the properties of films formed, it was seen that those formed at 623K had good opto-elctronic properties. Defect analysis using thermally stimulated current studies and photoluminescence in these samples helped in identifying the role of defects in controlling their opto-electronic properties.

Post deposition annealing treatments were carried out in air, vacuum and H_2S atmosphere. Pronounced change was observed in case of samples annealed in H_2S atmosphere. There were significant changes in the composition as well as the structural and optical properties. XPS depth profiling clearly indicated an improvement in uniformity of the samples. Except for the increase in resistivity and decrease in mobility, all other properties generally improves on sulfurization. Present study gives a comprehensive idea on the properties of sprayed $CuInS_2$. Such a study is a pre-requisite for using this material effectively in solar cells.

Chapter 4 is dealing with the deposition of Indium Sulfide (In_2S_3) thin films and their characterization. Preparation conditions like volume of spray, In/S ratio, substrate temperature and spray rate were varied to study the variation in properties. It was seen that variation in thickness of the films affected the properties of the films. Resistivity of the films increased with increase in thickness which directly affected the series resistance when applied in device. Hence optimum thickness of In_2S_3 film was selected for cell applications. From studies on films prepared at different substrate temperatures, it was seen that crystalline films were formed from substrate temperature of 573 K onwards. Study of In/S ratio variation on the properties of films showed that film composition is largely affected by variation in the concentrations of precursors used. Spray rate of the films also affected structural and electrical properties. Crystallinity decreased while photosensitivity increased with increase in spray rate. Effects of copper incorporation in In_2S_3 films were also

investigated. This was mainly done to find how diffusion of Cu from $CuInS_2$ to In_2S_3 in the cell will affect the properties. It is seen that there is a gradual variation in properties like bandgap and resistivity due to the incorporaton of copper.

Chapter 5 is on $CuInS_2/In_2S_3$ cell fabrication and analysis. Samples selected from characterization studies (as described in previous chapters) were used for the fabrication. By controlling the thickness of $CuInS_2$ and In_2S_3 layers, we could achieve efficiency of ~1% for a simple bilayer structure, without any post deposition treatments. This result was obtained for small ($0.01cm^2$) as well as larger area (0.25 cm^2) devices. The repeatability of the result was confirmed and the cells were found to be stable without any lamination. Diffusion of silver over the In_2S_3 layer in cell and depositing silver electrode over it resulted in drastic increase in the current collected. Enhancement of current collection in this device points towards the applicability of using silver diffusion as a method of increasing current collection in large area devices and higher efficiencies can be expected for such solar cells.

Chapter 6 is summary of the work, where important conclusions are highlighted. Future scope of the work is also presented.

List of Publications

Journal Publications:

1. Role of substrate temperature in controlling properties of sprayed $CuInS_2$ absorbers; Tina Sebastian, Manju Gopinath, C. Sudha Kartha, K. P. Vijayakumar, T. Abe, Y. Kashiwaba; Solar Energy. 83 (2009) 1683.

2. Characterization of spray pyrolysed $CuInS_2$ thin films; Tina Sebastian, R. Jayakrishnan, C. Sudha Kartha, K. P. Vijayakumar; The Open Surface Science Journal.1 (2009) 1.

3. Effects of incorporation of Na in spray pyrolysed $CuInS_2$ thin films; Teny Theresa John, Tina Sebastian, C. Sudha Kartha, K. P. Vijayakumar, T. Abe, Y. Kashiwaba. Physica B. 388 (2007) 1.

4. Photoconductivity in sprayed β-In_2S_3 thin films under sub band gap excitation of 1.96 eV; R. Jayakrishnan, Tina Sebastian, Teny Theresa John, Sudha Kartha, K. P. Vijayakumar; Journal of Applied Physics. 102 (2007) 043109.

5. Room temperature photoluminescence surface mapping; R.Jayakrishnan, Tina Sebastian, C. Sudha Kartha and K. P. Vijayakumar; Journal of Physics: Conference Series. 28 (2006) 62.

6. Implantation assisted copper diffusion: a different approach for the preparation of $CuInS_2/In_2S_3$ p-n junction; K.C.Wilson, Tina Sebastian, Teny Theresa John, C. Sudha Kartha and K. P. Vijayakumar; Applied Physics Letters. 89 (2006) 013510.

Conference Publications:

1. Comparative study of Cu rich and In rich $CuInS_2$ thin films prepared using automated spray system; Tina Sebastian, Teny Theresa John, R. Jayakrishnan, K. P. Vijayakumar, C. Sudha Kartha, Deepthi Jain, Ganesan V.; International Conference on Optoelectronic Materials and Thin Films (OMTAT-2005); Cochin, India, 24-26 October (2005).

2. Room temperature photo-luminescence surface mapping; R.Jayakrishnan, Tina Sebastian, C. Sudha Kartha, K. P. Vijayakumar; International Conference on Materials for Advanced Technologies; Singapore, 3-8 July (2005).

3. Non-destructive evaluation of carrier transport properties in $CuInS_2$ and $CuInSe_2$ thin films using Photothermal deflection technique; Anita R. Warrier, Deepa K. G., Tina Sebastian, C. Sudha Kartha, K. P. Vijayakumar; XVII International Materials Research Congress –IMRC 2008; Cancun, Mexico, 17-21 August (2008).

4. Effect of H_2S treatments on the properties of spray pyrolysed $CuInS_2$; Tina Sebastian, Shihabuddin Mohammed, C. Sudha Kartha, K. P. Vijayakumar; National conference on emerging areas in thin film science and technology; PSG College, Coimbatore, 13-14 February (2009).

5. Material properties of $CuInS_2/In_2S_3$ interface; Tina Sebastian, C. Sudha Kartha, K. P. Vijayakumar; MRSI-AGM; Kolkotta, India, 10-12 February (2009).

6. Indigenously developed chemical spray pyrolysis unit to deposit semiconductor thin films for solar cell applications; Tina Sebastian, C. Sudha Kartha, K. P. Vijayakumar; 19^{th} Kerala Science Congress; Kannur, India, 29-31 January (2007).

7. On the properties of Copper rich $CuInS_2$; Tina Sebastian, Deepa Raj, Manju Gopinath, C. Sudha Kartha, K. P. Vijayakumar; Current Trends in Material Science; Christian College, Chengannur, 25-27 Mach (2007).

8.Preparation of device quality $CuInS_2$ using chemical spray technique for PV applications; Tina Sebastian, R. Jayakrishnan, Manju Gopinath, C. Sudha Kartha, K. P. Vijayakumar; MRSI-AGM; NPL, New Delhi, 12-14 February (2007).

9. Deposition of copper indium sulfide films with widely varying opto-electronic properties by chemical spray pyrolysis; Tina Sebastian, Teny Theresa John, Meril Mathew, K. P. Vijayakumar, C. Sudha Kartha; MRSI-AGM; Lucknow, India, 13-15 February (2006).

10. An inexpensive automatic spray pyrolysis unit to deposit thin films; Tina Sebastian, K. P. Vijayakumar; National Symposium on Instrumentation; Cochin, India, 30th December-2nd January (2005).

11. PL surface scan of sprayed $CuInS_2$ thin films; R. Jayakrishnan, Tina Sebastian, C. Sudha Kartha, K. P. Vijayakumar; National Conference on Luminescence Application; Banglore University, 2-4 February (2005).

12. Tunable photodetectors based on β-In_2S_3 thin films; R. Jayakrishnan, Tina Sebastian, C. Sudha Kartha, K. P. Vijayakumar; Smart Structures and MEMS Systems for Aerospace Applications; RCI Hyderabad, 1-2 December (2006).

13. Photothermal deflection technique for non destructive evaluation of semiconductor thin films; Anita R. Warrier, Tina Sebastian, K. P. Vijayakumar, C. Sudha Kartha; National symposium on Ultrasonics (NSU-XVI); STIC, Cochin, 17-19 December (2007).

14. Measurement of thermal and electronic transport properties of semiconductor thin films using photothermal deflection technique; Anita R. Warrier, Tina Sebastian, K. P. Vijayakumar, C. Sudha Kartha; 9th International symposium on Measurement and Quality control (ISMQC-2007); Chennai, November 21-24 (2007).

15. Photothermal investigation of minority carrier mobility in $CuInS_2$ thin films prepared by chemical spray pyrolysis; Anita R Warrier, Tina Sebastian, K. P. Vijayakumar, C. Sudha Kartha; New Horizons in Experimental and Theoretical Physics (NHTEP-2007); Cochin, 8-10 October (2007).

16. Chemical spray pyrolysed β-In_2S_3 thin films for sensors and energy conversion applications; R. Jayakrishnan, Teny Theresa John, Tina Sebastian, Meril Mathew, C. Sudha Kartha, K. P. Vijayakumar; 18th MRSI-AGM, 12-14 February (2007).

CONTENTS

CHAPTER 2

Fabrication of Automated Chemical Spray Pyrolysis Unit

CHAPTER 3

Deposition and Characterization of $CuInS_2$ Absorber Layer

CHAPTER 4

Deposition and Characterization of In_2S_3 Buffer Layer

CHAPTER 5

$CuInS_2/In_2S_3$ Junction Fabrication and Analysis

CHAPTER 6

Concluding Remarks and Future Prospects

CHAPTER 1

An Introduction to Photovoltaics

1.1.Introduction

Satisfying world's growing energy demand is one of the most significant challenges facing society. Today, major share of the energy produced by mankind comes from fossil fuels. Given that such fuels are on the decline, and that green house gases are known to contribute to global warming, there is urgent need to rely on technologies that are economically feasible and environmental friendly. Solar energy is ideal for power generation as it is clean, quiet and renewable. It is also plentiful as an average of 125000 TW of solar power strikes our planet at any time. Photovoltaic (PV) devices directly harness solar energy and convert optical power into electrical.

Most photovoltaic technologies work under the same general principle. Each cell consists of two layers of two different types of semiconductor materials – viz., p and n. When cell is struck by a photon with appropriate energy, electrons are knocked free and their movement from one layer to the other generates electricity. Existing technologies exploit this phenomenon with varying degrees of success. But cost remains the main setback that has slowed the technology's spread. Even after fifty years of intensive research and development works, PV systems continue to be expensive to build, install and maintain. Although prices have trended downward in recent years, solar power remains a pricey proposition.

A PV system is comprised of PV cells assembled into modules, which are connected into arrays, and the so called balance of system (BOS) components. The BOS components refer to batteries, inverters, charge controllers, wiring, fuses and fittings for holding/tilting the modules for sun tracking, which account for a significant portion of the total cost of PV. Considering the cost and the fact that PV systems are put out of action every time night falls, achieving the highest possible

efficiency is critical for solar power's viability. Reducing the cost of PV systems will be accomplished through improved materials and higher efficiencies.

1.2.Solar cells- some historical facts

Photovoltaic effect was reported initially in 1839 by French physicist Edmond Becquerel who observed light dependent voltage between electrodes immersed in an electrolyte [1]. This effect was further observed in 1883 by Charles Fritts in an all solid state system of selenium. Efficient silicon solar cells were reported by Chapin, Fuller and Pearson in 1954 [2]. Solar cells were developed during the 1950's, primarily at the Bell Telephone laboratories. These cells proved to be the best power sources for extra-terrestrial missions, and more than 1000 satellites using solar cells were utilized between 1960 and 1970. In mid seventies, efforts were initiated to make solar cells for terrestrial applications. Since 1974, the emphasis has shifted from space applications to terrestrial applications. Last three decades saw newer device technologies enabling reduction in cost and hence opening new horizons for commercial applications of solar cells.

1.3.Solar cell – basic principles

Three major processes are involved in the conversion of sunlight into electrical energy. They are (i) absorption of photon by the material, (ii) generation of electron hole pairs and (iii) their separation. Absorption of photon causes promotion of electron to an excited state. For extra electronic energy to be extracted efficiently, the excited state should be separated from the ground state by an energy gap and semiconductors are good examples of such systems. With band gap in the range 0.5-3 eV, semiconductors can absorb visible photons to excite electrons across band gap. High absorption of light can be achieved by increasing thickness of the absorbing material, but this along with requirement of perfect charge collection make high demands on material quality.

Some intrinsic asymmetry is then needed to separate the electrons and holes which are created by spatial variations of semiconductor parameters like band gap,

work function, electron affinity or density of states [3]. This can be achieved by preparing a junction which is an interface between two electronically different materials or between layers of the same material treated differently. The junction is usually large in area to maximize the amount of solar energy intercepted.

Once separated, the charges should be allowed to travel without loss in an external circuit to do electrical work. To conduct the charge to the external circuit, the material should be a good electrical conductor. The carriers should not recombine with defects or impurities and should not give up energy to the medium. There should be no resistive losses (low series resistance) or current leakage (high shunt resistance). The material around the junction should make good ohmic contact to the external circuit. Also the load resistance should be chosen so as to match the operating point of the cell.

Mechanisms of excitation, charge separation and transport can be provided by the semiconductor p-n junction, which is the classical model of solar cell. Here, a p-type material is brought together with an n-type material. Diffusion of carriers occurs across the junction, leaving behind fixed charges due to ionised atoms on either side. This region where electrons have diffused across the junction is called the 'depletion region' because it no longer contains any mobile charge carriers. The diffusion of carriers does not happen indefinitely as the electric field created by the imbalance of charge on either side of the junction opposes the diffusion and equilibrium is reached. When the junction is illuminated, light creates electron-hole pairs in p, n and depletion regions. The electric field at the junction separates the pairs by driving minority carriers across the junction.

1.4.Metrics for solar cells

In the simplest form, the electrical characteristic of photovoltaic device may be modeled by a diode and current source connected in parallel, where current source describes the process in which solar cell converts the sunlight or optical power, directly into electrical power [4]. Unlike photo detectors that operate in reverse bias, photovoltaic cells operate in the fourth quadrant of the current-voltage characteristic

graph, where voltage is positive and current density is negative. When device is under illumination, two quantities can be easily determined experimentally: the intercepts of electrical characteristics with vertical and horizontal axes, which corresponds to short circuit current density (J_{sc}) and open circuit voltage (V_{oc}).

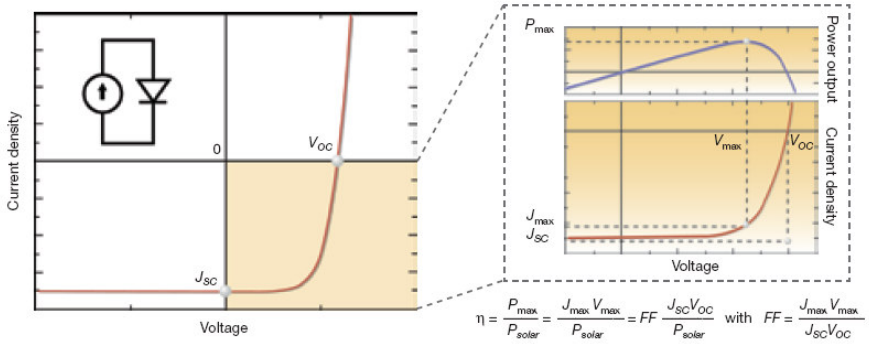

Figure 1.1.I-V characteristic along with idealized equivalent circuit of solar cell (left) and close up of fourth quadrant with an illustration of the point of maximum power (right).

At any point on the electrical characteristic in the fourth quadrant, the solar cell produces electrical power density given by the product of voltage and current density. This product is maximum at a point that corresponds to a voltage V_{max} and current density J_{max}, which is the point of maximum power. The power conversion efficiency (η), which is the most important metric of a solar cell, is then defined as the power density produced at the point of maximum power divided by the incident optical power density. The cell is combined with a matched load to operate at maximum power condition. Power conversion efficiency is a function of the magnitude of irradiance and the incident spectral distribution. Therefore, the performance of PV cells is reported for standard test conditions of 1 kWm^{-2} at a temperature of 298K and for a solar reference spectrum AM 1.5 [5]. Power conversion efficiency (η) is alternately defined as a function of fill factor (FF) and is

given by the product FF. J_{sc}. V_{oc} divided by incident optical power density. FF is a measure of the rectifying property of the current-voltage characteristic. Figure.1.1 (left) illustrates the electrical characteristics and idealized equivalent circuit for a solar cell, together with the definition of V_{oc} and J_{sc} and (right) the close-up of the fourth quadrant with an illustration of the point of maximum power.

Quantum efficiency refers to the percentage of photons that are converted to electric current (i.e., collected carriers) when the cell is operated under short circuit conditions [3, 6]. External quantum efficiency is the fraction of incident photons that are converted to electric current, while internal quantum efficiency is the fraction of absorbed photons that are converted to electric current. Quantum efficiency should not be confused with energy conversion efficiency, as it does not convey information about the power collected from the solar cell. Furthermore, quantum efficiency is most usefully expressed as a function of photon wavelength or energy. Since some wavelengths are absorbed more effectively than others in most semiconductors, spectral measurements of quantum efficiency can yield information about which parts of a particular solar cell design are most in need of improvement [3].

1.5.Different types of solar cells and current technological trends

Most photovoltaic cells produced are currently deployed for large scale power generation in centralized power stations or in 'building integrated photovoltaics' (BIPV). Although crystalline silicon solar cells were the dominant cell type used through most of the latter half of the last century, other types of cells have been developed that compete either in terms of reduced cost of production or improved efficiencies. The best efficiencies obtained with some of the important cell types are given in Table.1.1. The key aim of all the technologies is to reduce production cost to 1$ per peak Watt (1$/Wp) to compete on cost with other forms of power generation. The technologies also need to have an acceptable energy payback time which is the time taken by a device to generate as much energy as was needed to fabricate the device.

In this section, we have listed different types of solar cell technologies which are currently in use along with some new concepts which are yet to be made practical. For convenience they are grouped as silicon based cells, cells based on compound semiconductors, dye sensitized cells, organic/polymer solar cells and some new concepts.

Type of solar cell	**Highest reported small area efficiency**	
	Efficiency (%)	**Laboratory/Institution**
Crystalline Si	24.7	University of New South Wales
Multicrystalline Si	20.3	Fraunhofer Institute for Solar Energy Systems
Amorphous Si	10.1	Kaneka
HIT cell	23	Sanyo Corporation
GaAs cell	26.1	Radboud University Nijmegen
InP cell	21.9	Spire Corporation
Multijunction Concentrators	40.8	National Renewable Energy Laboratory
CdTe	16.5	National Renewable Energy Laboratory
CIGS	19.9	National Renewable Energy Laboratory
$CuInS_2$	12.5	Hahn Meitner Institute
DSSC	11.1	Sharp
Organic Solar Cells	6.1	Gwangju Institute of Science and Technology

Table.1.1.Best efficiencies reported for different types of solar cells.

Another mode of classifying solar technology is based on the different generations. First generation solar cells are the silicon-based photovoltaic cells that still dominate the solar panel market. These solar cells, using silicon wafers, account for 86% of the solar cell market. Despite their high manufacturing costs, they are dominant due to their high efficiency. Second generation cells, also called thin-film solar cells, are significantly cheaper to produce than first generation cells but have lower efficiencies. The great advantage of second generation thin-film solar cells along with low cost, is their flexibility. Thin-film technology has spurred lightweight, aesthetically pleasing solar innovations such as solar shingles and solar panels that can be rolled out onto a roof or other surface. It has been predicted that second generation cells will dominate the residential solar market as new, higher-efficiency cells are developed. The most popular materials used for second generation solar cells are copper indium gallium selenide, cadmium telluride (CdTe), amorphous silicon and micromorphous silicon. The third generation is somewhat ambiguous in the technologies that it encompasses, though generally it tends to include non-semiconductor technologies (including polymer cells and biomimetics), quantum dot technologies, tandem/multi-junction cells, hot-carrier cells, upconversion and downconversion technologies, and solar thermal technologies.

1.5.1.Silicon based solar cells

a.Crystalline Si solar cells

For crystalline silicon devices, boron doped p-type Si boule is grown using Czochralski method and wafers are sawn from it. Since Si has indirect band gap resulting in a low optical absorption coefficient, the wafers need to have thickness greater than 200μm to absorb most of the incident light. The wafer surfaces are textured to minimize reflection losses and to enhance optical path length in Si. A p-n junction is formed by diffusing phosphorus into the wafer. Ag contacts are used on n-type surface to make electrical contact and Al is used as back contact in p region. An antireflection (A/R) coating of TiO_2 or silicon nitride is deposited over the top surface [7]. The passivated emitter rear locally diffused (PERL) solar cell, which has an efficiency of 24.7% is the most efficient Si solar cell produced in laboratory [8].

The high efficiency is achieved by improving surface texturing and by inclusion of SiO_2 layer at the back of the device to passivate the back surface.

b.Multicrystalline Si solar cells

Here, molten Si is poured into a container and then allowed to cool, resulting in Si ingots with large columnar grains of typically 0.3 mm diameter growing from the bottom of the container upwards [9]. The grains are so large that they extend through the wafers cut from the solidified block. Hydrogen is incorporated during device processing for passivating grain boundaries. Cell processing is similar to that of crystalline silicon devices. The advantages of using multicrystalline growth over Czochralski method include lower capital costs, higher throughput, less sensitivity to quality of Si feed stock and higher packing density of cells to make module, due to the square or rectangular shape of cells. Multicrystalline Si devices have efficiencies 2-3% less than those of crystalline Si and cost approximately 80%. It is also possible to draw multicrystalline silicon in the form of sheets or 'Si ribbon' from a Si melt. These are then processed to make solar cells [10].

c.Amorphous Si solar cells

Thin films of amorphous Si are usually produced using PECVD of gases containing Silane (SiH4) [11]. The layers can be deposited on rigid as well as flexible substrates allowing diversity of use. Solar cells use hydrogenated amorphous Si (αSi:H), an alloy of Si and hydrogen (5-20 at. % H), in which hydrogen plays the role of passivating dangling bonds that result from the random arrangement of Si atoms. Hydrogenated amorphous Si has a direct band gap of 1.7 eV and high optical absorption coefficient so that only few microns of material is required to absorb most of the incident light, thus reducing material usage and cost. Most devices have p-i-n structure. A major problem with amorphous Si solar cells is the Stebler-Wronski effect which is the increase in density of dangling bonds due to light-induced breakage of Si-H bonds, resulting in degradation of efficiency [11].

d.HIT solar cells

Heterojunction with intrinsic thin layer (HIT) is a novel device developed by Sanyo [12]. In this device, layers of amorphous Si are deposited on both faces of

textured wafer or single crystal Si. This results in 10 cm X 10 cm multijunction devices with efficiency more than 22% [13]. The advantages of this structure are potential for high efficiency, good surface passivation and low temperature processing (all steps except substrate production carried out at less than 473 K), which reduced energy pay back time and cost, compared to conventional Si devices.

1.5.2.Solar cells based on compound semiconductors

a.III-V solar cells

The III-V compounds like GaAs and InP have direct energy band gaps (1.4 eV), high optical absorption coefficients and good values of minority carrier lifetime and mobilities. This makes them excellent for photovoltaic application [14]. Solar cells using these materials can be made by diffusion of n–type dopants into wafers from single crystals, produced using liquid encapsulated Czocharalski (LEC method) or Bridgmann method [15]. But highest efficiencies achieved so far in both cases were by using epitaxially grown homojunction structures. The disadvantage of using III-V compounds in photovoltaic devices is the very high cost of producing device quality epitaxial layers of these compounds. Crystal imperfections and impurities severely reduce device efficiencies and hence low cost deposition techniques cannot be used. But these have been used for space applications due to high conversion efficiencies and radiation resistance. They have been effectively used in concentrator systems [16].

b.CdTe solar cells

With a direct band gap of 1.5 eV and high optical absorption coefficient, only few microns of CdTe are needed to absorb most of the incident photons. Since thin layers are needed, material cost is minimized and because short diffusion length is adequate, expensive material processing can be avoided. In a typical cell, front contact is provided by depositing a transparent conducting oxide (TCO) onto glass substrate, followed by deposition of CdS window layer and CdTe absorber. CdTe has been deposited using a variety of ways such as closed space sublimation (CSS), chemical bath deposition (CBD), physical vapour deposition (PVD), chemical spray pyrolysis (CSP) etc. But for commercial devices, CSS and CBD are used. To produce

most efficient devices, an activation process is required in the presence of $CdCl_2$ irrespective of the deposition technique used. Activation promotes re-crystallization and interdiffusion at the interface of CdTe and CdS [17, 18, 19]. In the most efficient CdTe cells, Cd_2SnO_4 is used as TCO and Zn_2SnO_4 buffer layer is included to improve quality of interface. Presently, two companies (First Solar and Antec Solar) manufacture CdTe based modules.

c.Solar cells based on chalcopyrite compounds

The first chalcopyrite solar cells developed were based on the use of $CuInSe_2$. Incorporation of Ga into $CuInSe_2$ to produce $CuInGaSe_2$ (CIGS) resulted in the widening of band gap to 1.3 eV and an improvement in material quality, thereby enhancing device efficiency. CIGS has high optical absorption coefficient for energies greater than its band gap, such that only few microns are required to absorb incident light effectively, thus reducing material cost. Another requirement is presence of Na, either directly from the substrate or incorporated chemically which helps in grain growth, passivation of grain boundary and decrease in resistivity [20, 21, 22]. The best CIGS solar cells are grown on soda lime glass in the sequence: back contact, absorber layer, window layer, buffer layer, TCO and top contact grid. CIGS solar cells have reached efficiencies up to 19.9% [23] and module efficiency of 13.4% [24]. The main manufacturers of CIGS cells are Würth Solar, Avancis (formerly Shell Solar) and Global Solar.

$CuInS_2$ has a band gap of 1.5 eV that is an ideal match for the solar spectrum and it can be produced in thin film form by a number of different processes. Cells with the structure Mo/p-$CuInS_2$/n-CdS/n^+ZnO/Al, where $CuInS_2$ was deposited by thermal co-evaporation and CdS by chemical bath deposition, were reported to have an efficiency of 10.2% [25]. The p-type $CuInS_2$ was prepared with Cu/In ratio between 1.0 and 1.8 and excess copper phases were removed chemically. Both co-deposition and sequential deposition produced device efficiencies of 11 to 12% [26]. Cells based on RTP absorbers have reached confirmed total area efficiency of 11.4% [27]. $In_x(OH,S)_y$ has been used to replace CdS as buffer layer in 11.4% solar cells based on $CuInS_2$ [28].

1.5.3.Dye sensitized solar cells

In dye-sensitized solar cell, the bulk of the semiconductor is used solely for charge transport while the photoelectrons are provided from a separate photosensitive dye [29]. Charge separation occurs at the semiconductor/dye/electrolyte interface.The dye molecules are quite small and hence to capture a reasonable amount of the incoming light, the layer of dye molecules need to be made fairly thick, much thicker than the molecules themselves. Hence, a nanomaterial is used as a scaffold to hold large numbers of the dye molecules in a 3-D matrix, increasing the number of molecules for any given surface area of cell. In existing designs, this scaffolding is provided by the semiconductor material, which serves a double duty. The dye-sensitized solar cell depends on a mesoporous layer of nanoparticulate titanium dioxide to greatly amplify the surface area [30]. The photogenerated electrons from the light absorbing dye are passed onto the n-type TiO_2, and the holes are passed to an electrolyte on the other side of the dye. The circuit is completed by a redox couple in the electrolyte, which can be liquid or solid. This type of cell allows a more flexible use of materials, and is typically manufactured by screen printing, with the potential for lower processing costs than bulk solar cells. However, the dyes in these cells also suffer from degradation under heat and UV light, and the cell casing is difficult to seal due to the solvents used in assembly. This, along with the fact that the solvents permeate plastics, has precluded large-scale outdoor application and integration into flexible structure [31]. In spite of the above demerits, this is a popular emerging technology with some commercial impact forecast within this decade.

1.5.4.Organic/Polymer solar cells

Organic solar cells differ from inorganic semiconductor solar cells in that they do not rely on the large built-in electric field of a p-n junction to separate the electrons and holes created during photon absorption. The active region of an organic device consists of two materials, one of which acts as an electron donor and the other as an acceptor. When a photon is converted into an electron-hole pair, typically in the donor material, the charges tend to remain bound in the form of an exciton, and are separated when the exciton diffuses to the donor-acceptor interface. The short exciton

diffusion lengths of most polymer systems tend to limit the efficiency of such devices. Nanostructured interfaces, sometimes in the form of bulk heterojunctions, can improve performance [32].

Organic solar cells and polymer solar cells are built from thin films (typically 100 nm) of organic semiconductors such as polymers and small-molecule compounds like polyphenylene vinylene, copper phthalocyanine (a blue or green organic pigment) and carbon fullerenes. Energy conversion efficiencies achieved to date using conductive polymers are low compared to inorganic materials, with the highest reported efficiency of 6.1% for a bulk heterojunction [33]. However, these cells could be beneficial for some applications where mechanical flexibility and disposability are important.

1.5.5.Some new concepts

Some novel methods have been put forward lately with the aim to achieve high efficiency devices using second generation deposition methods. Increasing efficiency strongly leverages lower costs. To achieve such efficiency improvements, devices aim to circumvent the Schockley-Quiesser limit for single band gap devices that limit efficiency to 31% or 40.8%, depending on concentration [34]. This requires multiple threshold devices. The two important power-loss mechanisms in single band gap cells are the inability to absorb photons with energy less than the band gap and thermalisation of photon energies exceeding band gap. These two mechanisms alone amount to the loss of about half of the incident solar energy in the cell. In the new approaches, which are popularly known as third generation concepts, the amount of work done per photon is increased by (i) increasing the number of band gaps to utilize different photon energies (tandem or multi-band solar cells), (ii) reducing dissipation of thermal energy (hot carrier cells) and (iii) multiple carrier generation per photon (impact ionization cells) [35]. Of these, tandem cells are the only ones that have, as yet, been realized with efficiencies exceeding Shockley-Queisser limit.

a.Multiple energy level approaches

The concept of using multiple energy levels to absorb different sections of the solar spectrum is achieved in tandem solar cells and intermediate band solar cells.

In tandem cells, p-n junctions using different semiconductors with increasing band gap are stacked such that the highest band gap material intercepts the sunlight first. The elegance of this approach is that both spectrum splitting and photon selectivity is achieved by the stacking arrangement. This approach was first suggested by Jackson in 1955 [36]. To achieve highest efficiency from a tandem device, power from each cell must be optimized. This is done by choosing appropriate band gaps, film thicknesses, junction depths and doping characteristics such that the incident spectrum is split between the cells most effectively.

In intermediate band cells, one or more energy levels within the band gap absorb photons in parallel with the normal operation of single band gap cell. These additional sub-band gap absorbers can either exist as discrete energy levels in an impurity PV (IPV) or as a continuous band separated from valance and conduction band in intermediate band solar cell (IBSC). Both types of cells can absorb below band gap photon to create electron-hole pairs, but IBSC has the advantage that photons do not necessarily have to be absorbed by the same electron, giving more time for the absorption of second photon. IPV cells are made by incorporation of deep defects in a cell. Defects with energy one third of the band gap energy of the absorber are found to be optimum. Incorporation of boron in SiC [37] and indium in Si [38] are some suggested and tried examples. Formation of intermediate band for an IBSC has been suggested in some III-V, II-VI and chalcopyrite systems usually alloyed with transition systems [39, 40]. But in practice, neither IPV nor IBSC have yet achieved an efficiency advantage.

b.Hot carrier cells

An option for increasing efficiency is to allow absorption of a wide range of photon energies and to collect the photo-generated carriers before they have a chance to thermalize. The concept underlying hot carrier cell is to slow down the rate of photo-excited carrier cooling, which is caused by photon interaction in the lattice, to allow carriers to be collected while they are still at elevated energies. This allows higher voltages to be achieved and tackles major loss mechanism due to thermalization of carriers [41]. In addition to absorber material that slows down the

rate of carrier relaxation, hot carrier cells must also allow extraction of carriers from the device through contacts that accept very narrow range of energies.

c.Multiple carrier excitation

Carriers generated from a high energy photon having at least twice the band gap energy can undergo impact ionization, resulting in two or more carriers having energies close to band gap. In this process, an energetic electron collides with lattice and gives up its kinetic energy to excite a further electron across the band gap [42]. In the context of a PV device, this means that quantum efficiency for light with $E > 2Eg$ can be greater than one. These high energy photons are capable of multiple pair generation. This effect has been observed in Ge photodiodes at photon energies greater than 2.5 eV and in Si diodes for $E > 3.3$ eV [3].

1.6.Thin film solar cells: an overview

Thin film solar cells (TFSC) are a promising approach for terrestrial and space applications and offer wide variety of choices in terms of device design and fabrication. As requirements for material is reduced, they have potential for low cost mass production. TFSC can tolerate more imperfections and impurities than single crystal cells as the active semiconductor layer is thin. A variety of substrates (flexible or rigid, metal or non metal) can be used for depositing different layers (contact, buffer, absorber, anti-reflection etc.) using different techniques (physical vapour deposition, chemical vapour deposition, spray pyrolysis etc.). Such versatility allows tailoring and engineering of layers in order to improve device performance.

For large area devices required for realistic applications, thin film device fabrication becomes complex and requires proper control over the entire process sequence. Research and development in new, exotic and simple materials and simple manufacturing processes need to be pursued. Cheap and moderately efficient TFSC are expected to receive due importance in future.

TFSC generally uses polycrystalline and amorphous materials. The polycrystalline nature of the materials introduces grain boundaries which can degrade current generation, voltage and stability of cells. The method of deposition leads to non stoichiometry and post deposition recrystallization may create problems related

to material orientation. Suitability of substrate is also an important factor for proper functioning of TFSC.

1.6.1.Factors affecting thin film device performance

Electron affinity match: Interface states exists in all hetero junctions, in which case the electron affinity difference between the two materials determines the magnitude of the barrier which the carriers see as they cross the interface. To change the electron affinity mismatch, it is necessary either to alloy the material significantly or to change totally one of the junction components

Lattice constant match: Mismatch of lattice constants determine the density of interface states in the material. Therefore, it is essential to choose materials which have lattice constants as well matched as possible.

Grid contact: Grid contact on solar cell is an important efficiency controlling factor. Transmisssion through grid should be maximized and the grid material should make ohmic contact with the semiconductor. Also, the spacing between grid lines should be optimum.

Layer thickness: The optimum thicknesses of layers comprising a thin film solar cell are determined by a number of boundary conditions. For the absorber layer, the first requirement is that the product of absorbance and thickness be sufficient to ensure that virtually all the useful solar spectrum is absorbed and carriers are generated. This may be achieved in a single pass or in multipasses as a result of reflection from backcontact and light trapping effects. While satisfying the absorption requirement, the thickness must also be such that the minority carrier diffusion length should be equal to or greater than the thickness of absorber layer. Third requirement influencing the thickness of the semiconductor layers in a cell arise from resistance effects. The grid or substrate design should be so as to reduce series resistance so that fill factor is not affected whereas shunting paths arising from grain boundary penetration of dopants or impurities should be avoided.

Surface passivation: For an efficient thin film cell, it is essential that effective surface passivation prevent carrier loss by recombination at external or internal surfaces. Usually chemical polishing reduces surface recombination velocity. Another

approach is to produce a doping profile resulting in an internal electric field, which opposes minority carrier diffusion towards the surface.

Photon economy: It is essential to minimize the amount of light reflected from the surface of the device. One method is by texturing the surface so that the reflected light intercepts another entrance surface. Second method is to use anti-reflection coatings.

Substrate properties: For many solar cells, an important substrate characteristic is lattice constant match to the material deposited. This will promote epitaxial growth mode and good adherence to the surface. Good adherence is also assisted by matching thermal expansion constants of substrate and material being deposited. As deposition usually takes place at temperatures well above room temperature, difference in thermal expansion can produce destructive stresses on cooling. If substrate is being used as back contact, it is ideal to have it to be reflecting. This will assist multiple passages of light through the absorber, resulting in more effective use of photons.

1.6.2.Performance of thin film solar cells

A wide variety of materials have been used as the basis of thin film solar cells. But the reported efficiencies should not be taken as indicative of the achievable efficiencies. Poor efficiency can result from various causes many of which are of engineering nature. On the other hand, unjustifiably high values have been reported by using only active area, correcting for all reflection losses and using best values from very small devices. But these high values will not be attainable in practical devices. Also in large area polycrystalline devices, material nonuniformity may reduce the average efficiency to well below the best small area value.

The theoretical efficiency of a given solar cell may be computed for a given spectrum of light by assuming (1) that all incident photons of more than band gap energy contribute one electron each to the short circuit current, (2) that the open circuit voltage is limited only by the smallest band gap in the junction and (3) that the fill factor is not reduced by either series or shunt resistance effects [43]. But in practical devices, there are some fundamental losses like the inability of the

semiconductor to absorb below band gap photons, that due to thermalization of carriers and resistive losses etc. [6]. Knowing the theoretical efficiency value and by analysing unavoidable losses, one can compute the attainable efficiency. Although single crystal cells have achieved practical efficiencies much closer to theoretical limit than polycrystalline thin film cells, there is no fundamental reason why thin film cells should not reach high values.

1.7.Significance of the present work

In the present chapter, we have discussed the vital concepts of solar cells and came across the current technology trends in the PV field. It is clear that all other technologies other than silicon have to go a long way for achieving their predicted potential. Hence, there is enough room for further research in this area. New materials and new techniques need to be investigated comprehensively. Present work focuses on second generation concept, where thin film solar cells are developed using cost-effective techniques.

References

[1] A.E. Becquerel, Comptes Rendus. 9 (1839) 561.

[2] D.M. Chapin, C.S. Fuller, G.L. Pearson, J. Appl. Phys. 25 (1954) 676.

[3] Jenny Nelson, The Physics of Solar cells, Imperial College press, UK (2003).

[4] Eduardo Lorenzo, Gerardo L. Araújo, Philip Davies, A. Cuevas, M. Egido, J. Minano, R. Zilles, Solar Electricity: Engineering of Photovoltaic Systems, Progensa, Spain (1994).

[5] Stefan Mau et al., Proceedings of 19th EUPVSEC, Paris, France (2004).

[6] Tom Markvart, Louis Castañer, Practical Handbook of Photovoltaics: Fundamentals and Applications, Elsevier, UK (2003).

[7] Robert W Miles, Guilaume Zoppi, Ian Forbes, Materials Today. 10 (2007) 20.

[8]Jianhua Zhao, Aihua Wang, Martin A. Green, Francesca Ferrazza, Appl.Phys.Letters. 73 (1998) 1991.

[9] M.Ghosh et al., Proceedings of 19th EUPVSEC, Paris, France (2004).

[10] A. Eyer, A. Raeuber, A. Goetzberger, Optoelectronics. 5 (1990) 239.

[11] C.R. Wronski and D.E. Carlson, Amorphous Si Solar Cells. In: M.D. Archer and R. Hill, Editors, Clean Electricity from Photovoltaics, Imperial College Press, London, UK (2001).

[12] Maruyama E. et al., Proceedings of 4th World Conference on Photovoltaic Energy Conversion, Hawai (2006).

[13] http://www.sanyo.com.

[14] Bube R.H., Photovoltaic Materials, Imperial College Press, London,UK (1998).

[15] Partain L.D., Solar cells and their Applications, John Wiley and Sons (1995).

[16] Archer M.D., R. Hill, Clean electricity from photovoltaics, Imperial College Press, London, UK (1998).

[17] Zoppi G., K. Durose, S.J.C. Irvine, V. Barrioz, Semicond. Sci. Technol. 21 (2006) 763.

[18] Edwards P.R. et al., Proceedings of 2nd World Conference in Photovoltaic Solar Energy Conversion, Vienna, Austria (1998).

[19] Jensen D.G. et al., Proceedings of 25th IEEE Photovoltaic Specialists Conference, Washington, USA (1996).

[20] Rudmann D., D. Brémaud, A.F. da Cunha, G. Bilger, A. Strohm, M. Kaelin, H. Zogg, A.N. Tiwari, Thin Solid Films. 480-481 (2005) 55.

[21] Rudmann D., A.F. da Cunha, M. Kaelin, F. Kurdesau, H. Zogg, A.N. Tiwari, Appl. Phys. Lett. 84 (2004) 1129.

[22] Granata J.E. et al., Proceedings of 2nd World Conference on Photovoltaic Solar Energy Conversion, Vienna (1998).

[23] http://www.nrel.gov.in.

[24] Tanaka.Y. et al., Proceedings of the 17th European Solar Energy Conference, Munich, Germany (2001).

[25] R. Scheer, T. Walter, H.W. Schock, M.L. Fearheiley, H.J. Lewerenz, Appl. Phys. Lett. 63 (1993) 3294.

[26] Walter et al., 13th European Photovoltaic Solar Energy Conference, Nice, France (1995).

[27] Seimer Kai, Jo Klaer, Ilka Luck, Jürgen Bruns, Reiner Klenk, Dieter Bräunig, Sol. Energy Mater. Sol. Cells. 67 (2001) 159.

[28] Braunger D., Hariskos D., Walter T., H. W. Schock, Sol. Energy Mater. Sol. Cells. 40 (1996) 97.

[29] J. Bisquert, Journal of Physical Chemistry B. 108 (2004) 8106.

[30] Michael Grätzel, Inorganic Chemistry. 44 (2005) 6841.

[31] Yu Ba, Yiming Cao, Jing Zhang, Mingkui Wang, Renzhi Li, Peng Wang, Shaik M. Zakeeruddin Michael Gratzel, Nature Materials. 7 (2008) 626.

[32] Sam-Shajing Sun, Niyazi Serdar Sariciftci, Organic Photovoltaics: Mechanism, Materials, and Devices, CRC Press (2005).

[33] Jin Young Kim, Kwanghee Lee, Nelson E. Coates, Daniel Moses, Thuc-Quyen Nguyen, Mark Dante, Alan J. Heeger, Science. 317 (2007) 222.

[34] Shockley W., Queisser H., J.Appl.Phys. 32 (1961) 510.

[35] M.A. Green, Third Generation Photovoltaics, Springer (2003).

[36] Jackson E.D., Proceedings of Conference on the Use of Solar Energy, Tuscon, Arizona (1955).

[37] Richards B.S et al., 3rd World Conference on PV Energy Conversion, Osaka, Japan (2003).

[38] Keevers M.J., Martin Green, Sol. Energy Mater. Sol. Cells. 41-42 (1996) 195.

[39] Palacois P., J.J. Fernández, K. Sánchez, J.C. Conesa and P. Wahnón, Phys. Rev. B. 73 (2006) 085206.

[40] Yu K.M., W. Walukiewicz, J.W. Ager III, D. Bour, R. Farshchi, O.D. Dubon, S.X. Li, I.D. Sharp, E.E. Haller, Appl. Phys. Lett. (2006) 88, 092110.

[41] Wurfel P., Sol. Energy Mater. Sol. Cells. 46 (1997) 43.

[42] K. Tanabe, Electronics Letters. 43 (2007) 998.

[43] Lawrence L. Kazmerski, Polycrystalline and Amorphous Thin Film Devices, Academic Press (1980).

CHAPTER 2

Fabrication of Automated Chemical Spray Pyrolysis Unit

2.1.Introduction

Chemical spray pyrolysis (CSP) is used for depositing a wide variety of thin films, which are used in devices like solar cells, sensors, solid oxide fuel cells etc. It has evolved into an important thin film deposition technique and is classified under chemical methods of deposition. This method offers a number of advantages over other deposition processes, the main ones being scalability of the process, cost-effectiveness with regard to equipment costs and energy needs, easiness of doping, operation at moderate temperatures (100-500˚C) which opens the possibility of wide variety of substrates, control of thickness, variation of film composition along the thickness and possibility of multilayer deposition.

Many studies were done on CSP process since the pioneering work by Chamberlein and Skarman in 1966 on CdS films for solar cells [1]. Several reviews on this technique have also been published. Mooney and Radding reviewed CSP technique in which properties of specific films (particularly CdS) in relation to deposition parameters and their device applications were discussed in detail [2]. Tomar and Garcia discussed the preparation, properties and applications of spray-coated thin films [3]. Albin and Risbud presented a review of equipment, processing parameters and opto-electronic materials deposited using this technique [4]. R.Krishnakumar et al. did an exclusive review of sprayed thin films for solar cells in which a variety of solar cell materials and their preparative parameters were detailed [5]. Different atomization techniques and properties of metal oxide, chalcogenide and superconducting films prepared using CSP were discussed by Patil [6]. Recently, Perednis and Gaukler gave an extensive review on the effect of spray parameters on films as well as models for thin film deposition by CSP [7].

Present chapter discusses various aspects of CSP technique. Different models of deposition processes proposed in literature and the effect of spray parameters are included here. Details of the indigenously fabricated automated spray unit and the modifications made so as to obtain good quality films are also described.

2.2.The deposition process and models of deposition

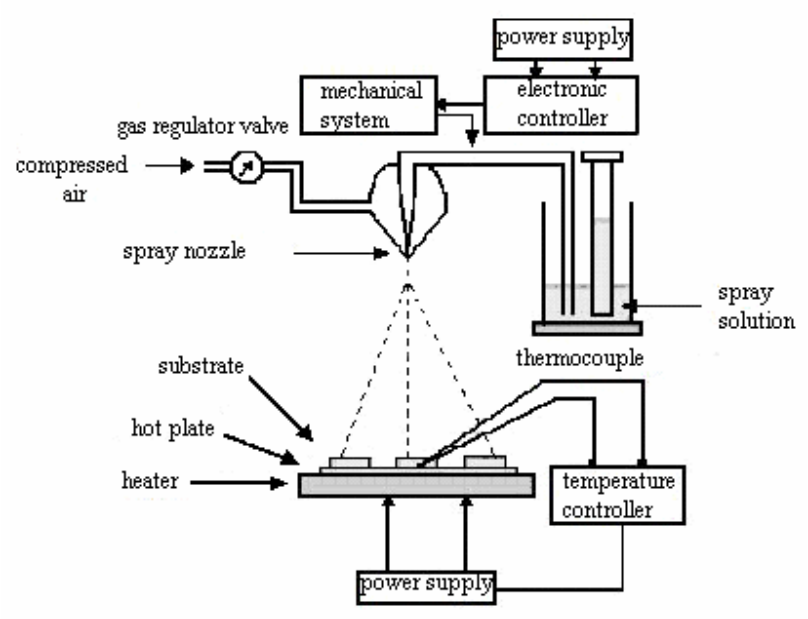

Figure.2.1.Schematic diagram of chemical spray pyrolysis unit.

CSP technique involves spraying a solution, usually aqueous, containing soluble salts of the constituents of the desired compound onto a heated substrate. Typical CSP equipment consists of an atomizer, a substrate heater, temperature controller and a solution container. Additional features like solution flow rate control, improvement of atomization by electrostatic spray or ultrasonic nebulization can be incorporated into this basic system to improve the quality of the films. To achieve uniform large area deposition, moving arrangements are used where either nozzle or

substrate or both are moved. The schematic diagram of a typical spray unit is given below (Figure.2.1).

Only crude models about the mechanism of spray deposition and film formation have been developed. There are too many processes that occur sequentially or simultaneously during the film formation by CSP. These include atomization of precursor solution, droplet transport, evaporation, spreading on the substrate, drying and decomposition. Understanding these processes will help to improve film quality. Deposition process in CSP has three main steps: atomization of precursor solutions, transportation of the resultant aerosol and decomposition of the precursor on the substrate.

Atomization of liquids has been investigated for years. It is important to know which type of atomizer is best suited for each application and how the performance of the atomizer is affected by variations in liquid properties and operation conditions. Air blast, ultrasonic and electrostatic atomizers are normally used. Among them, air blast atomization is the simplest. However this technique has limitation in obtaining reproducible droplets of micrometer or submicron size and in controlling their distribution [8].

In ultrasonic nebulized atomization, precursor solutions were fogged using an ultrasonic nebulizer [9]. The vapour generated was transported by carrier gas to the heated substrate. Precursor solution was converted to small droplets by ultrasonic waves and such droplets were very small with narrow size distribution and had no inertia in their movement. Pyrolysis of an aerosol produced by ultrasonic spraying is known as pyrosol process. Advantage of this technique is that gas flow rate is independent of aerosol flow rate, unlike in the case of air blast spraying.

Electrostatic spray deposition technique has gained significance only in recent years. Electrostatic atomization of liquids was first reported by Zeleny [10]. Grace et al. published a review on this type of atomization [11]. A positive high voltage applied to the spray nozzle generated a positively charged spray. Stainless steel discs acted as cathode and the droplets under electrostatic force moved towards the hot substrate where pyrolysis took place. In electrostatic spray, depending on the

spray parameters, various spraying modes were obtained. They were classified as cone-jet mode and multi-jet mode. Cone-jet mode split into multi-jet mode with increase in electric field, where number of jets increased with applied voltage.

During transportation of the aerosol, it is important that as many droplets as possible are to be transported to the substrate without forming powder. Sears et al. investigated the mechanism of SnO_2 film growth [12]. Gravitational, electric, thermophoretic and Stokes forces were taken into account in the proposed model. From the study, it was concluded that the film growth was from vapour of droplets which passed close to the hot substrate (in a manner similar to CVD), and that droplet on striking the substrate, formed a powdery deposit. However, spreading of the droplet on the substrate, which more significantly contribute to film growth, was not considered.

Yu and Liao proposed a model for evaporation of solution droplets [13]. The aerosol droplets experience evaporation during transport to substrate leading to size reduction and concentration gradient within the droplet. Precipitation may occur on the surface of droplet resulting in the formation of porous crust and hollow particles which is not desired because it increases surface roughness of the films. The probability of this is more if droplet size is large and number concentration low. Smaller droplets produce solid particles as diffusion distance for solute is shorter, leading to more uniform concentration distribution within the droplet. Increasing the number of droplet increases solvent vapour concentration resulting in delayed precipitation.

The reaction process taking place in CSP is interesting. Many models exist for the decomposition of precursor. Many simultaneous processes occur when a droplet hits the substrate surface: evaporation of residual solvent, spreading of droplet and salt decomposition.

Vigue and Spitz proposed that the following processes occur with increasing substrate temperature [14]. The below given figure illustrates the four possible processes that occur with increasing temperature (Figure.2.2).

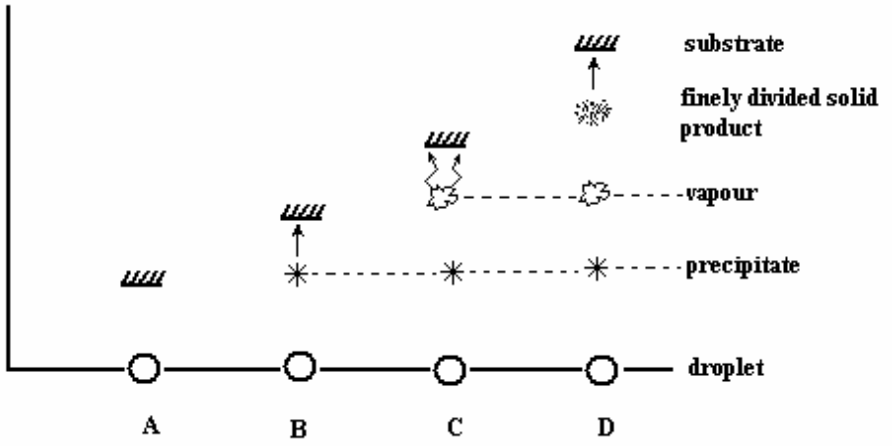

Figure.2.2.Spray processes occuring with increase in substrate temperature. A,B,C and D represents the different processes.

In *process A*, droplet splashes on substrate, vaporizes and leaves a dry precipitate in which decomposition occurs.

In *process B*, solvent evaporates before the droplet reaches the surface and precipitate impinges on the surface where decomposition occurs.

In *process C*, solvent vaporizes as droplet approaches the substrate, then solid melts and sublimes and vapour diffuses to substrate to undergo heterogeneous reaction there.

In *process D*, at highest temperature, the metallic compound vaporizes before it reaches the substrate and chemical reaction takes place in vapour phase.

Most of the spray pyrolysis deposition is of type A or B and our discussion will naturally center on these two.

2.3.Deposition parameters

Properties of film deposited depends on various deposition parameters like substrate temperature, nature of spray and movement of spray head, spray rate, type of carrier gas, nature of reactants and solvents used. The effect of some important spray parameters are discussed here.

2.3.1.Substrate temperature

Substrate temperature plays a major role in determining the properties of the films formed. It is generally observed that higher substrate temperature results in the formation of better crystalline films [15, 16]. Grain size is primarily determined by initial nucleation density and recrystallization. Recrystallization into larger grains is enhanced at higher temperature [17]. By increasing the substrate temperature, the film morphology can be changed from cracked to dense and then to porous [18]. Variation of substrate temperature over different points results in non-uniform films. Composition and thickness are affected by changes in substrate temperature which consequently affect the properties of deposited films. For example, while preparing SnS films using CSP, single phase films are obtained only in a narrow range of temperatures. Secondary phases like Sn_2S_3, SnS_2, SnO_2 etc. are present in films prepared at lower and higher temperatures [19].

High substrate temperature can also result in the re-evaporation of anionic species as in the case of metal sulfide films [20]. In metal sulfides, re-evaporation of sulfur from film occurs at high substrate temperature, leaving metal rich surface, which may react with oxygen to form oxides.

Though surface temperature is a critical factor, most investigators have not known the actual surface temperature of the substrate. Also, maintenance of substrate temperature at the preset value and its uniformity over large area are challenging. Liquid metal baths offer good contact at the interface and are widely used. But when solid surfaces are used, the actual area of contact is less than 1% of the surface area. Spraying in pulses or bursts also has been used to assure that surface temperature is reasonably constant [21].

2.3.2.Influence of precursors

Precursors used for spraying is very important and it affects the film properties seriously. Solvent, type of salt, concentration and additives influence the physical and chemical properties of the films. Usually, de-ionized water which is ideal for a low cost process is used as solvent. Use of alcohol as solvent has also been reported. It was observed that transparency of as deposited ZnO films increased when ethanol was used instead of water as solvent for zinc acetate [22]. Properties of films varied with type of precursors. For example, when In_2S_3 thin films were deposited from chloride based and nitrate based precursors, their properties differed significantly. Films from chloride based precursors were crystalline and highly photosensitive compared to those formed from nitrate based precursors which were amorphous [23, 24].

Concentration of spray solution also affects the nature of the films formed. Usually it ranges from 0.001 M to 0.1 M and it is seen that smooth films of columnar grains are obtained with low concentration and low spray rates [2]. Chen et al. observed that surface morphology of the films changed from cracked to crack free reticular, after introduction of acetic acid into precursor solution [25]. The change in morphology was attributed to the chemical modification of precursor solution.

Caillaud et al. investigated the influence of pH on thin film deposition and found that the growth rate depended on pH [26]. Formation of basic salts, adsorption compounds or precipitates slowed down the growth at higher pH. At low pH, deposition rate decreased drastically.

2.3.3.Spray rate

Spray rate is yet another parameter influencing the properties of films formed. It has been reported that properties like crystallinity, surface morphology, resistivity and even thickness are affected by changes in spray rate [27]. It is generally observed that smaller spray rate favours formation of better crystalline films. Smaller spray rate requires higher deposition time for obtaining films of the same thickness prepared at higher spray rate. Also, the surface temperature of substrate may deviate to a lower value at high spray rate. These two factors may

contribute to the higher crystallinity at small spray rates. Decrease in crystallinity at higher spray rates is observed in sprayed $CuInS_2$ thin films [27]. Decrease in crystallinity usually results in increased resistivity of the films.

Surface morphology of the films varies with spray rate. Higher spray rate results in rough films. Also, it is reported that films deposited at smaller spray rates are thinner due to the higher re-evaporation rate.

2.3.4.Other parameters

Parameters like height and angle of spray head, angle or span of spray, type of scanning, pressure and nature of carrier gas etc., influence the properties of deposited films. Different types of spray heads which produce different spray patterns are commercially available. Relative motion of the substrate holder and spray head should ensure maximum uniformity and large area coverage.

2.4.Fabrication of CSP unit

As already mentioned, CSP involves spraying of solution containing soluble salts of the constituent atoms of the desired compound onto a preheated substrate. The sprayed droplet reaching the hot substrate surface undergoes pyrolytic decomposition and forms a single crystallite or a cluster of crystallites. Other volatile byproducts and the excess solvent escape in the vapour form. The substrate provides the energy for the thermal decomposition of the constituent species and their subsequent recombination. This followed by sintering and recrystallization gives rise to a continuous film.

Hence, while fabricating a spray system, special attention must be given to maintain the substrate temperature, spray rate, type and pressure of carrier gas, movement of spray head etc. From our experience in working with the manual spray unit, we could fix the range of operating conditions. Photographs of the automated system are shown in Figure.2.3 and Figure.2.4.

Figure.2.3.Photograph of the automated CSP unit.

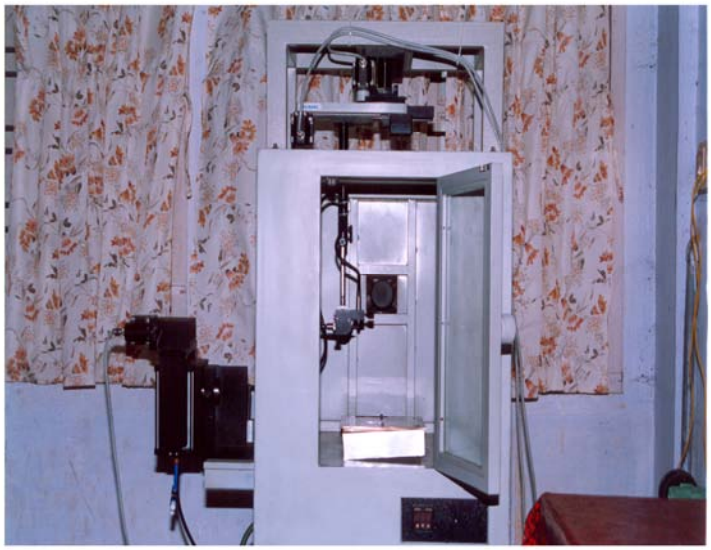

Figure.2.4.Photograph of the spray unit.

2.4.1.Substrate heating

Spray head, heater and substrate were kept inside a chamber provided with an exhaust fan for removing gaseous byproducts and solvent vapour. Initially, a stainless steel base plate of 20 cm X 20 cm area and 3 cm thickness with embedded heater rods was used. The required surface temperature was attainable even if one of the rods was malfunctioning. But while spraying, substrate temperature varied spatially along the plate and created non-uniformity over the film surface. To overcome this serious limitation, a single heater coil (1450 W) was embedded in ceramic grooves attached to the machined stainless steel base plate (15 cm diameter). In this setup, the heater was thermally insulated from the chamber.

Temperature of the substrate can be varied from room temperature to 723 K. K-type thermocouple was placed in a groove, close to the surface of the base plate, to detect the substrate temperature. During spray, substrate temperature was kept constant (with an accuracy of ±5 K) using a temperature controller equipped with a feed back circuit to control the heater supply.

2.4.2.Solution flow control and spray nozzle

In the present setup, solution was dispensed using a container with syringe-type arrangement (Figure.2.5). By varying the speed of the stepper motor attached to the container, dispensing rate of the solution could be controlled. The motor shaft was connected to a lead screw through a gear. During the rotation of the motor, a piston connected to the lead screw pushed out the liquid through the nozzle. Spray rate can be varied from 1ml/min to 15 ml/min. The container was made of Teflon, a corrosion free material. Plastic tubes were used for carrying the solutions from container to nozzle.

A surgical needle made of stainless steel was used as the spray nozzle which was replaced after every spray. It was ensured that solutions do not come into contact with any metal parts except the spray needle. Air nozzle was placed at right angles to the needle which was mounted horizontally (Figure.2.6). The spray was in the form of a solid cone with a circular impact area (~3.0 cm^2). Figure.2.7 shows full cone model spray and the resulting impact area pattern.

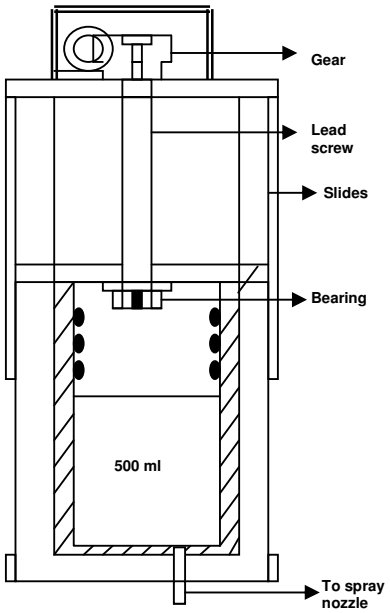

Figure.2.5.Schematic diagram of the syringe-type solution dispensing unit.

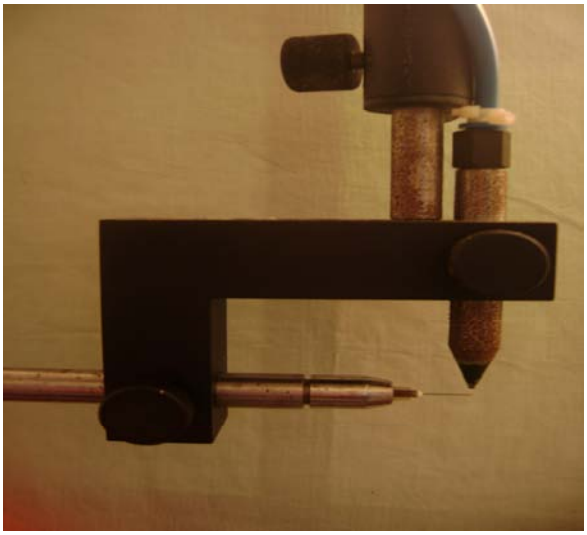

Figure.2.6.Photograph of the air blast type spray nozzle.

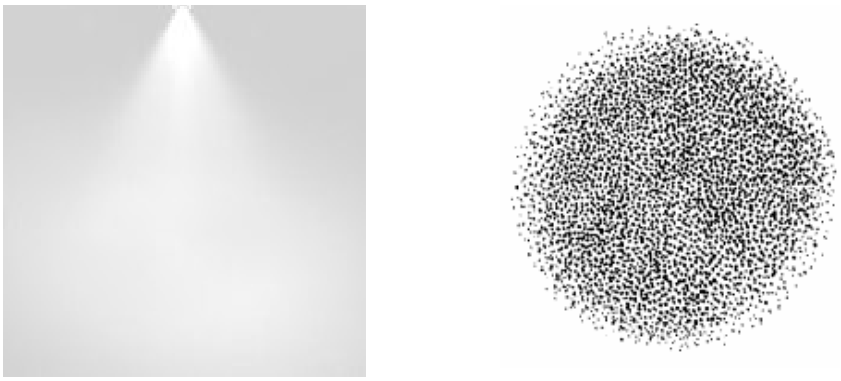

Figure.2.7.Full cone model spray (left) and the resulting impact area pattern (right).

2.4.3.Movement of spray head

Uniform coverage of large area was achieved by moving the spray head over the substrate surface by employing a mechanism having two stepper motors. The spray head could scan an area of 150 mm x 150 mm. The X-movement was at a speed of 100 mm/sec and the movement in Y-direction at a speed of 50 mm/sec. At higher spray rates, the speed of movement of spray head was found to be a critical factor. For slow movement (100 mm/s in X direction and 50 mm/s in Y direction in steps of 5mm), it was seen that films could not be deposited beyond the spray rate 4 ml/min without increasing the speed of X-movement (at ~573 K). When the spray head movement was slow and the spray rate was high, larger number of droplets reached unit area of the substrate surface. This resulted in substrate wetting and the deposited film detached from the substrate surface. Hence, the speed of spray head movement in X direction was increased to 200 mm/s. In the present setup, the distance between spray head and substrate as well as the angle of spray head can be varied.

2.4.4.Carrier gas control

Air blast type of atomization was used in the present setup. Filtered air used as carrier gas was compressed using a ½ HP compressor. The pressure of the gas fed to the nozzle was measured by a mechanical guage. The pressure can be varied

between zero and 10 kg/cm^2. Typical value of pressure used for deposition was ~ 0.6 kg/cm^2. Carrier gases other than air may also be used for spraying and we have deposited films using air as well as nitrogen. An air nozzle with orifice diameter of 0.1 mm was used in the unit.

2.4.5.Control and data storage

The set up fabricated as described above was controlled by a microprocessor which communicated with the computer through a serial port. The spray parameters could be stored in the PC. Parameters of each spray were fed into the unit via. a user friendly window (Figure 2.8). Interfacing between the system and PC was done using Visual C++ programming and the microprocessor was programmed separately.

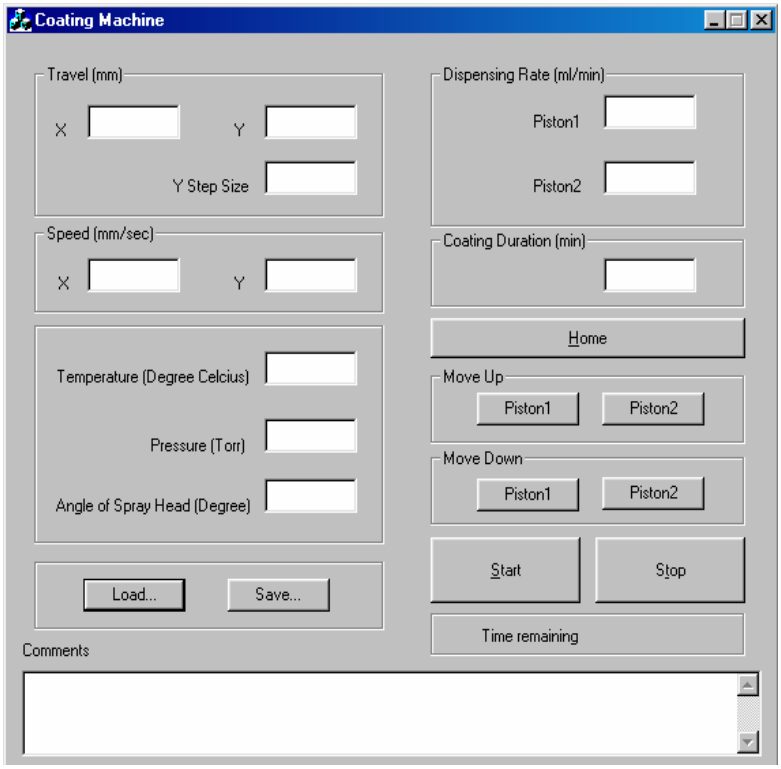

Figure.2.8.User friendly window for inputting spray parameters.

2.5.Conclusions

Using the spray system fabricated, thin films of $CuInS_2$ and In_2S_3 were successfully deposited. It was observed that uniform films could be deposited over an area of 10 cm X 10cm [28]. The figure given below shows the thickness profile of $CuInS_2$ film deposited over an area, 2.5 cm x 10 cm. The thicknesses were measured from thirty points using stylus profiler and surface mapping was done. The result of the mapping is presented in Figure 2.9. It is seen that the thickness variations are prominent at the edges and a major portion of the film has thickness within the range 315 nm - 370 nm. In other words, the spatial variation of thickness is less significant in the central region of the film.

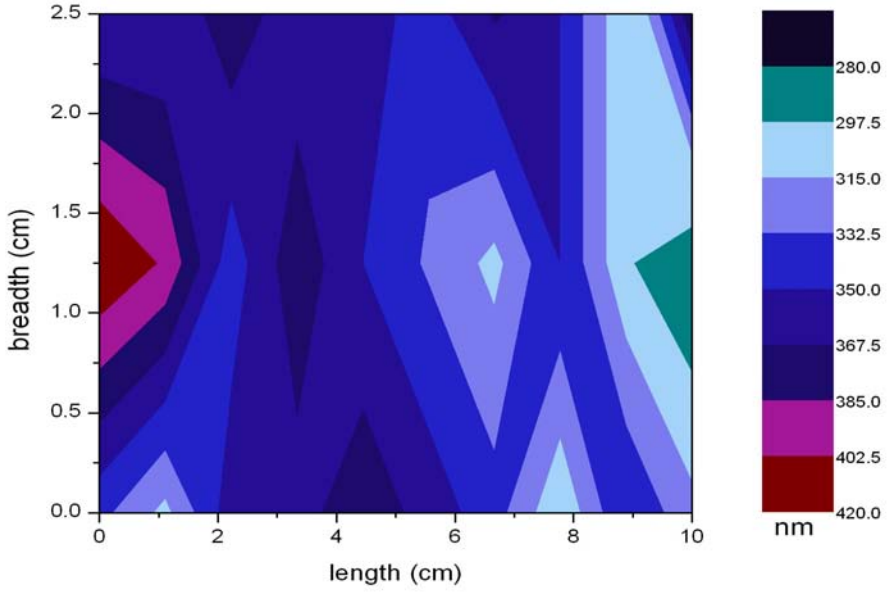

Figure 2.9.Two dimensional surface mapping of sample thickness over an area of 10cm x 2.5 cm.

The spray system has been designed as per our know-how and requirement by M/s Holmarc Opto-Mechatronics Pvt. Ltd., Kalamassery, Kochi. We have so far made three systems and all are working consistently for the past four years without

any major repairs or breakdowns. Several modifications have been made on X-Y movement. We have been able to deposit binary, ternary and quaternary compounds using it. The effect of different spray parameters on the properties of $CuInS_2$ and In_2S_3 films deposited using this system has been detailed in the next chapters.

References

[1] Chamberlein R.R, Skarman J.S., J. Electrochem Soc. 113(1) (1996) 86.

[2] J.B. Mooney, S.B. Radding, Annu. Rev. Mater. Sci. 12 (1982) 81.

[3] M.S. Tomar and F.J.Garcia, Progress in Crystal Growth and Characterization of Materials. 4(3) (1981) 221.

[4] D.S. Albin, S.H. Rishbud, Advanced Ceramic Materials. 2(3A) (1987) 243.

[5] R. Krishnakumar, V. Subramanian, Y. Ramprakash, A.S. Lakshmanan, Materials Chemistry and Physics. 15 (1987) 385.

[6] Pramod S. Patil, Materials Chemistry and Physics. 59 (1999) 185.

[7] Dainius Perednis, Ludwig J. Gauckler, Journal of Electroceramics. 14 (2005)103.

[8] Lampkin C.M., Prog. Cryst. Growth Characterization of Materials. 1(4) (1979) 405.

[9] S.P.S Arya, H.E.Hintermann, Thin Solid Films. 193 (1990) 841.

[10] J. Zeleny, Phys. Rev. 3(2) (1914) 69.

[11] J.M. Grace, J.C.M. Marijnissen, J. Aerosol Sci. 25 (6) (1994) 1005.

[12] W.M. Sears, M.A. Gee, Thin Solid Films. 165(1) (1984) 267.

[13] H.F. Yu, W.H. Liao, Int.J. Heat and Mass Transfer. 41(8-9) (1998) 993.

[14] J.C Viguiě, J. Spitz, J. Electrochem. Soc: Solid State Science and Technology. 122(4) (1975) 585.

[15] H.H. Affify, S.A. Nasser, S.E. Demian, J. Mater. Sci.: Materials in Electronics. 2(3) (1994) 700.

[16] A. Goswami, Thin Film Fundamentals, New Age International (P.) Ltd, India (1996).

[17] K.L. Chopra, Indrajeet Kaur, Thin Film Device Applications, Plenum Press, Newyork (1983).

[18] N.H.J. Stelzer, J. Schoonman, J. Materials Synthesis and Proceedings. 4(6) (1996) 429.

[19] T.H. Sajeesh et al., MRSI-AGM, New Delhi (2007).

[20] K.L. Chopra, S.R. Das, Thin Film Solar Cells, Plenum Press, Newyork and London (1983).

[21] Minoura H., Nakamura T., Uneo Y., Tsuiki M., Chem. Lett. 8 (1977) 913.

[22] Ratheesh Kumar P.M., Ph.D Thesis, Cochin University of Science and Technology, India (2007).

[23] Teny Theresa John, Ph.D Thesis, Cochin University of Science and Technology, India (2004).

[24] Teny Theresa John, C. Sudha Kartha, K.P. Vijayakumar, T. Abe, Y. Kashiwaba, Appl. Surf. Sci. 252 (2005) 1360.

[25] C.H. Chen, E.M. Kelder, J. Schoonman, J. Eur. Ceram. Soc. 18 (1998) 1439.

[26] F. Caillaud, A. Smith, J.F. Baumard, J. Amer. Ceram. Soc. 76(4) (1993) 998.

[27]Tina Sebastian, R.Jayakrishnan, C.Sudha Kartha, K.P.Vijayakumar, The Open Surface Science Journal. 1 (2009) 1.

[28] Tina Sebastian et al., Proceedings of 19th Kerala Science Congress, Kannur Kerala (2007).

CHAPTER 3

Deposition and Characterization of $CuInS_2$ Absorber Layer

3.1.Introduction

$CuInS_2$ is a chalcopyrite material belonging to the group of ternary semiconductors with molecular formula ABX_2. The system of copper chalcopyrite includes a wide range of band gap energies (E_g) from 1.04 eV (for $CuInSe_2$) up to 2.7 eV (for $CuAlS_2$), covering most parts of the visible spectrum [1]. This along with the wide range of carrier mobility offered by these semiconductors has resulted in their applications in photovoltaics, light emitting diodes and non linear optical devices. The crystal structure of ternary chalcopyrite has eight atoms per unit cell and can be considered as a superlattice of zincblende structure (Figure.3.1). Each anion is tetrahedrally coordinated to two atoms of both cations, while each cation is coordinated to four anions.

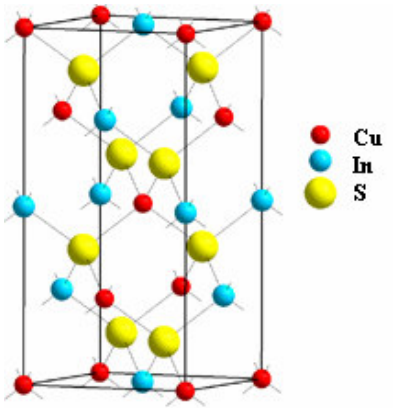

Figure.3.1.Structure of $CuInS_2$.

$CuInS_2$ (E_g=1.5 eV) has nearly optimum band gap for energy conversion, large absorption coefficient and good stability for solar radiation. The higher band gap favours the device response at higher temperatures and improves blue response of the cell. Large number of possible intrinsic defects and tolerance of this material to off stoichiometries make it all the more interesting. Important progresses in understanding the properties of $CuInS_2$ have been made during the last few decades, though a lot of questions still remain unanswered.

3.2.Spray pyrolysed $CuInS_2$: A brief review

Various routes to prepare $CuInS_2$ thin films exist and many have been atleast partially explored. $CuInS_2$ has been successfully deposited using techniques such as three-source evaporation [2], rapid thermal process (RTP) [3], RF sputtering [4], chemical spray pyrolysis (CSP) [5], sulfurization of Cu/In bilayers [6] etc. But as reduction in manufacturing cost is an important factor for the ultimate success of photovoltaic device in the market, thin film deposition techniques like CSP has gained importance.

CSP has been used by several groups to prepare $CuInS_2$ thin films. Two types of precursors are generally used for preparing sprayed $CuInS_2$ thin films. One uses solution containing $CuCl_2$+ $InCl_3$+Thiourea [7, 8, 9]. Works on nitrate based precursors instead of chlorides have also been reported [10]. The second type uses single source precursors of the type ($\{L\}_2Cu(SR)_2In(SR)_2$) where R=alkyl, aryl; L=neutral donor ligand [11]. In both the cases the deposition temperature was well below 723 K. In an aqueous solution of $CuCl_2$, $InCl_3$ and $SC(NH_2)_2$, which is the mainly used precursor solution to deposit $CuInS_2$ thin films, the copper chloride forms a complex compound with thiourea and indium chloride forms ammonium indium chloride. Formation of $CuInS_2$ from this mixed precursor has been followed by thermal analysis techniques by Krunks et al. They observed that thermal decomposition of precursor was a multistep process where $CuInS_2$ was formed at 523 K, independent of the atmosphere in which the reaction takes place [12].

Deposition of $CuInS_2$ under different deposition conditions were carried out by different groups. Structure and composition of sprayed films were strongly

affected by the temperature (at which film growth takes place) and copper to indium ratio in the precursor solution. Growth and recrystallization of sprayed $CuInS_2$ films were studied by Krunks et al. [13]. They observed that the growth temperature required to deposit single phase films depended on Cu/In ratio in the spray solution.

$CuInS_2$ can be successfully deposited on differnt types of substrates like glass [9], alumina [14], metal oxide [15] and polymer substrates [16]. Nature of substrate contribute to the growth and structure of as deposited films. $CuInS_2$ films deposited using CSP technique exists in either sphaletite or chalcopyrite structures. Tiwari et al. showed that sphalerite structure changes to chalcopyrite on annealing [17]. Single phase films with preferential orientation in (112) plane and having characteristic peak along (103) plane corresponding to chalcopyrite structure were obtained for sulfur rich films [18]. But generally, stoichiometric $CuInS_2$ deposited by CSP process is characterized by broad XRD peaks compared to films grown by other techniques.

It was observed that deviation from the stoichiometric composition affects the microstructure and surface morphology [8, 13]. Use of In rich solutions results in films with smooth surface and small grains whereas copper rich starting solutions promote formation of sharp edged crystallites with larger grain size. Also increasing copper concentration results in increase in number and area of agglomerations from SEM micrographs.

In almost all the studies it was seen that sulfur rich starting solution was required for formation of p-type stoichiometric films. Also, it is observed that Cu/In ratio and S/metal ratio can be varied to obtain films with resistivity ranging from 10^4 ohm cm to 10^{-2} ohm cm [19]. Band gap of the films also varied in the range 1.3 eV to 1.5 eV with variation in stoichiometry.

Sprayed $CuInS_2$ has to be chemically etched in alkaline KCN solution to remove copper rich phases which covers large crystals and fills cavities between grains [7]. Compositional analysis of sprayed $CuInS_2$ filmscshowed presence of chlorine, nitrogen and carbon containing residues. It was observed that the concentration of residues was mainly controlled by substrate temperature. Inversely to the residues orginated from precursors, oxygen content of the films increased at

higher temperatures [20]. XPS analysis showed that oxygen was found bounded to cations [21].

Post deposition treatments in H_2S atmosphere, vacuum and sulfur atmosphere have been carried out in sprayed $CuInS_2$. Hydrogen treatment at 400^0C and above purifies the film from chlorine and oxygen containing residues [20]. Annealing in dynamic vaccuum at temperatures close to 500^0C results in n-type $CuInS_2$ films containing In_2O_3 [22]. Post deposition annealing in H_2S atmosphere significantly improves the crystallinity and stoichiometry of the films. Optical band gap also increased on H_2S treatment. But it had adverse effect on electrical properties particularly when cooled rapidly [23].

Effect of incorporation of Na in sprayed $CuInS_2$ was investigated by Teny et al. using Na_2S as dopant [5]. It was observed that crystallinity, band gap, conductivity and photosensitivity of the samples improved on doping with low Na concentration. Incorporation of Al and Mn in sprayed $CuInS_2$ has also been reported. Mn doping resulted in increase of the band gap. It was found that Mn creates donor levels close to conduction band and this compensates hole concentration [24]. Kamoun et al. found that incorporation of Al in $CuInS_2$ increased work function of the material and induced formation of surface barrier [25].

From the above works it is clear that preparation conditions play a crucial role in controlling the properties of $CuInS_2$ thin films deposited using CSP technique. Subsequent sections discusses in detail the deposition and characterization of spray pyrolysed $CuInS_2$ thin films deposited under different conditions.

3.3.Outline of the work done

$CuInS_2$ films were deposited using the automated spray system with $CuCl_2$, $InCl_3$ and thiourea as precursors. Parameters like precursor ratio, thickness, spray rate and substrate temperature were varied so as to study their effects on properties of films formed. Effects of post deposition annealing treatments in air, vacuum and H_2S atmosphere on the properties of $CuInS_2$ films were also investigated.

For studying the effect of spray parameters on the properties of films deposited, depositions were carried out by varying only one spray parameter, keeping

all other conditions same. Structural, optical and electrical characterizations were carried out in these films. In some cases, studies on transport properties as well as defect analysis were carried out. Results of these studies are illustrated in the following sections.

3.4.Effect of precursor ratio (change in composition)

Systematic study was conducted on samples deposited by varying the molarities of precursor solutions. Fixing the spray rate at optimum value, Cu rich, equimolar and In rich samples were prepared, in which Cu/In ratio was 1.5, 1 and 0.5 respectively, keeping S/Cu ratio constant (S/Cu=5). Here, molarity of indium alone is changed to achieve variation in Cu/In ratio keeping S/Cu ratio constant. These samples were named as CIS 0.5-5, CIS 1.0-5 and CIS 1.5-5 respectively. To study the effect of variation of chalcogen concentration in the film, S/Cu ratio was changed, keeping Cu/In=1. The S/Cu ratios were varied as 2, 5 and 10 and the samples were named as CIS 1.0-2, CIS 1.0-5 and CIS 1.0-10 (the sample C1.0-5 is same as that mentioned above in Cu/In variation studies). In all the cases, the substrate temperature was maintained at 573 K, and volume of the spray solution was 40 ml. Properties of the films were studied using different characterization tools and the results are described below.

3.4.1.Scanning Electron Microscopy (SEM) and Energy Dispersive X-ray Analysis (EDAX)

SEM is a method for high resolution imaging of surfaces. It is the most widely used instrument for obtaining micro structural and surface features of thin films. The SEM uses electrons for imaging, such as an optical microscope uses visible light. The advantages of SEM over optical microscopy include much higher magnification (>100,000X) and depth of field upto 100 times that of light microscopy. A finely focused electron beam is scattered over the surface of the specimen and the secondary electrons emanating from the specimen are used for imaging the surface. Since secondary electrons come from the surface layer, the picture obtained is a faithful reproduction of the surface features. Secondary electron imaging can provide high-resolution imaging of fine surface morphology.

Quantitative and qualitative chemical analysis information can also be obtained using EDAX (Oxford model 7060).

Atomic concentrations of Cu, In and S in the films were obtained through EDAX analysis and the results are given in Tables.3.1 and 3.2. For each sample, EDAX was taken from different points on the surface and their mean value was taken as the actual composition. It was observed that variation of Cu/In ratio in the spray solution resulted in corresponding change in the composition of the films, as expected. But the Cu/In ratios from EDAX were not exactly same as the ratios taken in the solution. However it was difficult to control sulfur concentration.

Sample Name	Cu/In ratio in solution	Cu%	In%	S%	Cl%
CIS 0.5-5	0.5	14.8	30.25	47.8	7.15
CIS 1.0-5	1	22.37	24.26	46.58	6.78
CIS 1.5-5	1.5	28.3	22.85	48.8	0.05

Table.3.1.Atomic concentration from EDAX of samples prepared with different Cu/In ratio keeping S/Cu=5 in solution.

Percentage of Cu increased from 14.8 to 28.3 in the sample, as Cu/In ratio was changed from 0.5 to 1.5 in the solution. In these films, S concentration remained more or less constant. In CIS 1.5-5, the composition varied largely from point to point due to the formation of agglomerated Cu rich areas, as seen in SEM micrograph (Figure.3.2). EDAX taken specifically from the agglomerated area showed copper concentration as 36.01% and Cu/In ratio in this region as 2.01.

For CIS 1.0-2, the film obtained was deficient in sulfur (37.49 %). Also, this sample was Cu rich (35.98%), though we had kept the Cu/In ratio in the solution to

be 1. Sulfur concentration increased to 46.54 % for the sample CIS 1.0-5. But no further significant increase was observed even after increasing the S/Cu ratio in the solution to 10. Chlorine was present in all the samples.

Sample Name	S/Cu ratio in solution	Cu%	In%	S%	Cl%
CIS 1.0-2	2	35.98	16.47	37.49	10.06
CIS 1.0-5	5	22.37	24.26	46.58	6.78
CIS 1.0-10	10	25.66	23.21	46.45	4.68

Table.3.2.Atomic concentration from EDAX of samples prepared with different S/Cu ratio keeping Cu/In=1 in solution.

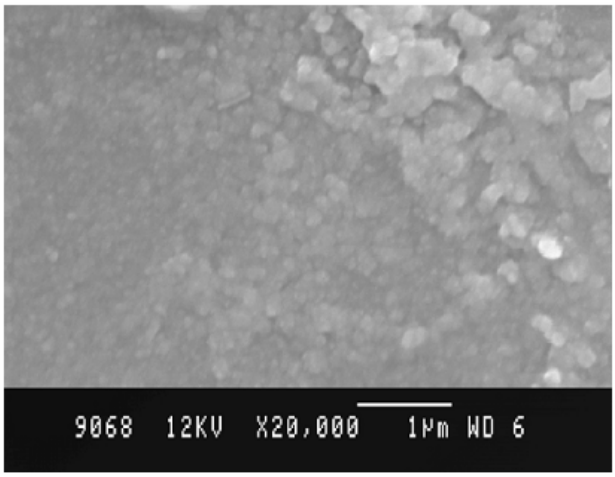

Figure.3.2.Scanning Elecron Micrograph of Cu rich $CuInS_2$ (CIS 1.5-5).

3.4.2.Atomic Force Microscopy (AFM)

AFM is a form of Scanning Probe Microscopy (SPM) where, a small probe is scanned across the sample to obtain information about the sample's surface. The information gathered from the probe's interaction with the surface can be as simple as physical topography or as diverse as measurements of the material's physical,

magnetic or chemical properties. These data are collected as the probe is scanned in a raster pattern across the sample to form a map of the measured property relative to the X-Y position.

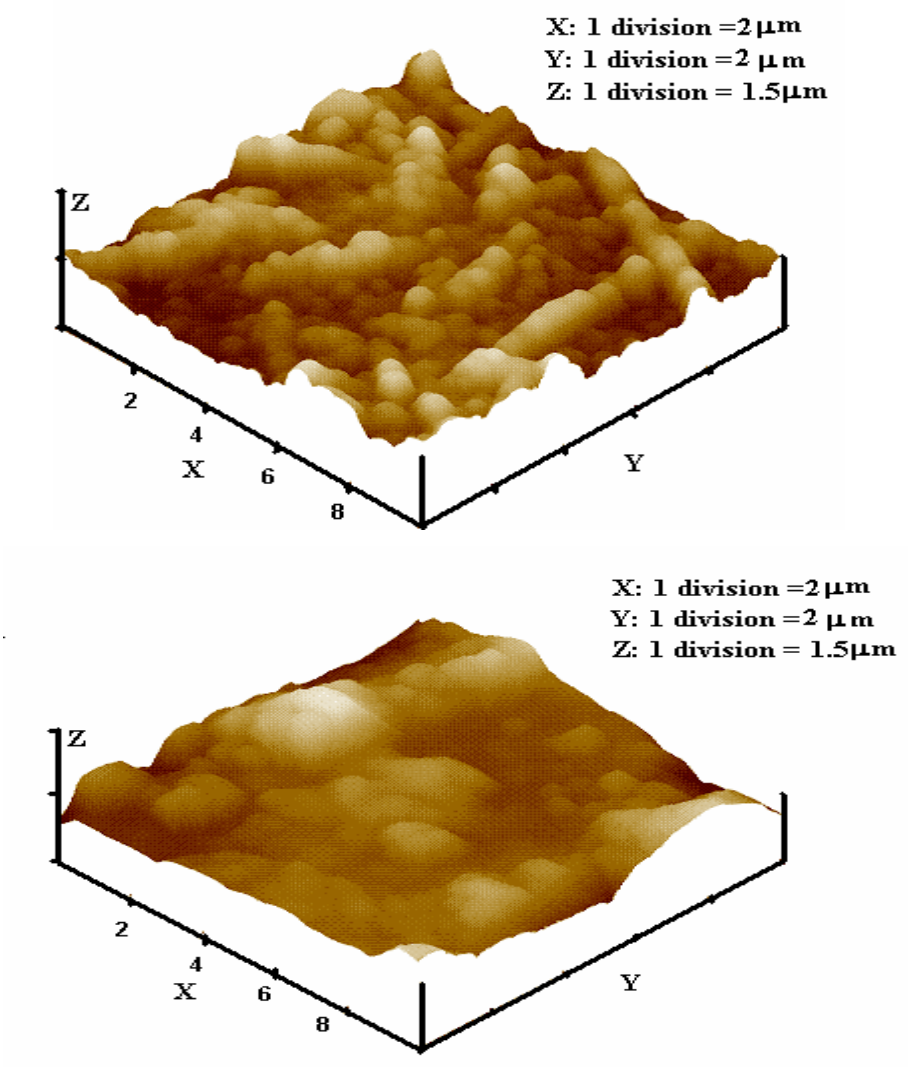

Figure.3.3.AFM images of Cu rich (top) and In rich (bottom) $CuInS_2$.

The AFM probe has a very sharp tip, often less than 100 Å diameter, at the end of a small cantilever beam. The probe is attached to a piezoelectric scanner tube, which scans the probe across a selected area of the sample surface. Inter-atomic forces between the probe tip and the sample surface cause the cantilever to deflect as the sample's surface topography (or other properties) changes. A laser light reflected from the back of the cantilever measures the deflection of the cantilever. This information is fed back to a computer, which generates a map of the topography and/or other properties of interest. Areas as large as 100 μm square to less than 100 nm square can be imaged.

AFM studies revealed significant variations in the surface morphology of the samples (Figure.3.3). Films formed from Cu rich solutions showed formation of sharp edged crystallites as observed from increase in surface roughness, while indium rich samples promoted formation of smoother film surface. Krunks et al. have observed similar results on spray pyrolysed $CuInS_2$ thin films [13].

3.4.3.Structural analysis

X-ray diffraction (XRD) technique, which is a precise and nondestructive tool, is used for structural analysis. XRD gives whole range of information about crystal structure, orientation, crystalline size, phase content and stresses in films. Experimentally obtained diffraction pattern is compared with the Joint Council Powder diffraction (JCPDS) data to obtain information about different crystallographic phases, their relative abundance and preffered orientations. From the width of the diffraction peak, average grainsize can also be calculated. Interplanar spacing d was calculated from the X-ray diffraction profiles using the formula,

$$2d \sin\theta = n\lambda \qquad (3.1)$$

where θ is the Bragg angle, n is the order of the spectrum and λ is the wavelength of X-rays. Using the d values the set of lattice planes (h k l) were identified from the standard data and the lattice parameters are calculated using the following relations.

For the tetragonal systems,

$$\frac{1}{d^2} = \frac{(h^2 + k^2)}{a^2} + \frac{l^2}{c^2} \qquad (3.2)$$

where a and c are lattice parameters. The grain size (D) can be evaluated using Scherrer's formula,

$$D = \frac{k\lambda}{\beta \cos\theta} \qquad (3.3)$$

where k is a constant which is nearly equal to one and β is the full width at half maximum (FWHM), usually measured in radians.

In the present work, x-ray diffraction studies were done using Rigaku (D. Max. C) X-ray diffractometer employing CuK_α line (λ=1.5405 Å) and Ni filter operated at 30 kV and 20 mA. XRD pattern of the films, deposited with different Cu/In and S/Cu ratios, are depicted in Figure.3.4 and Figure.3.5. The d values coincided with those of $CuInS_2$ (JCPDS data card 270159) with preferential orientation along (112) plane. Lattice constants were calculated to be a=5.53Å and c=11.00 Å, which also matched well with the standard values a=5.52 Å and c=11.12 Å. No characteristic peaks corresponding to the chalcopyrite phase were observed.

Intensity of the peak corresponding to (112) plane increased with increase in Cu concentration, as shown in Figure.3.4. Grain size was calculated to be 25 nm for Cu rich films and decreased to 9 nm for indium rich films, which was evident from the broadening of maximum intensity peak. XRD peak corresponding to (109) plane of In_2S_3 was observed in indium rich films (JCPDS data card 25-390).

In sample CIS 1.0-2, there was an unintentional increase of Cu concentration (observed from EDAX), which might be the reason for the increase in intensity of (112) peak. It had been observed that Cu-rich spray solutions promoted recrystallization and crystal growth in the film. Improvement of crystallinity of Cu rich films may be attributed to Cu mobility [19]. Samples CIS 1.0-5 and CIS 1.0-10 had broad peaks, indicating poor crystalline nature of these samples. Also, In_2S_3 was present as secondary phase in these two samples.

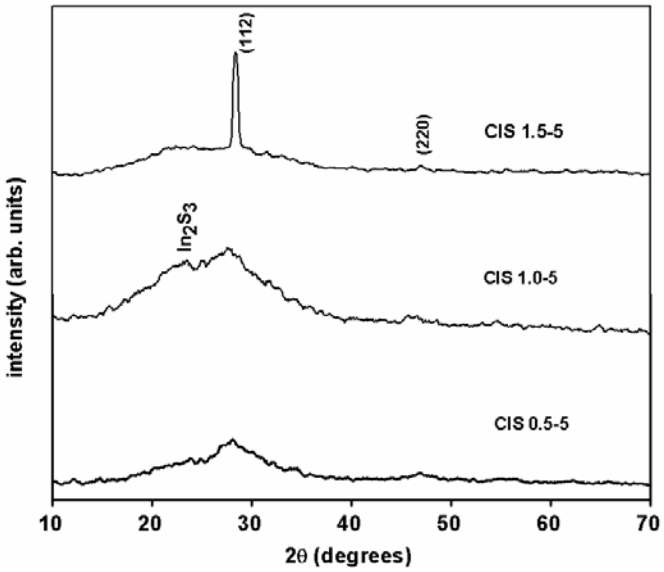

Figure.3.4.XRD pattern of samples prepared with different Cu/In ratio keeping S/Cu=5.

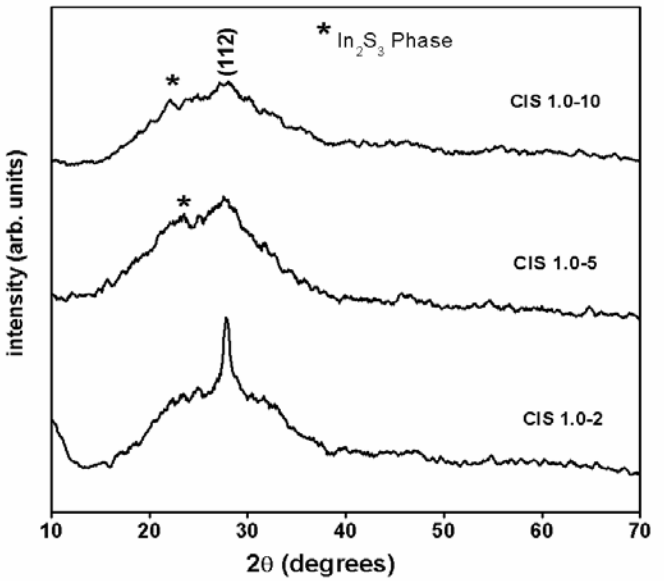

Figure.3.5.XRD pattern of samples prepared with different S/Cu ratio keeping Cu/In=1.

3.4.4.Optical properties

The most direct and the simplest method for probing the band structure of semiconductors is by studying the absorption spectrum. Absorption is expressed in terms of a coefficient *α(hν)* which is defined as the relative rate of decrease in light energy *L(hν)* along its propagation path [26]:

$$\alpha = \frac{1}{L(h\nu)} \frac{d[L(h\nu)]}{dx} \tag{3.4}$$

The absorption coefficient (*α)* is related to the energy gap E_g according to the equation,

$$\alpha h\nu = A(h\nu - E_g)^n \tag{3.5}$$

where *A* is a constant, *h* the Planck's constant, *ν* the frequency of the incident beam and *n* is equal to ½ for a direct gap and 2 for an indirect gap.

Optical band gap of $CuInS_2$ thin films were deduced from plot of $(\alpha h\nu)^2$ vs hν by extrapolating the straight line from high absorption region (Figures.3.6 and 3.7).

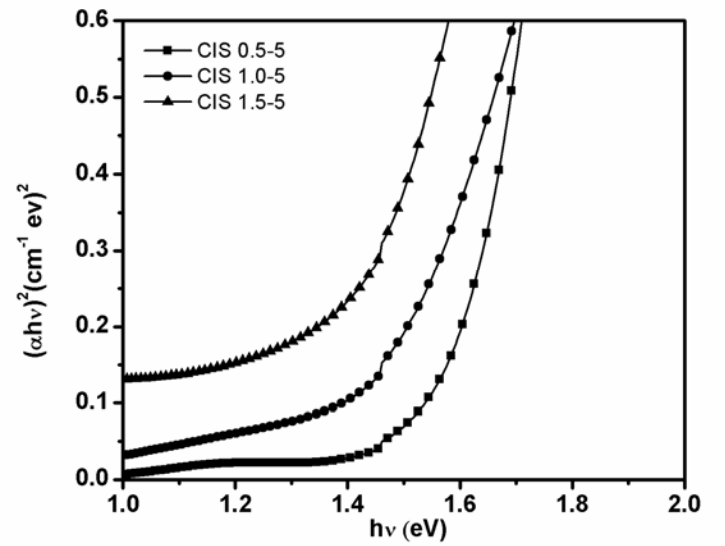

Figure.3.6.$(\alpha h\nu)^2$ vs. hν graph of films prepared with different Cu/In ratio, keeping S/Cu=5 in solution.

It was observed that the band gap decreased with increase of Cu/In ratio. It was found to be 1.55 eV for the sample CIS 0.5-5, 1.44 eV for CIS 1.0-5, and decreased further to 1.35 eV, in the case of CIS 1.5-5. Carrier degeneracy in $CuInS_2$ due to defects in the lattice was reported as a possible cause for this decrease in band gap [19].

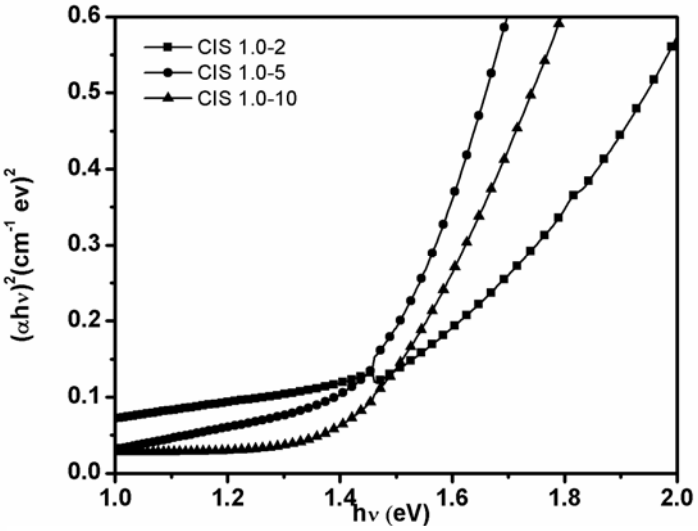

Figure.3.7.$(\alpha h\nu)^2$ vs. hν graph of samples prepared with different S/Cu ratio, keeping Cu/In=1 in solution.

In the case of CIS 1.0-2, the band gap was found to be 1.34 eV. When S/Cu ratio increased to 5, this increased to 1.44 eV. Interestingly, no change in band gap was observed when the sulfur concentration was further increased to 10. This might be due to the fact that, there was no significant difference between the composition of films with the increase in S/Cu ratio from 5 to 10, as seen from EDAX results.

3.4.5.Electrical studies

Type of conductivity in the films was checked using 'hot probe method'. CIS 0.5-5 was found to be n-type and CIS 1.0-5 and CIS 1.5-5 were p-type. It was observed that, as Cu/In ratio increased from 0.5 to 1.5, the photosensitivity decreased and resistivity decreased drastically by 5 orders (from 8000 ohm-cm to 0.023 ohm-cm). This might be due to the fact that decrease of indium (which formed donor states) was causing increase of carrier concentration in p-type samples.

Sulfur deficient films (CIS 1.0-2) showed a fluctuating nature between n and p-type i.e., the thermo emf changed between positive and negative. Sulfur deficient $CuInS_2$ usually tend to be n-type and variation of sulfur concentration over the sample area may be the cause of fluctuating nature. Resistivity was high for CIS 1.0-5 and CIS 1.0-10, compared to the one having S/Cu ratio 2. Interestingly, photosensitivity of the sample with S/Cu=5 was larger compared to the other two samples.

Dark conductivity of the films was measured as a function of temperature (100 K-450 K). Using this study, activation energies of intrinsic defect levels in sprayed $CuInS_2$ were obtained. This study opened up possibility of defect control in this type of samples, through intrinsic doping.

At low temperature range, conductivity increased slowly with increase in temperature, whereas in high temperature region it increased rapidly. From $\ln(\sigma)$ vs 1000/T graph, activation energies were calculated (Figure 3.8 and Figure 3.9). Two deep levels at 436 meV and 294 meV were obtained for CIS 0.5-5. Deep defects at 500 meV and 300 meV were reported for $CuInS_2$ in earlier works too, where films were prepared by a sequential process in which copper and indium were deposited by sputtering followed by annealing in S atmosphere [27]. Conductivity of the films increased when Cu/In ratio was increased from 0.5 to 1. Activation energies of 131 meV and 76 meV were obtained in this sample (CIS 1.0-5). These shallower levels were assigned to Cu_{In} and V_{Cu} respectively, which were acceptor defects. These defects were the most probable ones as the samples were p-type and EDAX measurements also revealed a slight deficiency of copper. Since Cu and In had comparable sizes, this type of antisite defect formation was possible. Reported values of activation energies of Cu_{In} (150 meV) and V_{Cu} (80 meV) were also in agreement with our results [26]. When Cu concentration was further increased (CIS 1.5-5), only very shallow levels (~10 meV) were obtained.

In CIS 1.0-5 and CIS 1.0-10, the defect levels obtained were Cu_{In} and V_{Cu}. When S concentration was decreased (CIS 1.0-2), in addition to the acceptor level due to V_{Cu}, a level at 50 meV was obtained. This level was assigned to be V_s (35-55

meV) which is a donor [28]. The EDAX results as well as type fluctuation in this sample also supported this analysis.

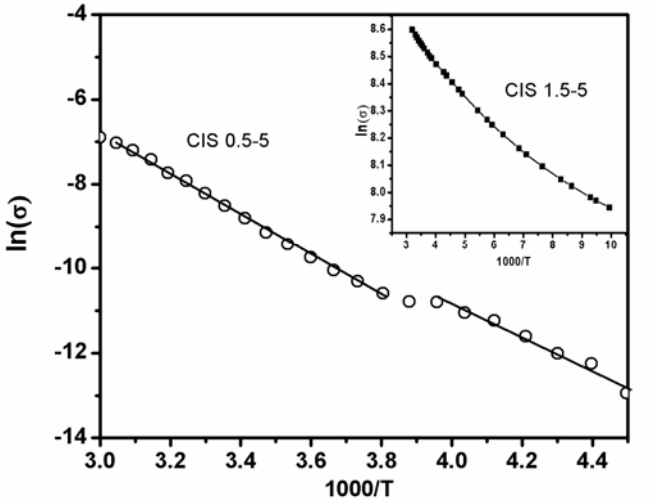

Figure.3.8.ln(σ) vs. 1000/T plot of In rich and Cu rich (inset) samples.

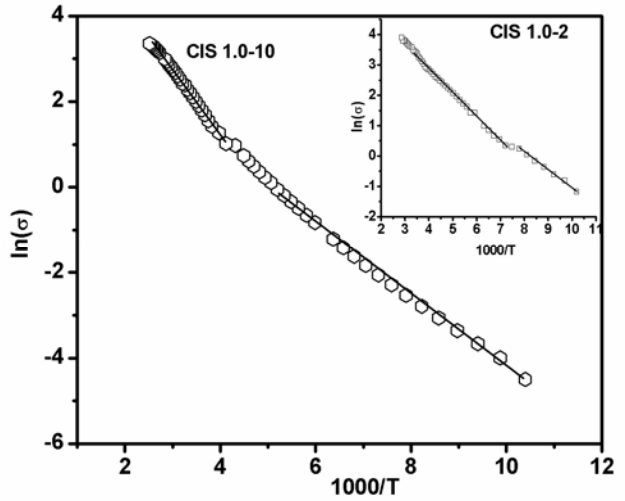

Figure.3.9.ln (σ) vs. 1000/T plot of S rich and S poor (inset) samples.

From the present study, it was observed that though S-rich starting solution was required for obtaining stoichiometric films, increasing S beyond a limit did not result in its incorporation in the film and hence had no effect on the properties.

Moreover, Cu rich films were good in terms of crystallinity and low resistivity, but these films had low photosensitivity and nonuniform composition over the surface. High resistivity and low crystallinity put limits on the use of In-rich films as absorber layer, inspite of their good photosensitivity. The sample with Cu/In=1 and S/Cu=5 (CIS 1.0-5), which showed intermediate value of photosensitivity, crystallinity and resistivity, may be better suited for device applications, if made free of secondary phases.

3.5.Effect of variation of thickness

In thin film solar cells, thickness of the absorber is a critical factor. Hence, it is essential to know how much thickness can be achieved in a single deposition process. In CSP, thickness of films is usually controlled by adjusting volume of solution sprayed. In case of some materials, thick films of the order of several microns can be deposited in a single spray just by increasing the volume sprayed. But in case of others, there is a critical thickness after which the films tend to peel off from the substrate. In case of $CuInS_2$ it is seen that the latter behavior prevails.

$CuInS_2$ thin films were deposited on glass substrates at a substrate temperature of 573K and a spray rate of 1 ml/min. $CuCl_2$, $InCl_3$ and Thiourea were used as precursors. The Cu/In ratio in solution was kept at 1.5 and S/Cu ratio at 5. Volume of spray solution was varied as 20ml, 30ml, 40 ml and 60 ml. In all the cases, the films were given a post deposition annealing by keeping them at the deposition condition for half an hour after spray. It was seen that continous films were obtained in the first three cases, but when 60 ml was sprayed, films peeled off from the substrate. But when same volume was deposited in two steps (multiple spray), thicker films could be obtained. The samples were named as C20, C30, C40 and C60 respectively.

3.5.1.Thickness measurements

Thickness of the films were measured using stylus depth profiler (Dektak 6M). This instrument can profile surface topography and measure the surface roughness. The instrument takes measurements electromechanically by moving the sample stage beneath a diamond tipped stylus. The stylus is mechanically coupled to

the core of an LVDT (Linear Variable Differential Transformer). As the stage moves, the stylus rides over the sample surface and surface variations cause stylus to be translated vertically. Electrical signals corresponding to stylus movements are produced as the core position of LVDT changes. The LVDT scales an ac reference signal propotional to the position change, which in turn is conditioned and converted to a digital format. Using the stylus profiler, thicknesses of samples C20, C30, C40 and C60 were measured and the values obtained were 0.13 μm, 0.17 μm, 0.25 μm and 0.33 μm respectively. Another interesting observation was that only lesser amount of spray volume was required in the automated spray system than in the manual system to achieve the same thickness. For example, in the above mentioned preparation conditions, 40 ml precursor solution was required to deposit 0.25 μm thick film whereas, in manual spray unit ~200 ml solution was required in order to achieve the same thickness. This was due to the lesser impact area of the spray cone, precisely controlled spray rate and scanning mechanism of the spray head in the automated system. Thus the material wastage was reduced to a large extend in the automated system.

3.5.2.Structural Analysis

From Figure.3.10, it was seen that the d values coincided with that of $CuInS_2$ (JCPDS data card 270159) with preferential orientation along (112) plane. X- ray diffraction studies of these films showed that crystallinity of the films increased with thickness. XRD data of the sample C40 in comparison with the standard data is given in Table.3.3.

2θ (degrees)	d (Å) (standard)	d (Å) (observed)	hkl	I/I_0 (standard)	I/I_0 (observed)
28.00	3.198	3.183	112	100	100
46.53	1.952	1.950	220	10	8.6

Table.3.3.XRD data of $CuInS_2$ thin films.

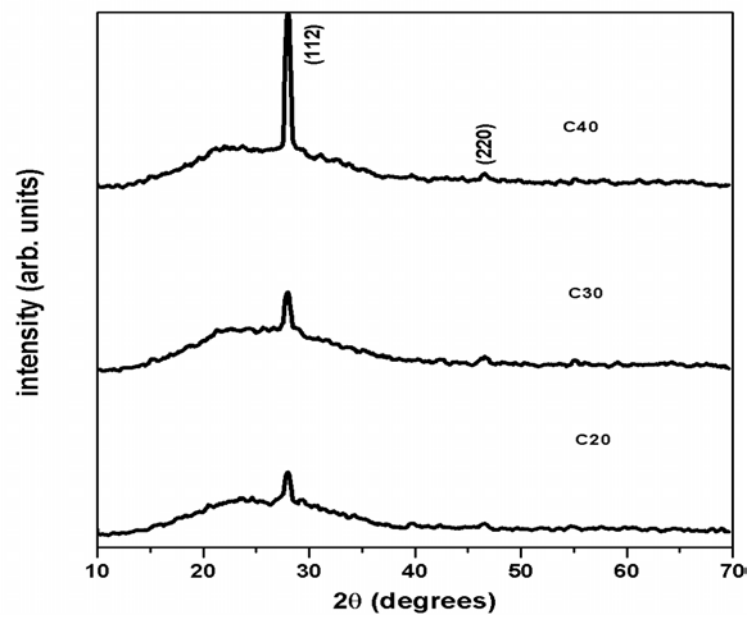

Figure.3.10. X-ray diffractograms of C20, C30 and C40.

3.5.3.Photothermal deflection technique

Transport properties of semiconductors play a crucial role in deciding the efficiency of the material when fabricated into a device. The knowledge of transport properties like minority carrier lifetime (τ_r), surface recombination velocity (V_{sr}) and thermal diffusivity (D_{th}) are necessary for optimizing the entire device fabrication process. Photothermal beam deflection technique offers a relatively simple non-contact and non-destructive approach for measurement of V_{sr}, τ_r and D_{th}. This technique deals with indirect detection of heat generated by the sample, due to non-radiative de-excitation processes, following the absorption of light. When the thin films are excited using the intensity-modulated beam, there arises a deflection of probe beam path, which is detected using a bicell PSD (photosensitive detector). A graph is plotted indicating the variation of the generated deflection signal amplitude with respect to the modulation frequency. A plot of $\log_e$ (signal amplitude) versus

(chopping frequency) $^{1/2}$ shows the dependence of the signal on frequency. The nature of dependence of signal amplitude on the chopping frequency depends on changes in the composition and surface morphology of the film. Thus we can analyse the graphs and study the origin of non-radiative process in the film. The detailed explanation regarding the theory and modeling used have been reported elsewhere [29].

Table.3.4 gives the values of thermal diffusivity, minority carrier lifetime and surface recombination velocity of the samples obtained through this technique. High thermal diffusivity, high minority carrier lifetime and low surface recombination velocity (V_{sr}) are recommended for a good absorber. High thermal diffusivity carries the information that the propagation of thermal waves happens with less scattering. The scattering of thermal waves occurs mostly due to the presence of impurities or defects in the film.

Sample Name	Thermal diffusivity (x 10^{-3} cm^2/s)	Lifetime (n s)	Surface recombination velocity (x 10^5 cm/s)
C20	0.73	0.7	50
C30	4.8	4.0	5
C40	1.9	1.0	5
C60	1.7	0.3	10

Table.3.4.Transport properties from PTD study**.**

From the present study, it is seen that spray volume is an important factor in controlling the surface properties of films. Low spray volume is insufficient for film formation and higher spray volume can result in increased porosity due to increased thickness. Though multiple spray is useful in depositing thicker films, the transport

properties of such films are not appealing compared to the thicker films deposited in single spray.

3.6.Effect of variation of spray rate

$CuInS_2$ thin films were deposited on glass substrates at 573 K. The Cu/In ratio in solution was kept at 1.5 and S/Cu ratio at 5. Fixed volume (40 ml) of $CuInS_2$ solution was sprayed at spray rates of 1ml/min, 2 ml/min and 4 ml/min. Films were not formed at still larger spray rates. These samples were named CIS1, CIS2, and CIS4 respectively and were characterized using x-ray diffraction (XRD), optical absorption and resistivity studies to find the most optimum spray rate.

3.6.1.Structural analysis

It was observed that spray rate played a decisive role in controlling the uniformity and adhesion of the films. Low spray rates favoured formation of uniform films devoid of pinholes or cracks. In the present work, all the three samples had thickness of ~0.25 μm, but the roughness increased with increase in spray rate from 28 nm for CIS1 to 40 nm for CIS4.

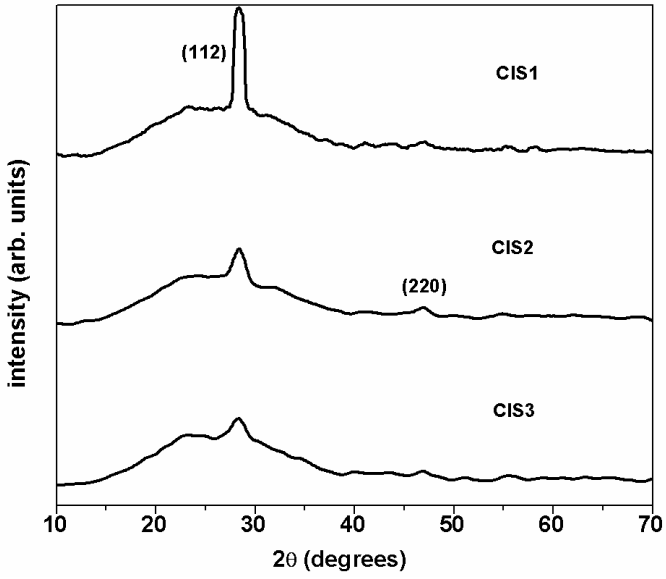

Figure.3.11.X-ray diffractograms of samples sprayed at different spray rates.

XRD pattern of films deposited at different flow rates are given in Figure 3.11. The d values coincided with that of $CuInS_2$ (JCPDS data card 270159) with preferential orientation along (112) plane. The grain size was calculated using Debye-Scherrer formula. Increase in spray rate resulted in formation of smaller crystallites as observed from the broadening of XRD peak. The calculated value of grain size decreased from 25.3 nm for CIS1 to 8.4 nm for CIS4.

3.6.2.Optical studies

From the plot of $(\alpha h\nu)^2$ vs $h\nu$, it was found that band gap increased from 1.3 eV to 1.4 eV as flow rate varies from 1 ml/min to 4 ml/min (Figure.3.12). Also, resistivity of the samples also increased which can be explained in terms of smaller grain size and higher band gap. For further studies the spray rate was fixed at 1ml/min as lower spray rate favoured formation of films with superior surface morphology, opto-electronic and structural properties.

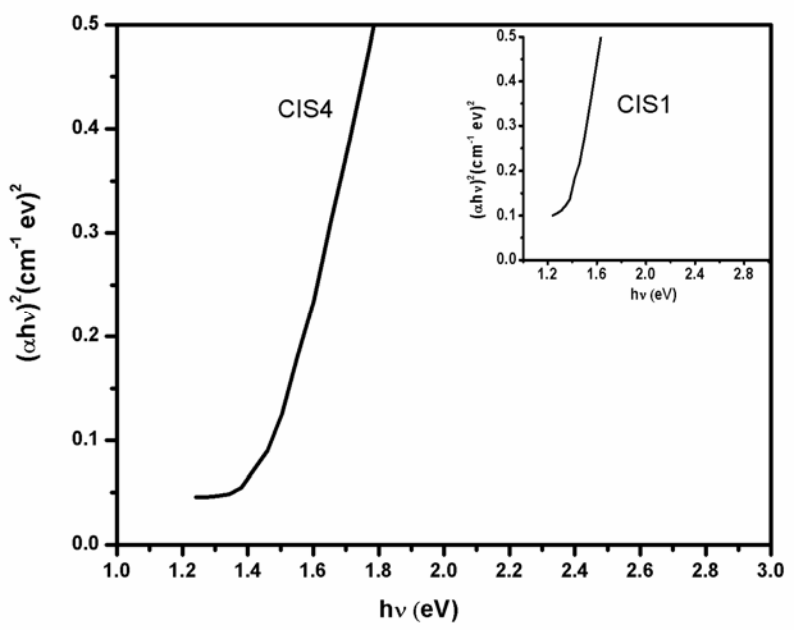

Figure.3.12.$(\alpha h\nu)^2$ vs. $h\nu$ graph of samples prepared at different spray rates.

Increasing the spray rate beyond 4ml/min resulted in powdery discontinuous deposits. One reason for this was the slow XY motion of the spray head which caused insufficient evaporation of the solvent. This obstacle was surmounted by increasing the XY speed to twice that was used previously. Thus films could be deposited with spray rates up to 8ml/min at 573 K.

3.7.Effect of substrate temperature

$CuInS_2$ thin films with Cu/In ratio 1 and S/Cu ratio 5 were prepared at substrate temperatures 523 K, 573 K, 623 K and 673 K, keeping all other parameters constant. The spray rate was 1ml/min and volume of spray solution used for each spray was 40 ml. The distance between spray head and substrate was maintained at 20 cm.

3.7.1 SEM and EDAX measurements

From SEM micrographs, it is seen that the sample prepared at 523K had cracks on the surface. Higher substrate temperatures yielded continuous films devoid of pinholes or cracks as evident from Figure.3.13. Hence in the present work, properties of samples prepared at 573 K, 623 K, 673 K (C300, C350, C400 respectively) were systematically studied.

EDAX was used to know the composition of films, whose results are given in Table.3.5. C300 is found to be indium rich and this may be the reason for the high resistivity of this sample. It is a well known fact that indium rich $CuInS_2$ is resistive due to the presence of donors, which compensates the p-type conductivity [17].

It was observed that films formed at higher temperatures were copper rich and also showed deficiency of sulfur. This might be due to the re-evaporation of anionic species at high temperature, leading to metal rich deposits. Chlorine was present in all the samples and its concentration decreased at higher substrate temperatures. Presence of chlorine is due to the use of chloride based precursors for deposition.

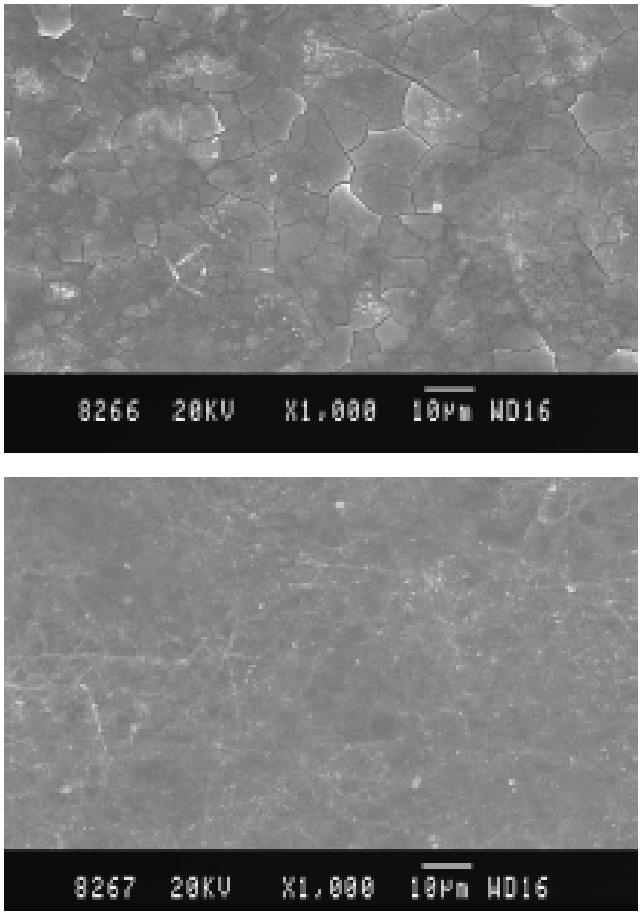

Figure.3.13.Scanning electron micrographs of C250 (top) and C400 (bottom).

Sample Name	Cu%	In%	S%	Cl%
C300	22.37	24.26	46.58	6.78
C350	26.91	21.62	44.52	6.95
C400	29.93	22.19	44.87	3.01

Table.3.5.EDAX results of samples prepared at different substrate temperatures.

3.7.2.Structural Analysis

X-ray diffractograms of $CuInS_2$ thin films deposited at different temperatures are depicted in Figure.3.14. The intensity of (112) peak corresponding to $CuInS_2$ (JCPDS Data card 270159) increased with substrate temperature. Lattice constants were calculated to be a=5.53 Å and c=11.00 Å which matched well with the standard values a=5.52 Å and c=11.12 Å. No peaks corresponding to secondary phases were observed in the diffractogram. In general, the peaks obtained were broad which is expected in near stoichiometric $CuInS_2$ films prepared by spray method [7]. Increase in substrate temperature leads to increase in size of crystallites as observed from the sharpening of the XRD peak. Grain size of a film is primarily determined by initial nucleation density and also recrystallization. Recrystallization into larger grains is enhanced at higher substrate temperature.

Thickness of the films grown at different substrate temperatures was measured using stylus depth profiler. Thickness decreased with increase in temperature. Values of thickness and surface roughness are given in Table.3.6. In spray pyrolysed films, it was generally observed that higher substrate temperatures yield thinner and continuous films [30]. Surface mobility of the adsorbed species increased with increase in substrate temperature, which resulted in smoother surface of the films by filling in the concavities.

Sample Name	Thickness (nm)	Roughness (nm)	Resistivity (Ω-cm)
C300	460	190	32.05
C350	350	100	0.5
C400	270	90	1139

Table 3.6.Thickness, roughness and resistivity values of samples prepared at different substrate temperatures.

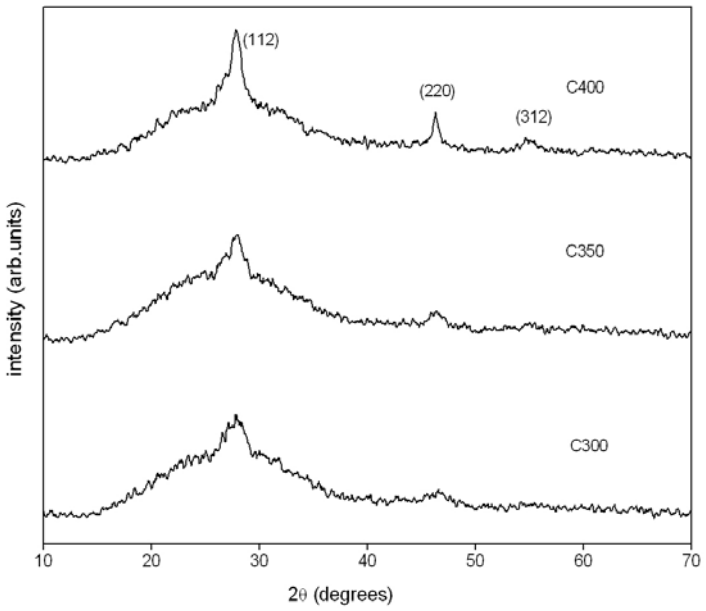

Figure.3.14.X-ray diffractograms of samples prepared at different substrate temperatures.

3.7.3.X-Ray Photoelectron Spectroscopy (XPS)

XPS is one of the major techniques for studying thin films. It provides information on the elemental composition of a sample as well as on the chemical state of the constituent atoms. In this technique, the sample is irradiated using electromagnetic radiation of energy hν. Due to the photoelectric effect, electrons are emitted with kinetic energy,

$$E_{kin} = h\nu - E_B - \phi \qquad (3.6)$$

where, E_B is the binding energy (BE) of a particular electron shell and Φ is the sample work function. Photoelectrons are energy-analysed in the spectrometer and, since the photon energy is known, one can determine characteristic binding energies of valence electrons coming from different elements present in the sample.

The chemical composition of the films was evaluated using XPS technique. XPS spectra of the samples were recorded using an ULVAC-PHI unit (model: ESCA 5600 CIM) employing argon ion sputtering (Voltage = 3 kV, Raster size = 3 x 3 mm^2, pressure 10^{-8} mbar). Al K_α X-ray (1486.6 eV) with a beam diameter of 0.8 mm and power of 400 W was used as the incident beam.

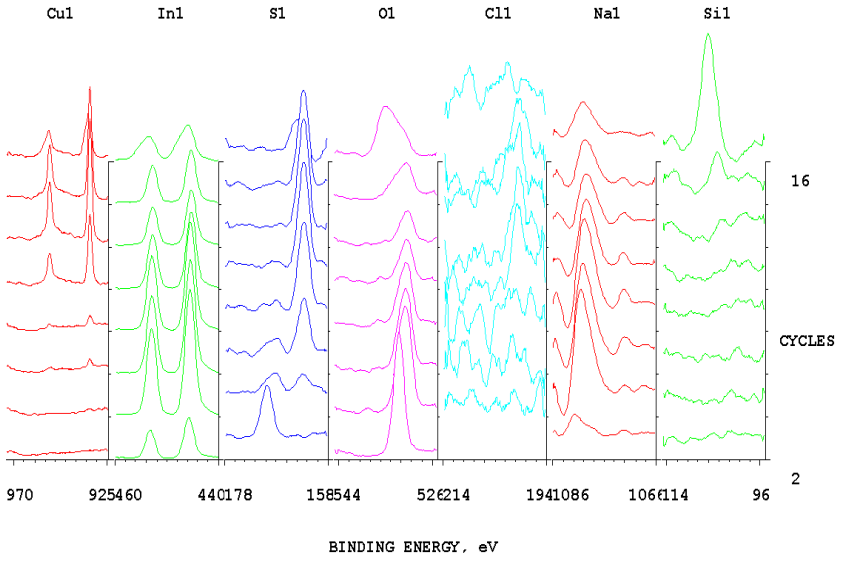

Figure.3.15.XPS depth profile of C350.

XPS depth profile of the sample C350 is given in Figure.3.15. Binding energies of $Cu2p_{3/2}$, $Cu2p_{1/2}$, $In3d_{5/2}$, $In3d_{3/2}$ and S2p are 933 eV, 952.5 eV, 445 eV, 453 eV and 162 eV respectively, corresponding to that of copper, indium and sulfur in $CuInS_2$ [9]. Sodium has diffused from the glass substrate into the sample and there is also the presence of oxygen (531 eV) throughout the depth. Binding energies of oxygen (532 eV) and sulfur (169 eV) at the surface corresponds to formation of sulfate as surface contaminant. Also, it may be noted that, in the XPS depth profile, concentration of copper on the surface of the film is significantly lesser than that in the bulk. This is a useful result because, in a photovoltaic device, it is favourable to

have a Cu-rich phase, which is more conductive, near the electrode and a Cu-poor phase, which is more photosensitive near the junction. Our result indicates that we could achieve this condition in our films without any deliberate variation in concentration of spray solution. Usually copper rich phases migrate towards the surface and segregates forming Cu_xS phases, which has to be removed by toxic KCN etching [13].

3.7.4.Electrical and optical studies

The type of conductivity of the samples was obtained using hot probe method. In hot probe or thermoelectric probe method, the conductivity type is determined by the sign of thermal emf generated by the temperature gradient between two probes kept in contact with the sample surface of which one is hot and the other cold. In a voltmeter (positive terminal connected to the hot probe and negative terminal to the cold probe) which is kept in contact with an n-type material, a positive voltage is detected. For a p-type material, the voltage detected is negative [26]. Here, it is seen that all the three samples exhibit p-type nature. The sample C350 is less resistive than the other samples by a few orders of magnitude (Table.3.6) as seen from resistivity studies. This behavior could not be explained in terms of crystallinity or band gap. A reason for this nature might be the copper rich nature of the films formed at higher temperatures, which enhances the grain growth [13]. But curiously, this enhancement in conductivity is absent for films C400 that had the highest copper concentration from EDAX.

Band gap was deduced from plot of $(\alpha h\nu)^2$ vs $h\nu$ by extrapolating the straight line from high absorption region (Figure.3.16). All the samples had a band gap of about 1.4 eV which did not vary with change in substrate temperature. A close look at the absorption spectrum of these samples showed a transition in the lower energy region (Figure.3.17) in addition to the direct transition at 1.4 eV. This sub band gap absorption was centered at 1.01 eV for C300 and 1.10 eV for C400. This low energy transition was absent for sample prepared at 623 K.

The anomalous decrease of resistivity and the absence of low energy transition in the absorption spectrum of C350 directly points to a defect related

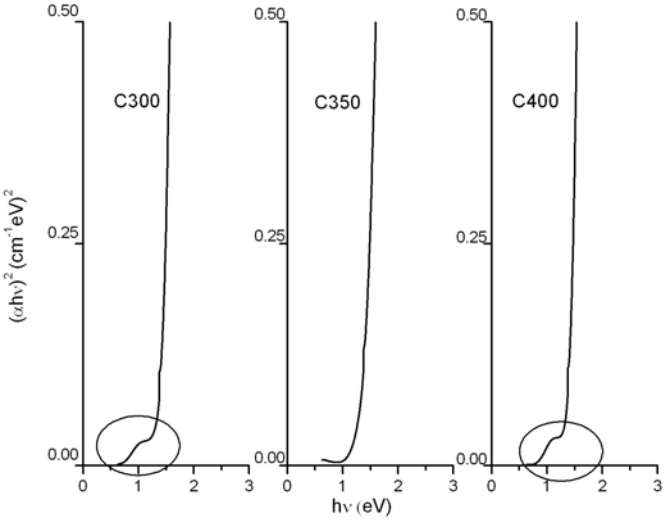

Figure.3.16.plot of $(\alpha h\nu)^2$ vs hν of C300, C350 and C400.

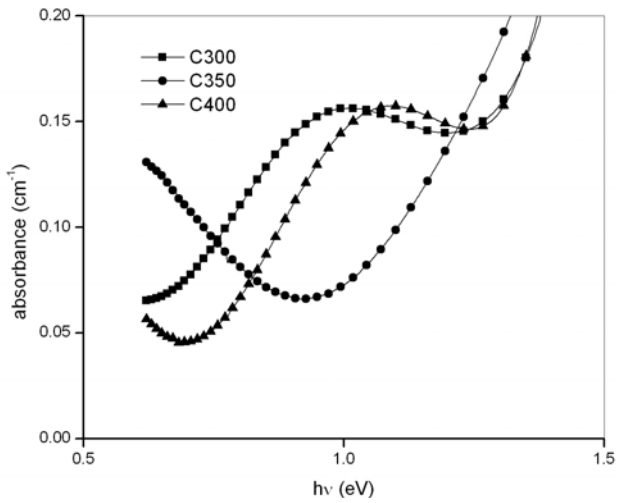

Figure.3.17.Sub band gap absorption in samples C300 and C400.

mechanism influencing the opto-electronic properties of these samples. It is well known that the doping in ternary chalcopyrites like $CuInS_2$ and $CuInSe_2$ is controlled by intrinsic defects. The high stoichiometric variations in these materials are usually accommodated in a secondary phase or electronically inactive defects. Incorporation of sodium (which diffuses from the substrate), oxygen (that occupies sulfur sites/ grain boundaries) or chlorine in the films can also affect the properties. Hence, a comprehensive defect analysis of these samples was conducted using TSC and PL.

3.7.5.Thermally Stimulated Current (TSC) studies

TSC (also called thermally stimulated conductivity) is used extensively as a defect characterization technique. This technique helps the identification and determination of the traps or defects and trap parameters of a material. A TSC spectrum consists of a number of peaks in current versus temperature graph called glow curve. Measured curve is then analysed to obtain the location of peak on the temperature scale, its width etc. These data are then utilized to compute the trapping parameters by applying appropriate theoretical models.

TSC spectra of the three samples were taken in the temperature range 100K to 450K (Figure.3.18). Activation energy of the defect levels were obtained using the formula

$$E = \frac{2k\ T_m^{\ 2}}{(T_2 - T_1)} \qquad (3.7)$$

where, T_m is the temperature at the peak maximum and T_2-T_1 is the width at half maximum of the peak. Presence of peaks and shoulders in the material indicated that the samples had continuous distribution of defects rather than a single defect level.

The glow curve of sample C300 and C400 had no peaks or shoulders up to room temperature, whereas C350 has a shoulder at 250 K whose activation energy was obtained as 68 meV using the relation (3.7). The absence of shallow defect levels contributing to the conductivity of the samples may be the reason for the high resistivity in C300 and C400. Deeper levels at 139 meV and 459 meV were obtained in C350.The level at 139 meV can be due to the antisite defect formation Cu_{In}, which

increased the p-type conductivity in the sample. This defect was probable as Cu and In has comparable sizes and EDAX measurements in the samples revealed a slight deficiency of Indium. Reported values of actvation energy of Cu_{In} (150 meV) are also in agreement with this result [31]. Shoulders obtained in the glow curve of C300 and C400 were curve fitted to obtain levels at 326 meV and 395 meV. The difference between activation energies of these levels and the band gap of the samples gives 1.07 eV and 1.00eV, which are close to sub band gap absorption energies obtained from absorption spectrum of these samples.

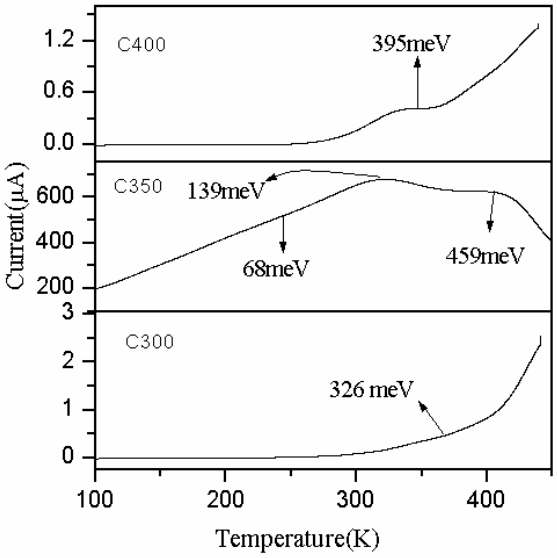

Figure.3.18.TSC glow curves of C300, C350 and C400.

3.7.6.Photoluminescence (PL) studies

PL spectroscopy is a non-contact, non-destructive method of probing the electronic structure of materials. Light is directed onto the sample, where it is absorbed and imparts excess energy into the material in a process called photo-excitation. This excess energy can be dissipated by the sample through the emission of light or luminescence. If the material was photo-excited, this luminescence is called PL. The intensity and spectral content of PL is a direct measure of various

material properties. In the present work, PL is used to determine defect levels in the samples.

For photoluminescence (PL) measurement, the sample was mounted on the cold finger of a liquid helium cryostat (Janis Research Inc) and cooled to 11K. The temperature was controlled to an accuracy of ±1K using a lakeshore temperature controller (321 Auto tuning). A He-Ne laser (632.8 nm, 5 mW) was used as the excitation source. The beam was focused onto the sample so as to get a spot of radius 0.5 mm. A 632.8 nm filter was placed in front of the window, from where the emission signal was collected. An optical fiber was placed behind the filter at 90^0 to the incident beam, outside the cryostat. The emission signal, collected by the fiber, was focused into the NIR 512 monochromator having slit width of 50 μm. The monochromator was attached to the 512-element InGaAs array detector, with a resolution of 1.5 nm/pixel.

From the PL spectrum of the samples taken at 12 K (Figure.3.19), it was clear that in C350, band edge emission (1.552 eV) dominated and persisted even at room temperature. The peak at 1.552 eV has a shoulder at 1.536 eV, which is quenched above 77K. The difference in their peak energies was 16 meV, which agreed well with the exciton binding energy in $CuInS_2$ [32]. But in C300, emission from defect state (1.46 eV) is prominent, which is a donor-acceptor transition between V_S and V_{Cu}. In C400, no band edge emissions were observed, which proved the absence of shallow donor bound excitons. However, broad emissions (1.527 eV and 1.482 eV) as well as above band gap emission (1.634 eV) which showed negative temperature quenching were observed in Figure.3.20. This indicated presence of large number of competitive radiative defects [27] and secondary phase impurities in this sample

The persistence of PL even at room temperature in C350 clearly indicated the better crystalline quality and absence of nonradiative losses in this sample (Figure.3.21). This accounted for the better properties of this sample. Also there was passivation of the donor acceptor transition in C300. This could either be due to the

difference in composition of C350, which is no longer Cu poor or due to formation of Na_{Cu} and O_S complex that annihilates level due to $V_{Cu\text{-}S}$ divacancy.

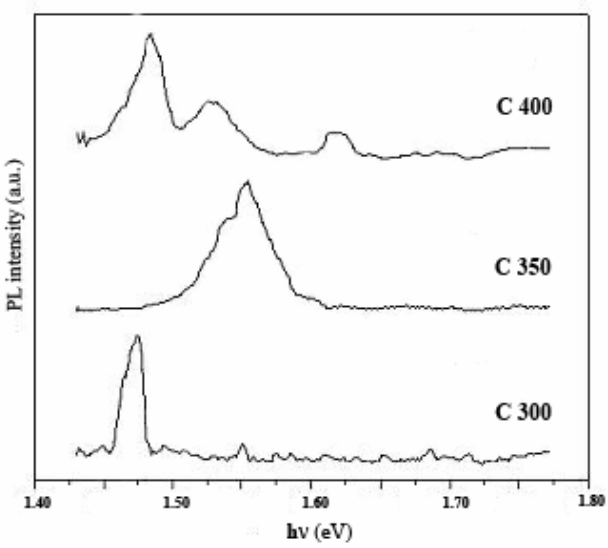

Figure.3.19.PL spectrum of C 300, C350 and C400.

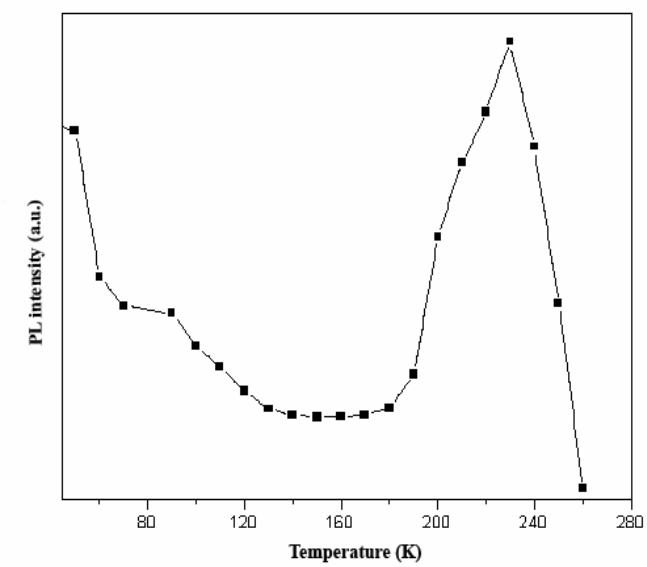

Figure.3.20.Negative temperature quenching of PL.

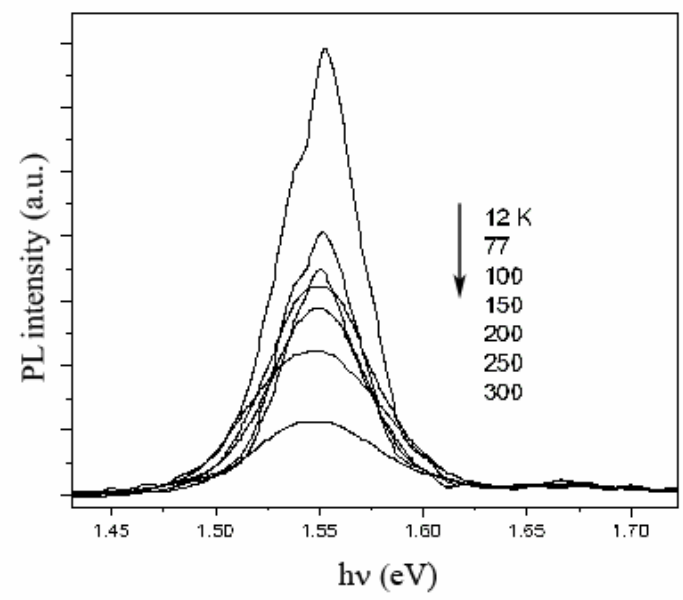

Figure 3.21.PL emission of sample C350 at different temperatures.

In the present work, we have tried to characterize $CuInS_2$ films prepared at different substrate temperatures to find the optimum preparation condition for the absorber. We could observe that the opto-electronic properties of sample C350 were better suited for device applications than the other samples.

3.8.Effect of post deposition treatments

In order to achieve good absorbers for solar cells, post deposition treatments are required. Inspite of deposition of $CuInS_2$ through cost-effective single phase process, there remain some questions whether there can be further improvement of the film crystalline quality by a post deposition annealing. In addition, how do they influence the optical as well as electrical properties of the films? Following these questions, we performed various post deposition treatments on the as-grown films like annealing in vacuum, air and H_2S environment.

3.8.1.Effect of air and vacuum annealing

Post growth treatments like annealing in air and vacuum were performed on $CuInS_2$ films. Samples with Cu/In ratio as 1 and S/Cu ratio as 5 prepared at substrate temperature 573 K and spray rate 8 ml/min were used for the study. The samples were annealed in air and vacuum for 30 minutes. The effects on structural, optical and electrical properties were studied. In general it was observed that post deposition treatments improve the opto-electronic properties. However, crystallinity of the films improved only slightly. Also the absorption edge sharpened indicating annihilation of defects which was more pronounced in vacuum annealing. It was also observed that air annealing resulted in lowering of resistivity whereas vacuum annealing increased the resistivity. Figure.3.22 and 3.23 shows the x-ray diffractograms and absorption spectra of the pristine, air annealed and vacuum annealed samples.

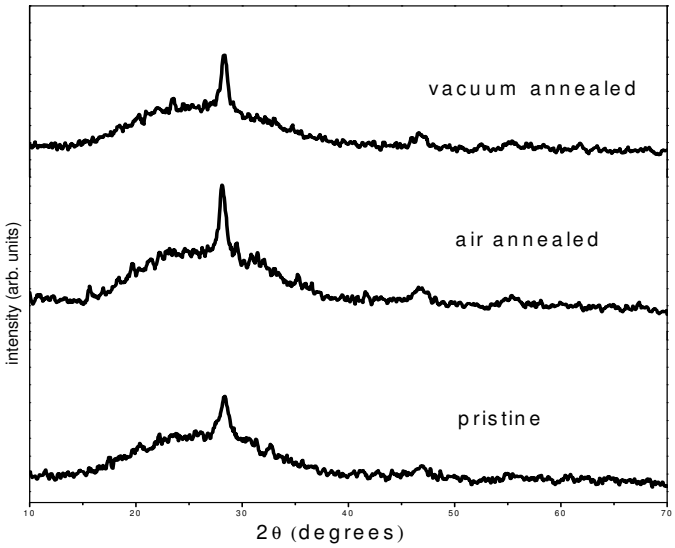

Figure.3.22.X-ray diffractograms of as prepared, air annealed and vacuum annealed samples.

As evident from the study, no radical change in opto-electronic properties were achieved due to air or vacuum annealing.

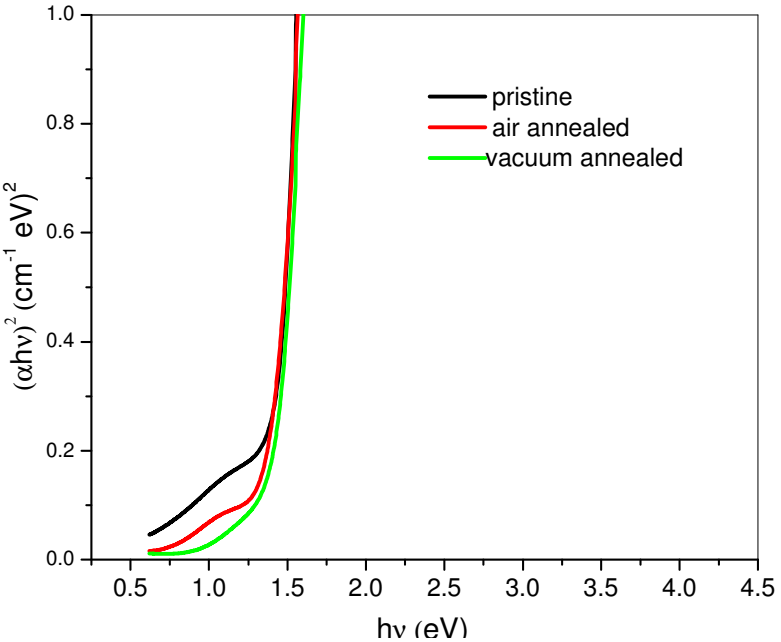

Figure.3.23.Absorption spectra of as prepared, air annealed and vacuum annealed samples.

3.8.2.Effect of annealing in H_2S atmosphere

$CuInS_2$ samples prepared at 573 K and spray rate of 8 ml/min with Cu/In ratio as 1 and S/Cu ratio as 5 were annealed in H_2S atmosphere at 673 K for one hour.The pristine and H_2S treated samples were named cis and cis-s respectively.

Thickness of the $CuInS_2$ films was measured using stylus profiler and found to be ~0.3 microns. XRD pattern of samples cis and cis-s is given in Figure.3.24. The d values coincided with that of $CuInS_2$ (JCPDS data card 270159) with preferential orientation along (112) plane. It was clearly seen that crystallinity increased on sulfurization. The grain size increased from 12.6 nm to 39.4 nm on sulfurization.

Optical band gap of $CuInS_2$ thin films were deduced from plot of $(\alpha h\nu)^2$ vs $h\nu$ by extrapolating the straight line from high absorption region (Figure.3.25). It was observed that the band gap of sulfurized samples were higher than that of pristine sample. The band gap increased from 1.38 eV to 1.41 eV. Observed widening of

optical band gap could be explained by the improved crystallinity and higher purity of annealed films [33].

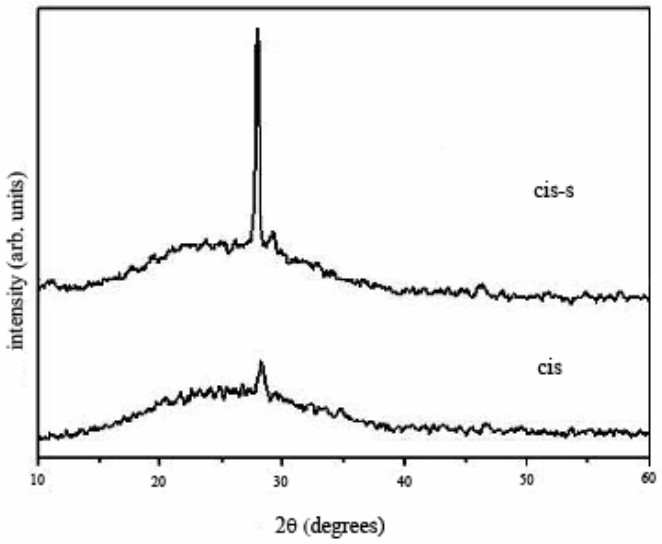

Figure.3.24.X-ray diffractograms of as prepared and H_2S annealed samples.

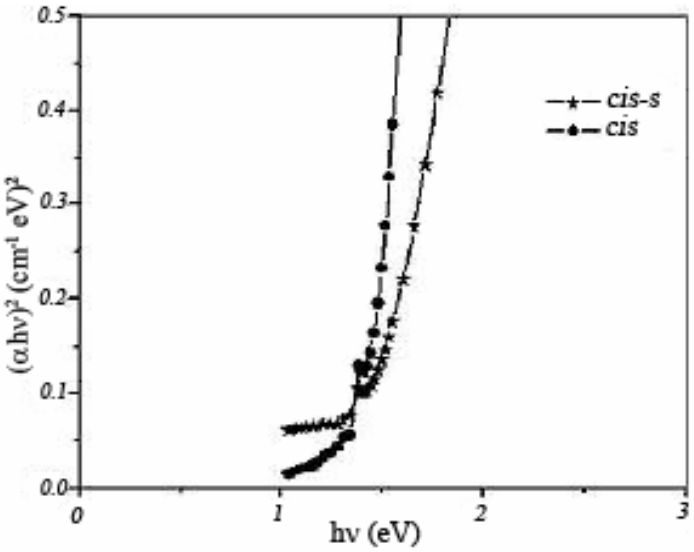

Figure.3.25.Absorption spectra of as prepared and H_2S annealed samples.

EDAX spectrum of the samples cis and cis-s are given below (Figure.3.26A and 3.26B) which clearly shows peaks indicating the presence of copper, indium, sulfur and traces of chlorine in the samples. Since the substrate used in the present work is soda lime glass, peaks due to silicon and oxygen also appears in the spectrum. Cu, In, S and Cl are present in the samples in the percentage as seen in Table.3.7. It is seen that percentage of sulfur in cis-s exceeds 50%. Usually, sprayed samples are sulfur deficient which forces to have precursors with excess sulfur while spraying. Incorporation of sulfur into films does not improve beyond a limit even if we heavily increase the sulfur concentration in solution. Here it is seen that H_2S treatment has catalyzed the incorporation of sulfur in the films.

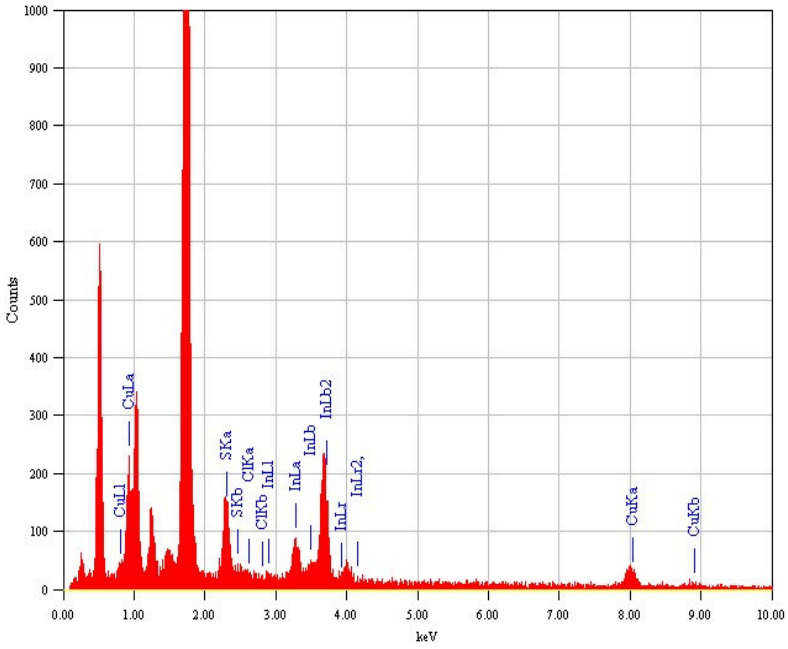

Figure.3.26A.EDAX spectrum of pristine samples.

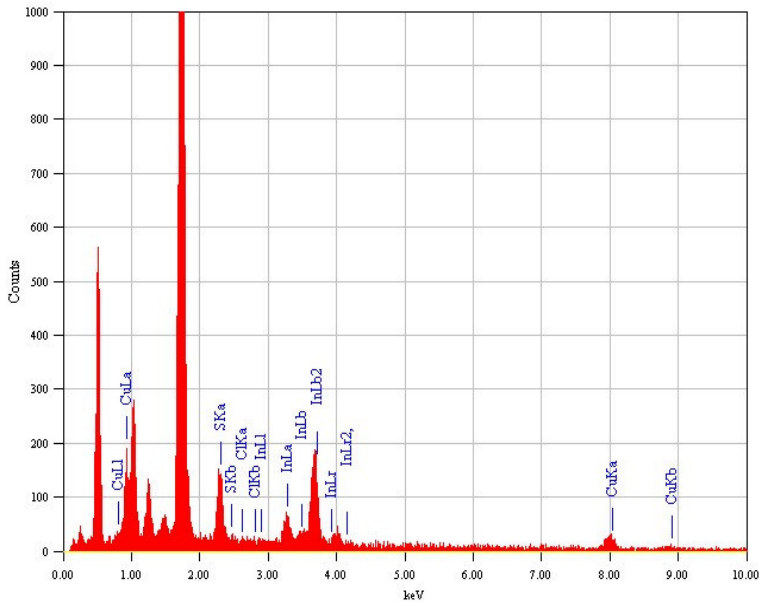

Figure.3.26B.EDAX spectrum of sulfurized samples.

Sample Name	Cu%	In%	S%	Cl%
CIS	28.54	23.91	46.08	1.47
CIS-S	24.92	19.81	53.06	2.21

Table.3.7.Atomic concentration from EDAX of pristine and sulfurized samples.

Depth wise analysis of the samples was done using x-ray photoelectron spectroscopy (Figure.3.27) which revealed that formation of $CuInS_2$ throughout the depth of the film is observed in case of sulfurized samples. But the as-prepared samples had surface devoid of sulfur and copper. Thus annealing in H_2S atmosphere has made the films more uniform.

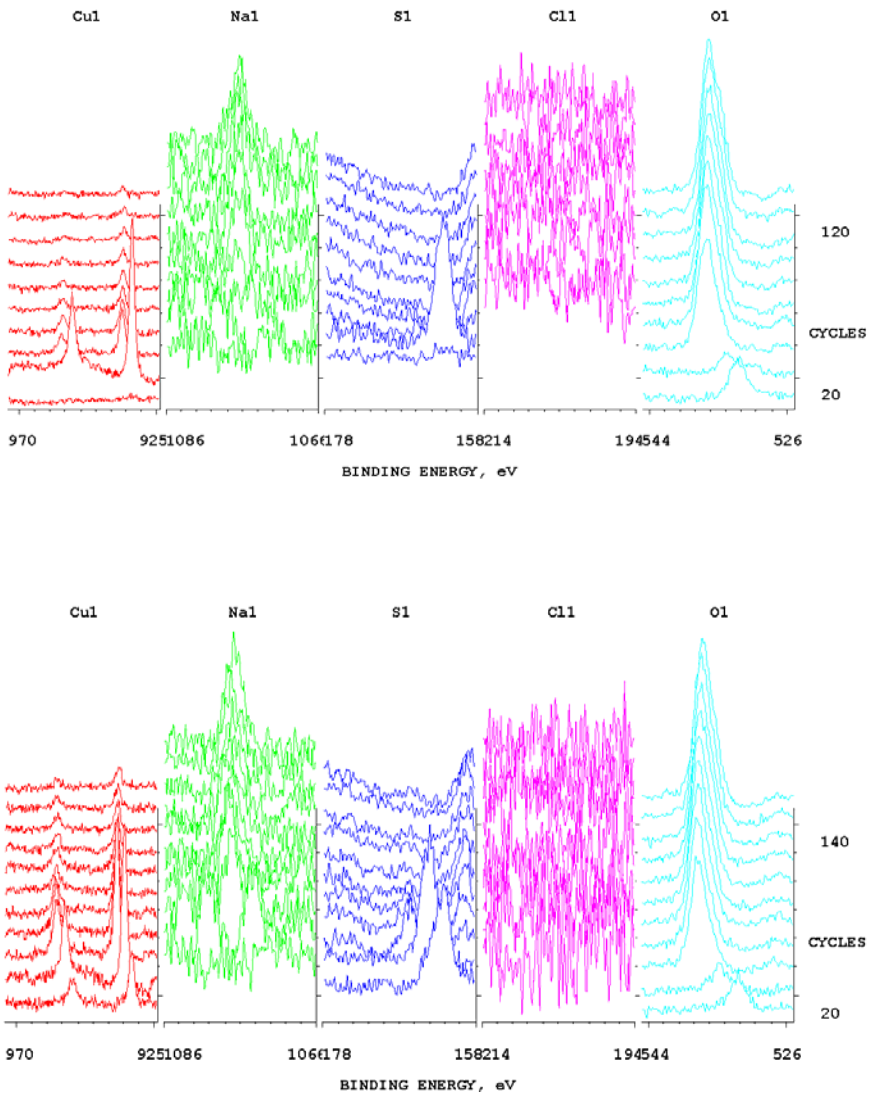

Figure.3.27.XPS depth profile of as prepared (top) and sulfurized (bottom) samples.

Transport properties of the films were studied using PTD method and Table. 3.8 depict the values of thermal diffusivity, minority carrier lifetime, surface recombination velocity and mobility.

Sample Name	Thermal diffusivity (x 10^{-3} cm^2/s)	Lifetime (n s)	Surface recombination velocity (x 10^5 cm/s)	Mobility (cm^2/Vs)
cis	$0.8x10^{-7}$	$0.9x10^{-6}$	$1x10^5$	1.2
cis-s	$1.6x10^{-7}$	$2x10^{-6}$	$0.7x10^5$	0.37

Table.3.8.Transport properties from PTD studies.

Although stoichiometric $CuInS_2$ films can be deposited by CSP method, post deposition treatments significantly improve the composition as well as the structural, and optical properties. Also, the shift towards optimum band gap for energy conversion will be beneficial in device applications. XPS depth profiling clearly indicates improvement of uniformity in the samples. But decrease in mobility and high resistivity of sulfurized samples poses serious doubts regarding their use in devices.

3.9.Conclusions

From the present work, effect of different preparation conditions and post deposition treatments on the properties of sprayed $CuInS_2$ films was investigated. From the study of effect of precursor ratio variation, it was seen that the near stoichiometric sample with Cu/In = 1 and S/Cu = 5 (CIS 1.0-5) which showed intermediate value of photosensitivity, crystallinity and resistivity, was better suited for device applications. From thickness variation studies it was seen that very thick $CuInS_2$ films could not be prepared by continuous spray. Multiple spray resulted in thicker films, but their transport properties showed detrimental nature. Also, in comparison with the manual spray unit, the automated unit required lesser amounts of precursor solution for achieving a particular thickness. Low spray rates resulted in

films with better crystallinity and good opto-electonic properties.The study of the effect of substrate temperature on the properties of film, showed that films formed at 623K had good opto-elctronic properties, where as films formed at 573 K showed better transport properties from photothermal studies.

Post deposition annealing treatments were carried out in air, vacuum and H_2S atmosphere. Pronounced change was observed in case of annealing in H_2S atmosphere. There was significant improvement in the composition as well as the structural and optical properties on H_2S treatment. A shift in band gap towards the optimum value for energy conversion was observed. XPS depth profiling indicated improvement of uniformity in the samples. Except for the increase in resistivity and decrease in mobility, all other properties generally improved on sulfurization.

Present study gives a comprehensive idea on the properties of $CuInS_2$ prepared using automated spray unit. We observe that the properties of films can be tailored effectively with the automated system, due to the better control of spray parameters. Such a study is a pre-requisite for using this material and the equipment effectively in preparing solar cells.

References

[1] Shay J.L. and Wernick J.H., Ternary Chalcopyrite Semiconductors: Growth, Electronic Properties and Applications, Pergamon press, New York (1975).

[2] Vequizo Reynaldo Magdaro, Kobayashi Satoshi, Tsuboi Nozomu, Oishi Koichiro, Kaneko Futao. Jpn. J. Appl. Phys. 46 (2007) 716.

[3]Siemer Kai, Klaer Jo, Luck Ilka, Bruns Jürgen, Klenk Reiner, Braunig Dieter, Sol. Energy Mater. Sol. Cells. 67 (2001) 159.

[4] A.N.Y. Samaan, S.M. Wasim, A.E. Hill, D.G. Akmour, R.D. Tomlinson, Physica Status Solidi (A). 96 (2006) 317.

[5] Teny Theresa John, Tina Sebastian, C. Sudha Kartha, K.P. Vijayakumar, T. Abe, Y. Kashiwaba, Physica B: Condensed Matter. 388 (2007) 1.

[6] Yoshio Onuma, Kenji Takeuchi, Sumihiro Ichikawa, Yasunari Suzuki, Ryo Fukasawa, Daisuke Matono, Kenji Nakamura, Masao Nakazawa, Koji Takei, Sol Energy. 80 (2006) 132.

[7] Krunks M., O. Kijatkina, A. Mere, Varema T., I. Oja, V. Mikli., Sol. Energy Mater. Sol. Cells. 87 (2005) 207.

[8] Tina Sebastian, R. Jayakrishnan, C. Sudha Kartha, K.P. Vijayakumar, The Open Surface Science Journal 1 (2009) 1.

[9] Teny Theresa John, Wilson K. C., Ratheesh Kumar P. M., Sudha Kartha C., Vijayakumar K. P., Kashiwaba Y., Abe T., Yasuhiro Y., Phys. Stat. Sol. (A). 202(1) (2005) 79.

[10] Teny Theresa John, Ph.D Thesis, Cochin University of Science and Technology, India (2004).

[11] Harris J.D. et al., 17th Space Photovoltaic Research and Technology Conference, Ohio (2001).

[12] Malle Krunks et al., Proceedings of International Conference on Solar Cells, Kochi, India (2008).

[13] Krunks M., Valdek Mikli, Olga Bijakina, Enn Mellikov, Applied Surface Science. 142 (1999) 356.

[14] Gorska M., Beaulieu R., Loferski J.J., Roessler B., Solar Energy Materials. 1(1979) 313.

[15] O. Kijatkina, Krunks M., A. Mere, B. Mahrov, L. Dlozik, Thin Solid films. 431-432 (2003) 105.

[16] Jin Michael H. et al., Proceedings of the 3rd World Conference on Photovoltaic Energy Conversion, Osaka, Japan (2003).

[17] A.N. Tiwari, D.K. Pandya, K.L. Chopra, Thin Solid Films. 130 (1985) 217.

[18] H. Bihri, M. Abd Lefdil, Thin Solid Films. 354 (1999) 5.

[19] M. Ortega-Lopez, Arturo Morales-Acevedo, Thin Solid Films, 330 (1998) 96.

[20] M. Krunks, O. Kijatkina, H. Rebane, I. Oja, V. Mikli, A. Mere, Thin Solid Films 403-404 (2002) 71.

[21] M.C. Zouaghi, T. Ben Nasrallah, S. Marsillac, J.C. Bernede, S. Belgacem, Thin Solid Films. 382 (2001) 39.

[22] Krunks M., O Bijakina, V. Mikli, H. Rebane, T. Varema, M. Altosaar, E. Mellikov, Sol. Energy Mater. Sol. Cells. 69 (2001) 93.

[23] M. Krunks, A. Mere, A. Katerski, V. Mikli, J. Krustok, Thin Solid Films. 511-512 (2006) 434.

[24] R.P. Vijayalakshmi, R. Venugopal, D. Raja Reddy, B.K. Reddy, Solid State Communications. 82 (1992) 997.

[25] N. Kamoun, N. Jebbari, S. Belgacem, R. Bennaceur, J. Bonnet, F. Touhari, L. Lassabatere, J. Appl. Phys. 91 (2002) 1952.

[26] Dieter K. Schroder, Semiconductor Material and Device Characterization, John Wiley and Sons Inc, Newyork (1998).

[27] N.S. Yusek, N.M. Gasanly, A. Aydinli, H. Ozkan, M. Acikgoz, Cryst. Res. Technol. 39 (2004) 800.

[28] Joechim Kneisel, Kai Siemer, Ilka Luck, Dieter Bräunig. J. Appl. Phys. 88 (2000) 9-5474.

[29] Anita R Warrier et al., XVII International Materials Research Congress – IMRC 2008, Cancun, México (2008).

[30] Chopra K.L., Das S.R., Thin Film Solar Cells, Plenum Press, New York and London (1983).

[31] Lewerenz H.J., Sol. Energy Mater. Sol. Cells. 83 (2004) 395.

[32] H.Y. Ueng, H.L. Hwang, J. Appl. Phys. 62(2) (1987) 434.

[33] I. Oja, M. Nanu, A. Katerski, M. Krunks, A. Mere, J. Raudoja, A. Goosens, Thin Solid Films. 480-481 (2005) 82.

CHAPTER 4

Deposition and Characterization of In_2S_3 Buffer Layer

4.1.Introduction

The substitution of cadmium sulfide (CdS) buffer layer by alternative materials is among the challenges faced by the researchers working on $Cu(In,Ga)(S,Se)_2$ thin film based solar cells since the end of 1990s. Due to environmental hazards connected with production and disposal of CdS layers, much attention has been focused on the development of other buffer layers. One such possible substitute for CdS is Indium sulfide (In_2S_3). This material has a variety of applications in the preparation of green and red phosphors and in the manufacture of picture tubes for colour televisions and dry cells [1].

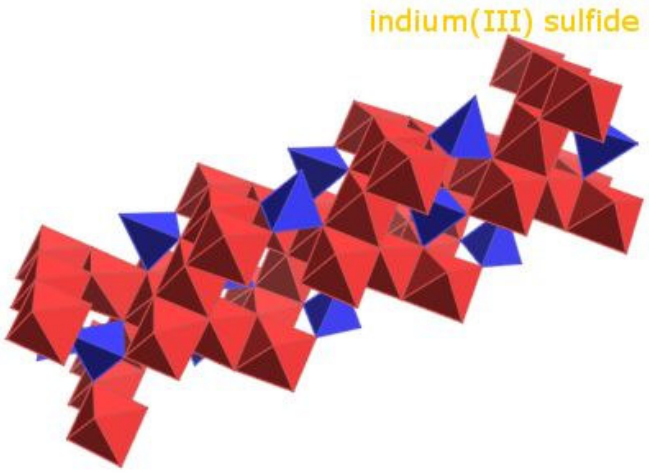

Figure.4.1.Crystal structure of In_2S_3 (indium atoms in red and sulfur in blue).

In_2S_3 exhibits different polymorphic structures such as α, β and γ depending on the processing parameters. β-In_2S_3 phase is found to be the stable crystalline phase of indium sulfide at room temperature with tetragonal structure (Figure.4.1). β-In_2S_3 is an n-type semiconductor with a direct band gap of 1.98 eV [2]. In this phase, it crystallizes in defect spinel structure with a high degree of disorder. Due to its high defect structure, β-In_2S_3 finds many applications in different fields [3].

In_2S_3 is a III–VI compound originating from the II–VI semiconductor by replacing group II metals by group III elements and exists in three crystallographic modifications α, β and γ with β-In_2S_3 being the stable state with a tetragonal structure at room temperature. In defect spinel structure, it has high degree of vacancies, ordering at tetrahedral cation sites [4]. It can be interpreted as a quasi-ternary compound, consisting of In, S and vacancies. Here 8 of the 12 tetrahedral sites are occupied by indium and the other 4 are empty (the latter are ordered). All octahedral sites are occupied by In and could be written as $In_6(In_2\square S)_{12}$, where, $\square$ indicates vacancies and the parentheses describe tetrahedral site [5]. However, a small fraction of indium atoms may leave their ordered positions and occupy crystallographically ordered vacancies. This results in a number of quasi-interstitial cations and an equal number of cation vacancies, so that in a stoichiometric crystal of β-In_2S_3, a considerable degree of disorder is always present [6].

The optical band gap of β-In_2S_3 single crystals is reported to be direct with a value of 2.0 eV at room temperature [7]. The electrical properties of this β phase have been accurately studied by Rehwald and Harbeke [6]. They have observed it to be an n-type material. However, the conductivity strongly depends on the sulfur concentration. Lack of sulfur compared to the In_2S_3 stoichiometry increases the electron density, i.e. increases the n-type character.

4.2.Indium sulfide thin films

Thin films of this material have been successfully synthesized using numerous techniques like thermal evaporation [8], RF sputtering [9], atomic layer deposition (ALD) [10], metal organic chemical vapour deposition (MOCVD) [11], Chemical spray pyrolysis (CSP) [12], spray ions layer gas reaction (ILGAR) [13],

spin coating [14] and chemical bath deposition (CBD) [15].The crystalline properties of the films depend strongly on their growth technique. It must be noted that all of the techniques leading to well crystallized films do not require substrate/process temperature higher than 150–300°C. The composition of the films also depends on the growth process. A general observation is that when the deposition technique requires the use of chemical precursors, it is very common to find residual precursor elements within the films. Typically, chlorine is frequently detected in the films grown by ALD (with $InCl_3$ precursor) [10], ILGAR [13] and spray pyrolysis [16]. In the case of CBD, Bayon and Herrero [17] as well as Hariskos et al. [18] concluded that the layers are of In(S,OH) compound, the S/OH ratio decreasing as the bath pH is increased. The techniques leading to the least contaminated films appear to be PVD processes such as evaporation and RF sputtering.

The optical properties of the indium sulfide films vary between the various studies. The band gap values reported in the literature extend from 2.0 eV up to 3.7 eV. It should be noted that values of the band gap were determined assuming a direct allowed transition. Contrary to this assumption, an indirect band gap was assumed by Sterner et al. [19] as well as Allsop et al. [13] for the ILGAR process. Such different assumptions may contribute to the large differences between reported values, i.e. from 2.10 eV to 2.85 eV. The most extended range of reported band gap values is found for the CBD grown layers. The strong impact of the bath composition and temperature on the composition and crystallinity of the film necessarily affects the optical properties. Yoshida et al. observed higher concentration of sulfur (much above the stoichiometric value) in films and suggested that this increased the band gap [20]. It is also argued that the band gap widening could be partly imputable to composition effects, they also agree that the small grain size (<10 nm) generated by the CBD process may induce quantization effects. Yasaki et al. have similar conclusions, they observed that the band gap of spin coated films widens as the grain size decreases [14]. In contrast to these results, Kaufmann et al. reported a 2.2 eV band gap although the crystallites are not larger than 2–4 nm and the films contained hydroxides [21].

Despite such optical behaviour, all the films are reported to be n-type. Nevertheless, a wide range of electrical conductivity is encountered; literature relates values from 10^{-1} to 10^{7} ohm-cm depending on the deposition process.

4.3.Spray pyrolysed In_2S_3 thin films: a brief review

As the focus of our work is on film preparation by chemical spray pyrolysis technique, here we present a brief review of works done on spray pyrolysed In_2S_3 films.

In_2S_3 was prepared by most of the groups using chloride based solutions as precursors. The chemical reaction taking place during the formation of In_2S_3 by CSP is as given below:

$$2InCl_3 + 3CS(NH_2)_2 + 6H_2O \rightarrow In_2S_3 + 3CO_2 + 6NH_4Cl \qquad (4.1)$$

An extensive study on the effect of substrate temperature and variation of In/S ratio was done by Teny et al. using $InCl_3$ and thiourea as precursors [22]. They observed that the optical band gap of the samples decreased with increase in sulfur concentration. XPS analysis of the samples revealed that films with low sulfur concentration had oxygen throughout the depth, whereas in sulfur rich films, oxygen was present only as a surface contaminant. Sulfur rich samples were also observed to be photosensitive and the sample with In/S ratio as 1.2/8 showed maximum photosensitivity.

Though chloride based precursors are widely used, preparation using new precursors like Indium nitrate have also been reported [23]. But it was observed that nitrate based precursors resulted in amorphous films compared to the crystalline films prepared using chloride based precursors. But better control over film stoichiometry was observed for films prepared from nitrate based precursor. Conductivity of the samples was greater than their chloride counterparts whereas photosensitivity was lower.

In_2S_3 films were also prepared using indium acetate and N-N-dimethyl thiourea as precursors [24]. Effect of substrate temperatures and precursor ratios were investigated. It was seen that substrate temperature affects the crystallinity as well as

opto-electronic properties of the material. Band gap increased with increase in substrate temperature and the films showed n-type conductivity.

The effect of substrate temperature on the properties of In_2S_3 was investigated by Bougila et. al [25]. Though XRD studies of the samples showed In_2S_3 as the main phase, the structure and allotropic phase of these samples were affected by substrate temperature. SEM and AFM analysis revealed that crystalline and homogeneous films were obtained at a substrate temperature of 613 K.

Effects of variation of sulfur concentration on the properties of CSP grown films were investigated by Kim et al. [26]. They obtained β-In_2S_3 films with tetragonal structure. Band gap of their samples increased with increase in sulfur concentration.

Bhira et al. deposited In_2S_3 films from chloride based precursors using nitrogen as carrier gas [4]. Well crystallized films showed β-In_2S_3 phase with preferential growth in (400) plane. Compositional analysis showed a deficit of sulfur in the films which is compensated by oxygen bonded to indium atoms and also presence of oxygen as surface contaminant. Traces of chlorine were also seen in these samples. Results of the photoconductivity studies conducted in these samples pointed towards presence of traps at grain boundaries or presence of structural defects or secondary phases. Mean absorption edge were measured from photocurrent studies using Devore's model and the band gap derived using this (2.05 eV) matched that obtained from absorption studies (2.08 eV).

Effects of post deposition treatments on CSP grown films have also been studied [27]. Annealing of films in vacuum at 300^0 C and 400^0 C were carried out. It is seen that crystallinity of the films increased whereas resistivity decreased on annealing. But the optical properties remained unaffected.

Swift heavy ion (SHI) induced modification in sprayed β-In_2S_3 were studied by Ratheesh et. al [28]. Films were irradiated with 100 MeV Au ions with different fluences. XRD studies showed that crystallinity decreased as the fluence increased and at higher fluences recrystallization occured. A red shift in the absorption edge was observed for irradiated films.

Implantation assisted Cu diffusion was performed in sprayed In_2S_3 films by Wilson et al. [29]. A comparative study of copper diffusion was performed on pristine and ion implanted samples. Formation of $CuInS_2$ was better in ion implanted samples and a junction was fabricated which showed photoactivity. Mathew et al. found that diffusion of copper to pristine In_2S_3 films resulted in conversion of top layer into p-type $CuInS_2$ [16]. XRD analysis confirmed this formation and junctions were fabricated using this technique by adjusting the thickness of Cu and In_2S_3 layers at optimized temperatures.

Modification in properties of sprayed In_2S_3 films were investigated by Mathew et al. [3]. Doping with silver resulted in enhancement of crystallinity of the films up to an optimum value. This optimum value depended on thickness of the films as well as In/S ratio. Optimum doped samples showed lower resistivity and higher photosensitivity than pure In_2S_3 films.

Tin doping doping enhanced the conductivity of the samples [30]. Effect of ex-situ as well as in-situ doping was studied. Conductivity of films enhanced by five orders on ex-situ doping but there was no impact on physical properties like crystallinity or band gap. In situ doping resulted in low resistive films with wider band gap. Higher band gap was attributed to incorporation of oxygen and low resistivity due to donor action of tin.

As chlorine is an involuntary dopant in films prepared using CSP process with chloride based precursors, its role was studied by purposefully doping it in chlorine free films [16]. Chlorine was found to increase crystallinity of the films. Cluster formation on the surface was observed for higher chlorine doping. When chlorine doping was done in metal rich In_2S_3 films, formation of micro/ nano structures were observed. Chlorine was also found to be responsible for persistent photoconductivity in In_2S_3 films. Photosensitivity and resistivity of In_2S_3 films showed direct correlation to the atomic concentration of chlorine.

Kim et al. [31] found that when cobalt atoms were introduced into In_2S_3 lattice, structural defects increased and the impurity absorption in films increased

with increase in Co concentration. Photoconductivity and photoacoustic studies in these samples resulted in identification of defects due cobalt incorporation.

Aluminium incorporation in β-In_2S_3 was studied by L. Bhira et al. using $AlCl_3$, $InCl_3$ and $CS(NH_2)_2$ as precursors and nitrogen as carrier gas [32, 33]. Incorporation of Al in small quantities improved crystallinity of the films where as doping with high concentrations resulted in amorphous films with poor electrical and photoelectrical properties. Photoconductivity studies were used to understand the conduction mechanism and photo-carrier recombination.

Incorporation of sodium in sprayed In_2S_3 was also investigated [34]. $Na(NO_3)_3$, $InCl_3$ and thiourea were used as precursors. It was observed that crystallinity as well as photosensitivity of the samples increased up to an optimum value of doping. No variation in band gap was observed.

Defect studies on spray deposited β-In_2S_3 by thermally stimulated current studies were done by R.R.Pai et. al [35] . TSC studies revealed presence of four defect levels with their prominence varying with In/S ratio. Levels due to Indium vacancy (0.1 eV), sulfur vacancy (0.8 eV) and oxygen at sulfur vacancy (0.43 eV) were identified. The level at 0.26 eV was suggested to be as due to the presence of chlorine impurity.

PL studies on sprayed β-In_2S_3 films revealed the presence of two emission bands (A and B) with peaks at 568 nm and 663 nm [36]. The A band emission was found to be due to transition from sulfur vacancy (0.43 eV) which is a donor level, to indium vacancy (0.1 eV) which is an acceptor level. The B band emission was assigned to be due to transition from indium interstitial (0.059 eV) which is a donor level to an acceptor level (formed by oxygen replacing sulfur vacancy (0.83 eV)).

Here, we have tried to bring forth the major works done on CSP grown In_2S_3. The survey of previously done works helps to comprehend the peculiarities of this material and also to appreciate the potential of future works to be done on this material.

4.4.Outline of the work done

In the present work, In_2S_3 thin films were deposited using CSP technique with the help of automated spray system. $InCl_3$ and thiourea were used as the precursors in this study. We investigated the effect of variation of four spray parameters i.e spray volume/spray time which consequently affects the thickness, precursor ratio, substrate temperature and spray rate. Also, the effect of copper incorporation into the indium sulfide matrix was investigated.

For studying the effect of spray parameters, the films were deposited by varying the parameter under study, keeping all other factors constant. Characterizations of the films were then carried out to understand how the change in particular spray parameter influenced the structural, optical, electrical and compositional properties of the films formed. Copper incorporation was studied by doping different percentages of $CuCl_2$ into the precursor and analysing the properties of films formed. The results of these studies are described in the consequent sections.

4.5.Effect of variation in thickness

Thickness of buffer layer is an important factor in determining the output parameters of junctions and hence it is important to understand how to control the thickness of the films and also how the variation in thickness affects the properties of films. From the study, it was seen that unlike $CuInS_2$, thicker films of In_2S_3 could be deposited in a single spray. Films with In/S ratio as 1.2/8 were deposited by varying the volume of spray from 40 ml to 200 ml. The substrate temperature was maintained at 573 K and spray rate was kept constant at 8 ml/min. Figure 4.2 shows the variation of film thickness with volume of spray solution. Thickness up to ~ 2.5 microns were obtained by a single spray process. Thickness as well as roughness of the films was measured using stylus thickness profiler. The values are given in table 4.1.

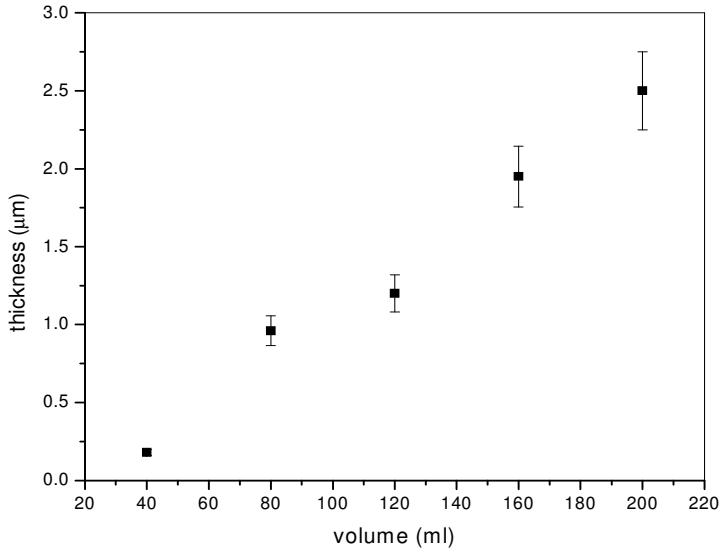

Figure.4.2.Variation in thickness of In_2S_3 films with spray volume.

Volume of spray (ml)	Thickness of films (nm)	Roughness (nm)	Resistivity (Ω-cm)
40	180.0	40.0	522
80	960.0	211.0	2592
120	1200.0	279.0	3000
160	1950.0	420.0	5070
200	2500.0	650.0	6750

Table.4.1.Variation in values of thickness, roughness and resistivity with spray volume.

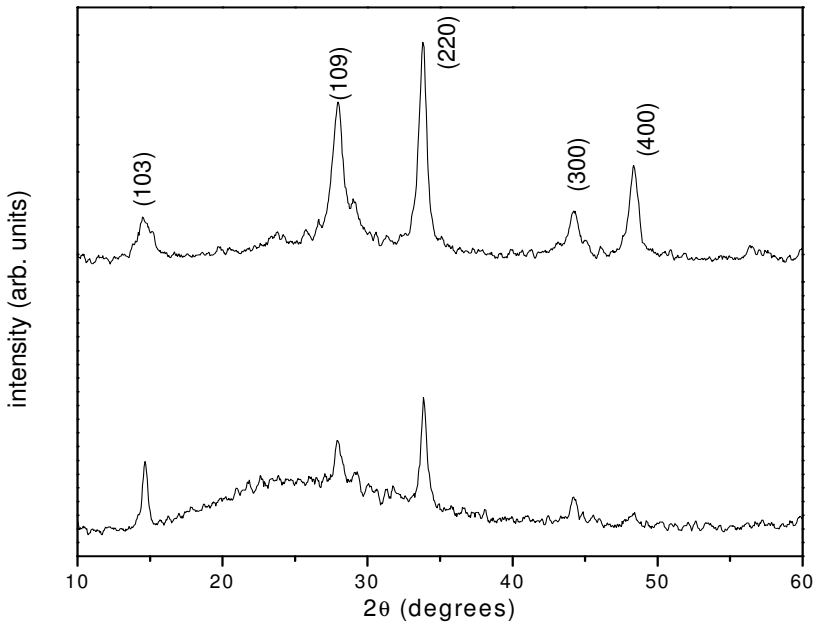

Figure.4.3.Comparison of x-ray diffractograms of thin and thick samples.

.

The x-ray diffractograms of the films with thickness 0.2 µm and 2.5 µm are depicted in Figure.4.3. It is observed that the intensity of diffractograms increases with increase in thickness of the films. But no significant improvement in grain size is observed. Resistivity of these films was measured and it was observed that resistivity increased with increase in thickness of the films. The values are as given in Table.4.1.

The absorption and transmission spectra of these films are given below (Figure.4.4 and 4.5). Naturally transmittance decreases with increase in thickness of the films. The band gap of the films decreases from 2.77 eV to 2.53 eV, as thickness varies from 0.2 µm to 2.5 µm.

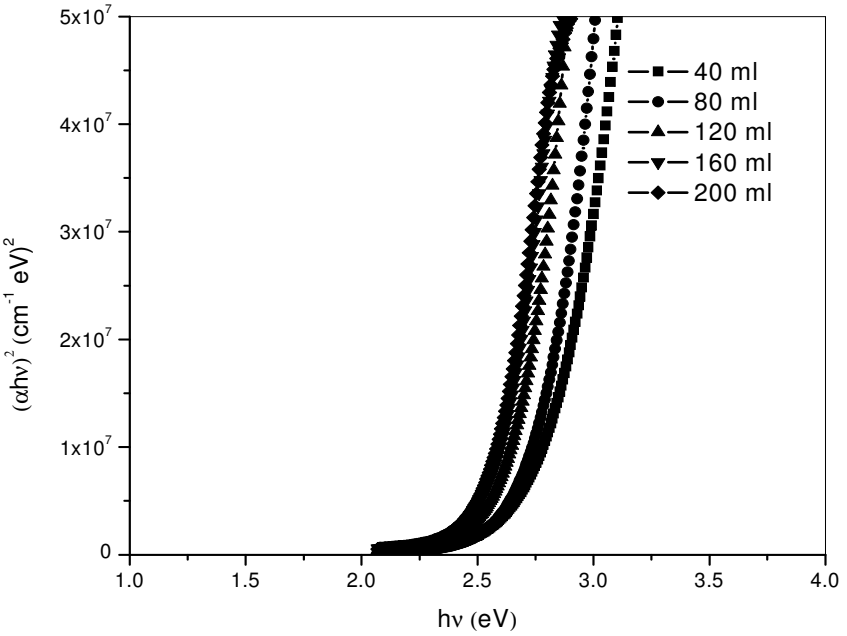

Figure.4.4.$(\alpha h\nu)^2$ vs. hν graph of samples prepared by varying the spray volume.

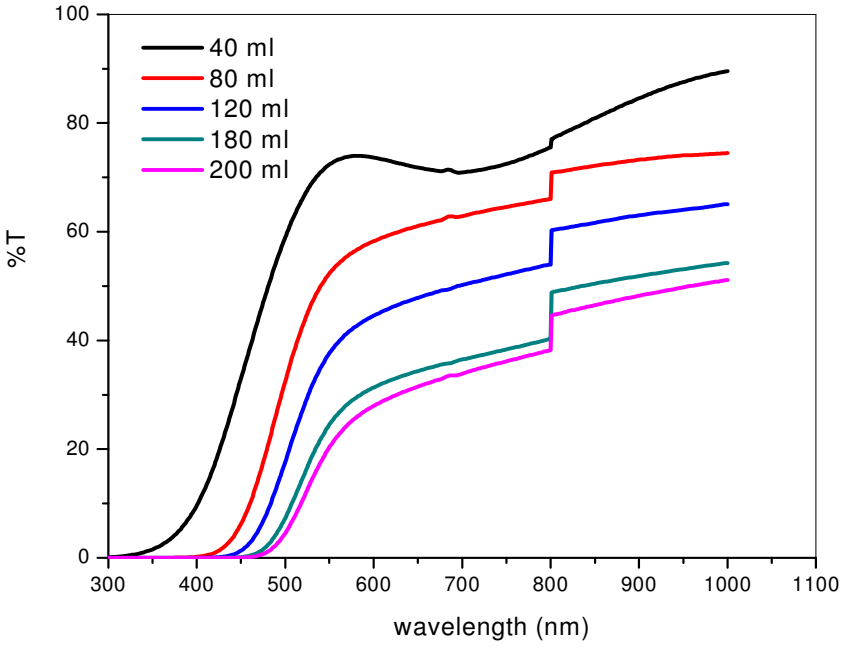

Figure.4.5.Transmission spectra of samples prepared by varying the spray volume.

From the above studies, it is evident that change in thickness of In_2S_3 films causes change in its properties. For application as buffer layer in solar cells, optimum thickness is an important factor which directly affects the cell parameters like series and shunt resistances. In our case, we could easily control the thickness of films by varying the deposition time or volume of spray.

4.6.Effect of variation of substrate temperature

Samples were prepared at different substrate temperatures in the range 523 K to 623 K keeping In/S ratio as 2/5 and spray rate at 2ml/min (volume of spray was 30 ml).

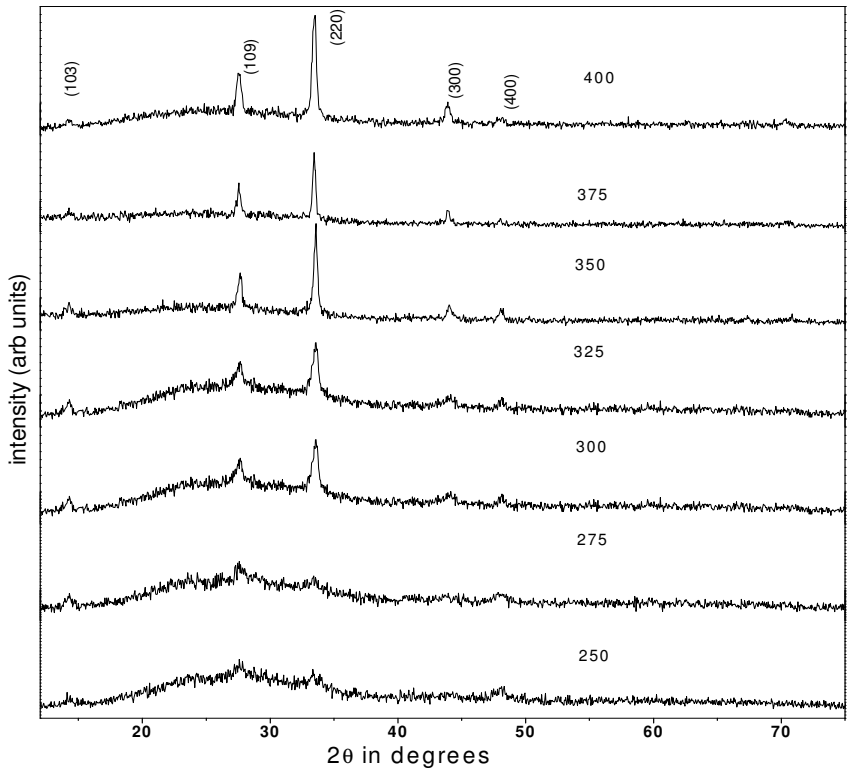

Figure.4.6.X-ray diffractograms of films prepared at different substrate temperatures.

The x-ray diffractograms of the films (Figure.4.6) proved that d values coincided with that of β-In_2S_3 with preferential orientation in (220) plane. At very low substrate temperatures the preferential orientation is along (109) plane. It is

evident that crystallinity of the samples increased with increase in substrate temperature. The grainsize increases from 18.9 nm for samples prepared at 573K to 29.95 nm for that prepared at 673K.

Optical properties of the films were studied. Band gap of the samples was found to vary between 2.67 eV and 2.85 eV (Table.4.2). Samples prepared at 573 K and above had more than 75% transmittance in the visible spectral range (Figure.4.7). The decrease in transmittance at low substrate temperatures may be due to the increase in thickness of the films.

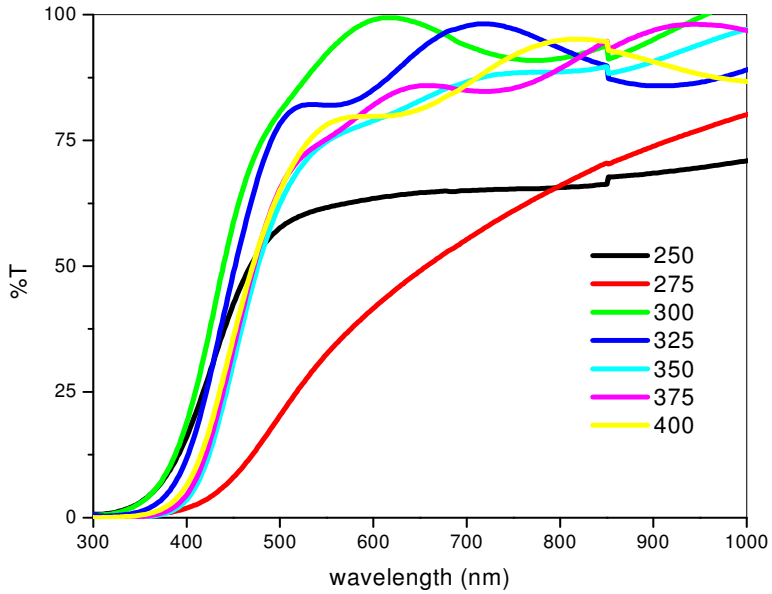

Figure.4.7.Transmission spectra of films prepared at different substrate temperatures.

Resistivities of the samples were also measured and tabulated (Table.4.2). It was observed that increase in substrate temperature caused decrease in resistivity of the samples.

Present study revealed that films with good transmission, wide band gap and orientation in (220) plane could be grown from 573 K onwards.

Substrate Temperature (K)	Band gap (eV)	Resistivity (Ω-cm)
523	2.79	322800
548	2.67	787500
573	2.83	378000
598	2.85	330000
623	2.85	231000
648	2.83	58800
673	2.83	70

Table.4.2.Band gap and resistivity of samples prepared at different substrate temperatures.

4.7.Effect of varying precursor ratio

Effect of variation of atomic ratio on the properties of In_2S_3 films was investigated. In_2S_3 with In/S ratio 2/3, 2/5, 2/8 and 1.2/8 were studied. These films were prepared at a substrate temperature of 573 K and the spray rate was 2 ml/min. Structural, optical, compositional as well as electrical studies were done on these samples. It was seen that crystallinity increased as In/S ratio changes from 2/3 to 2/5 and then decreased for samples 2/8 and 1.2/8 (Figure.4.8). Such a behaviour was previously observed in the case of manually sprayed samples.

The optical properties of these samples were also analysed. Absorption and transmission spectra are given below (Figure.4.9 and 4.10). Band gap of the samples were calculated from plot of $(\alpha h\nu)^2$ vs. $h\nu$ by extrapolating the straight line from high absorption region. From the transmission spectra it was evident that films have above 70% transparency in visible spectral range.

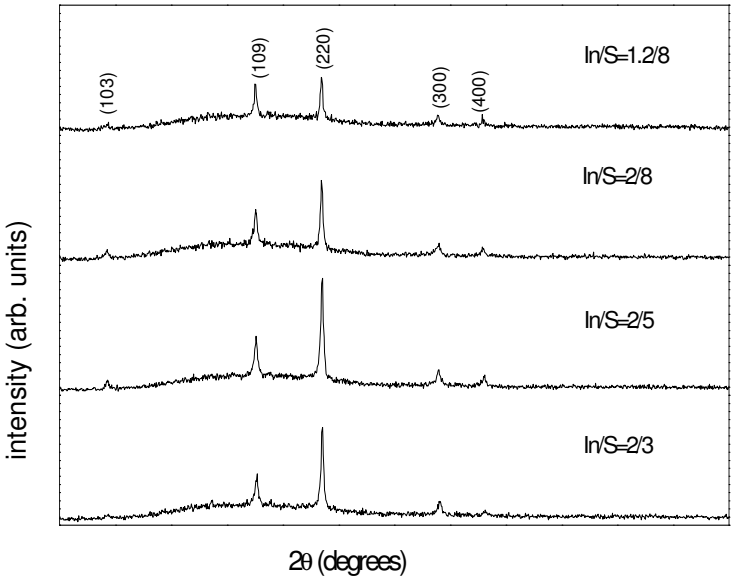

Figure.4.8.X-ray diffractograms of samples with different In/S ratio.

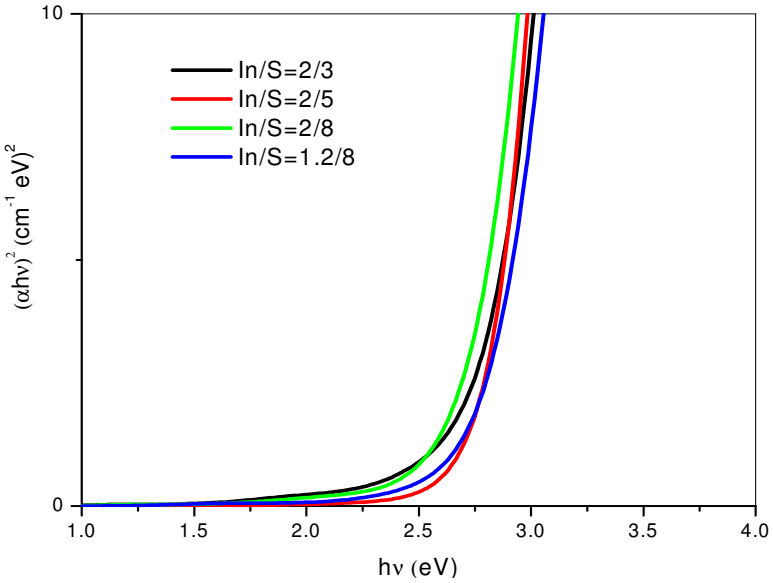

Figure.4.9.$(\alpha h\nu)^2$ vs. hν graph of samples prepared by varying the In/S ratio.

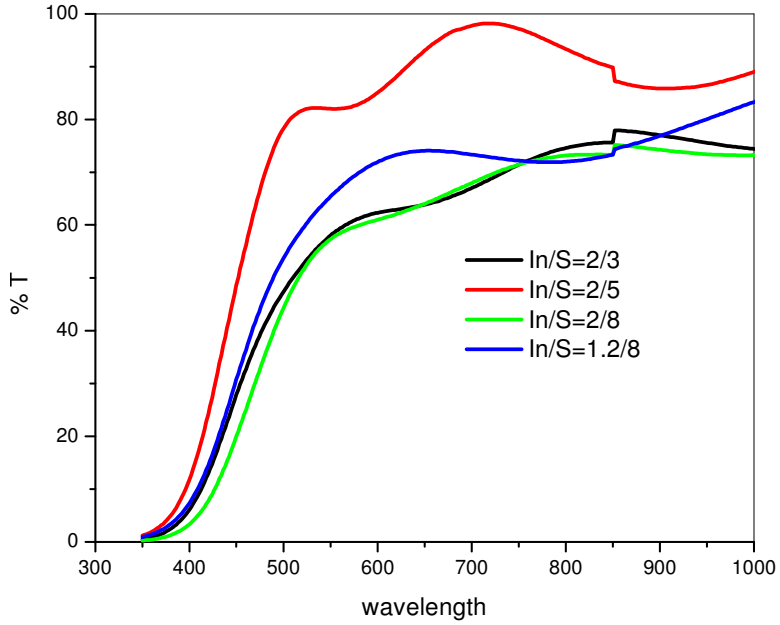

Figure.4.10.Transmission spectra of samples prepared by varying the In/S ratio.

EDAX analyses of the samples with In/S ratio as 2/3 and 2/8 were performed. It was clearly seen that concentration of sulfur in the samples increased with increase of sulfur concentration in the precursor solution (Table.4.3). High percentage of chlorine was present in both the samples.

In/S ratio	In (%)	S (%)	Cl (%)
2/3	38.43	43.68	17.88
2/8	28.17	52.78	19.05

Table.4.3.Stoichiometry variation of samples with In/S ratio as 2/3 and 2/8.

In order to understand the variation in stoichiometry as well as the chemical state of the elements along the thickness of the samples, XPS depth profiling was done. Presence of In, S, Cl, O, Na and Si was examined throughout the depth of the samples. Binding energies of indium and sulfur clearly indicated formation of In_2S_3.

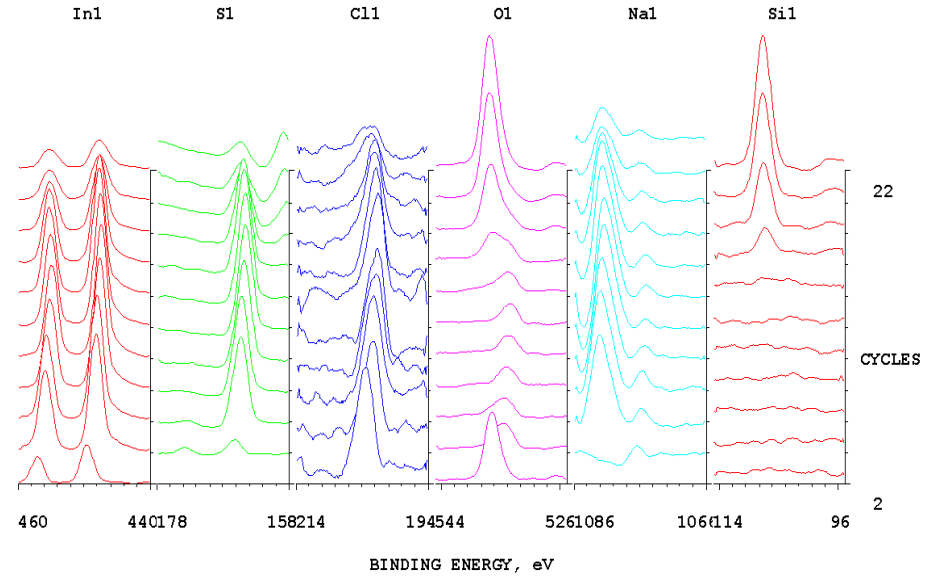

Figure.4.11.XPS depth profile of In_2S_3 with In/S ratio 2/3.

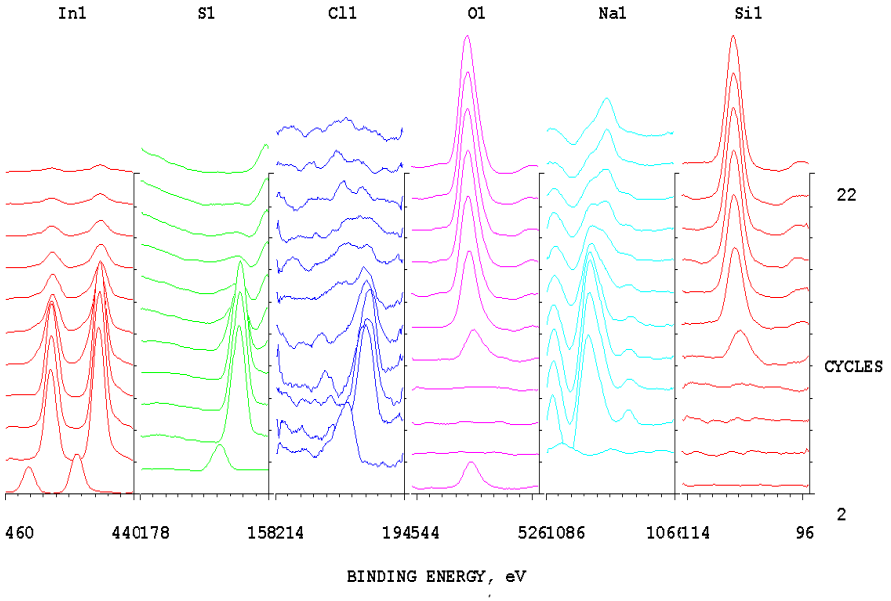

Figure.4.12.XPS depth profile of In_2S_3 with In/S ratio 2/8.

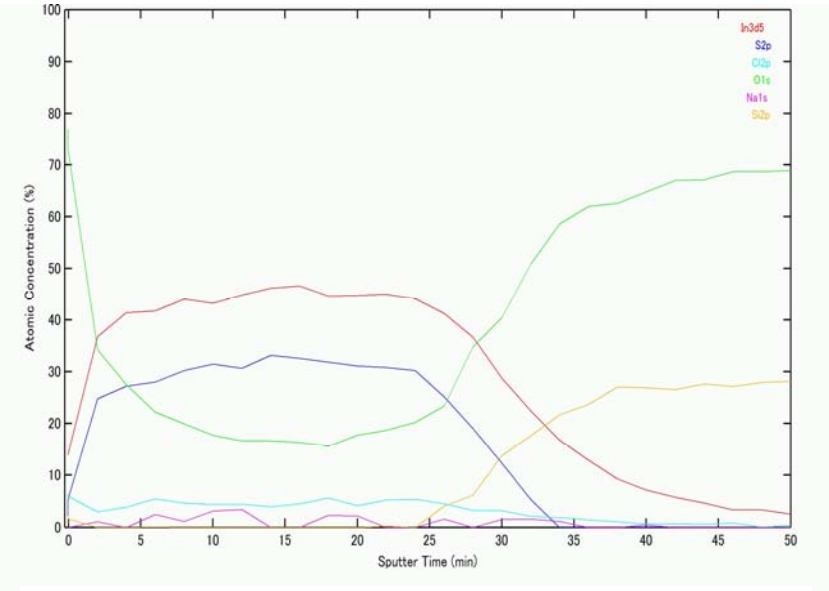

Figure.4.13.Atomic concentration vs. sputter time of different elements in In_2S_3 with In/S ratio 2/3.

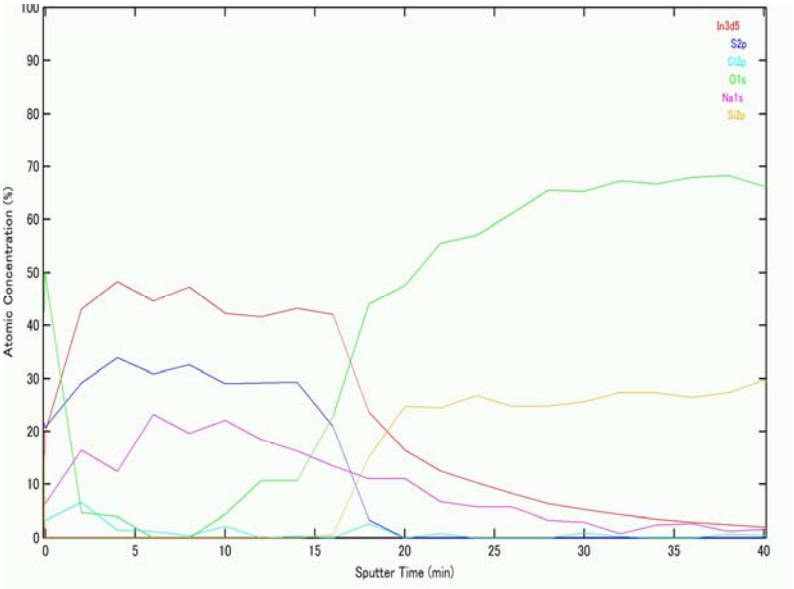

Figure.4.14.Atomic concentration vs. sputter time of different elements in In_2S_3 with In/S ratio 2/8.

Depth profile of the samples with In/S ratio as 2/3 showed the presence of oxygen throughout the depth (Figure.4.11). The binding energy peak corresponding to oxygen in the sample was at 532.49 eV. This can be attributed to the contamination of the sample in the form of sulfate. On increasing the sulfur concentration (In/S=2/8), it was seen that oxygen was present only as a surface contaminant (Figure.4.12). The decrease in peak height of sulfur at the surface of the film indicated that sulfur in the top layer was substituted by oxygen.

Atomic concentration of constituents of the films was also analysed (Figure. 4.13 and 4.14). One interesting observation was the presence of higher percentage of sodium in the sample with In/S ratio 2/8. It has been observed that in the presence of excess of sulfur as compared to the In_2S_3 stoichiometry, elements like sodium and copper can easily be introduced within the indium sulfide matrix. Here, sodium from soda lime glass substrates has diffused into the films. But the role of sodium in these films is yet to be investigated.

In this study we tried to study variation in properties of the films with change in precursor ratios. It is found that composition of the films varies with change in precursor ratio which consequently affects other properties.

4.8.Effect of variation of spray rate

Effect of spray rate on the properties of sprayed In_2S_3 films was investigated. In fact this parameter could be varied as we used the automated spray machine. If it was manual spray process, it is not possible to do this study. In_2S_3 films with In/S ratio as 1.2/8 was selected for the study. Films were prepared at substrate temperature of 573 K by varying the spray rate as 2 ml/min, 4 ml/min and 8 ml/min. Volume of pray was 50 ml.The variations in structural as well as electrical properties were investigated in detail.

From the x-ray diffraction studies, it was seen that crystallinity of the films decreased with the increase in spray rate as evident from the broadening of the peak (Figure.4.15). More interestingly, it was proved by the electrical studies that resistivity as well as photosensitivity increased with the increase in spray rate. Resistivity of the films increased from 131 x 10^3 Ω-cm to 525 x 10^3 Ω-cm and

photosensitivity from the ~10 to ~200 as spray rate was increased from 2 ml/min to 8 ml/min.

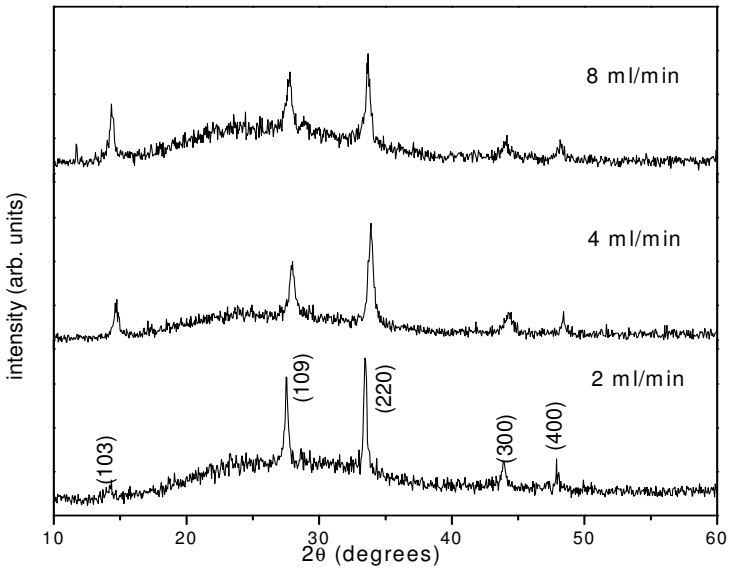

Figure.4.15.X-ray diffractograms of In_2S_3 deposited at different spray rates.

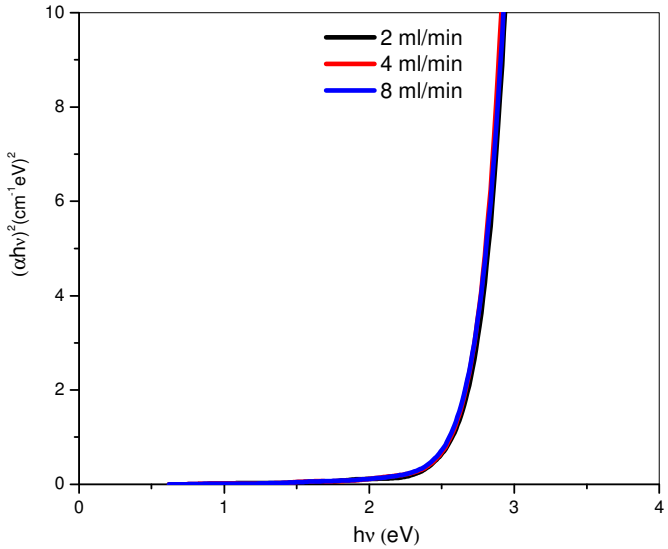

Figure 4.16. $(\alpha h\nu)^2$ vs. hν graph of samples prepared at different spray rates.

However, the optical studies of these samples proved beyond doubt that there is no variation in the band gap or transmittance of the films. Absorption and transmission spectra are given below (Figure.4.16 and 4.17).

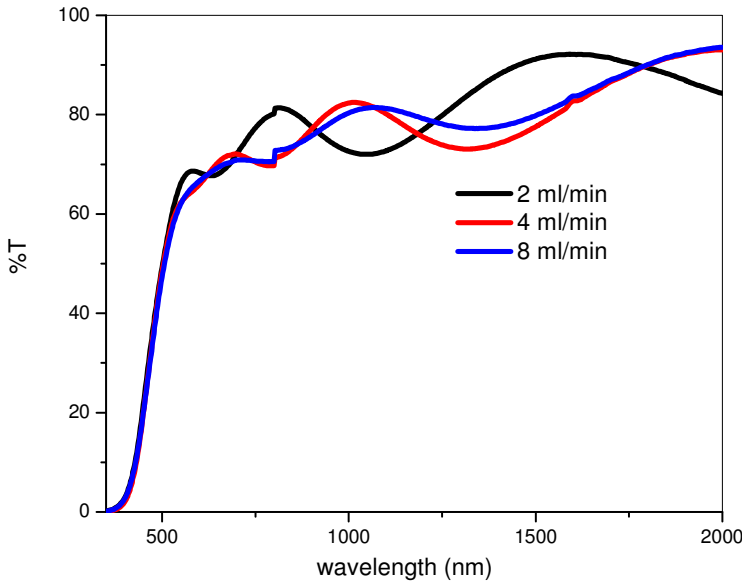

Figure.4.17.Transmission spectra of samples prepared at different spray rates.

Therefore, it is clear that photosensitive films could be obtained only at high spray rates. Spray rate could not be increased above 8 ml/min keeping all other parameters constants as the films then peeled off from the substrate.

4.9.Effect of copper incorporation in In_2S_3

One major observation in sprayed $CuInS_2/In_2S_3$ solar cells is the uncontrolled diffusion of Cu to the In_2S_3 layer. To overcome this, the In_2S_3 layer is made thick so that an undiffused layer of pure In_2S_3 remains even after the diffusion of copper during the deposition of Indium sulfide layer. This is found to improve the photo-activity of the cell. Thick In_2S_3 layer does not affect the light reaching the junction, as the cell is illuminated in front-wall configuration i.e. from $CuInS_2$ side. The $CuInS_2/In_2S_3$ cell is rather a graded junction in which Cu concentration is increasing from the In_2S_3 side to the $CuInS_2$ side. Study of the material properties of this

junction is essential for understanding the junction mechanism. One method to characterize the different junction layers is to chemically etch it layer by layer from top surface, and study the properties of each layer. But then, the bulk properties cannot be studied, as the underlying layers may affect the measurements. Hence, In_2S_3 films were prepared by incorporating varying amounts of $CuCl_2$ in the precursor solution so that composition changes gradually from In_2S_3 to that of $CuInS_2$. Each set of films correspond to different layers of the junction. The films were then characterized to understand their structural and opto-electronic properties.

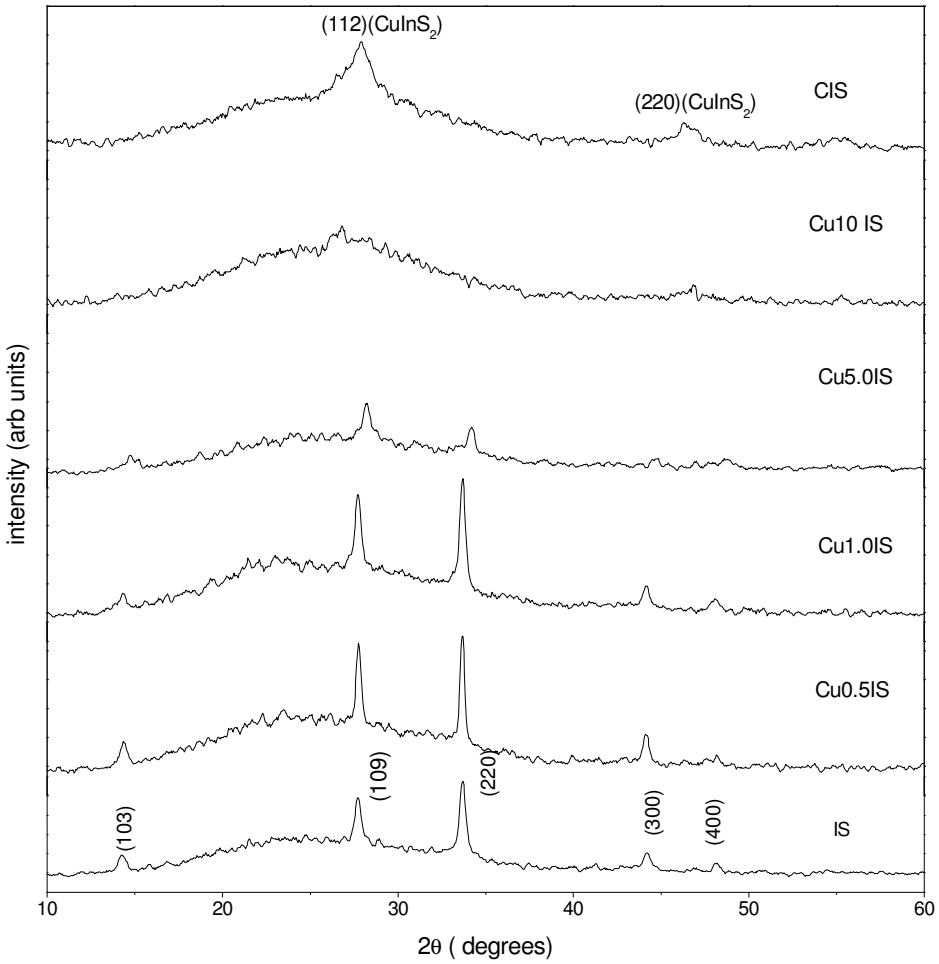

Figure.4.18.X-ray diffractograms of In_2S_3 with increasing copper concentrations.

Possibility of a third element substitution in the In_2S_3 matrix has been investigated in the past. It was seen that when introduced into the lattice, sodium and copper can occupy cationic vacancies. In the case of copper, it was seen that an excess of copper leads to the formation of $CuInS_2$ even at substrate temperatures as low as 473 K.

In the present case, $CuCl_2$ was used for doping copper into the In_2S_3 matrix. Doping percentages were 0.5%, 1%, 5% and 10% and the samples were named Cu0.5IS, Cu1.0IS, Cu5.0IS, Cu10IS. Pristine In_2S_3 (IS) and $CuInS_2$ (CIS) were also prepared and compared with these doped samples.

The films were analysed using x-ray diffraction technique to study the structural properties. The XRD pattern revealed that there was a gradual change from In_2S_3 to $CuInS_2$ (Figure.4.18). The peaks corresponding to In_2S_3 and $CuInS_2$ were identified. An amorphous state was observed in between the transition from In_2S_3 to $CuInS_2$.

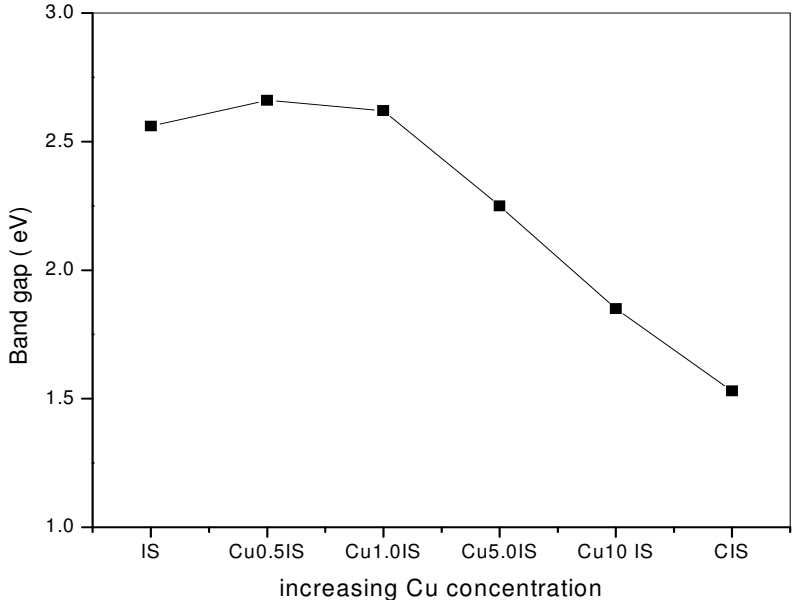

Figure.4.19.Band gap variation with increasing copper concentration.

Band gap of the samples changed from 2.60 eV to 1.53 eV with the incorporation of copper (Figure.4.19). Also, the transmision spectra clearly indicated the shift in transmission edge towards larger wavelengths with increased concentration of copper (Figure.4.20). Resistivity was also reduced by 3 orders as the films changed from In_2S_3 to $CuInS_2$.

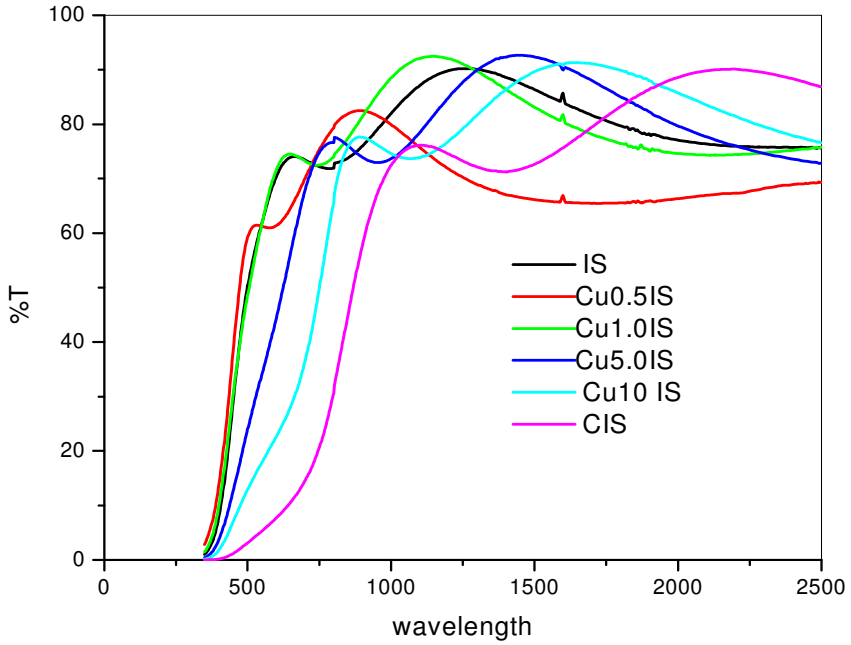

Figure.4.20.Transmission spectra of In_2S_3 with increasing copper concentration.

From the present work, it has been observed that the diffusion of copper into the layer of In_2S_3 can result in a change of the indium sulfide phase to that of the $CuInS_2$, making the junction a graded one, without forming any other phases of Copper. This will naturally improve the junction by forming an intrinsic layer between In_2S_3 and $CuInS_2$.

4.10.Conclusion

Indium sulfide thin films were prepared in the automated spray system and characterized. Preparation conditions like volume of spray, In/S ratio, substrate temperature and spray rate were varied to study the variation in properties of the

samples. It was seen that variation in thickness of the films affected the resistivity of the films. Resistivity of the films, which will directly affect the series resistance of the cell, increased with increase in thickness. Hence, optimum thickness of In_2S_3 film should be selected for cell applications.

From the studies on films prepared at different substrate temperatures it was seen that crystalline films with good optical properties were formed from substrate temperature of 573 K onwards. Study of In/S ratio variation on the properties of films showed that film composition was largely affected by concentration of precursors. Spray rate of the films affected the structural and electrical properties. Crystallinity of the films was found to decrease with increase in spray rate while the photosensitivity increased. Effects of copper incorporation in In_2S_3 films were also investigated. This was mainly done to find how diffusion of Cu from $CuInS_2$ to In_2S_3 will affect the properties at the junction. It was noticed that there was a regular variation in the opto-electronic properties with increase in copper concentration.

References

[1] Yu S., Shu L., Qian Y., Xie Y., Yang J., Yang L., Mater. Res. Bull. 33 (1998) 717.

[2] Bube R.H., J. Phys. Chem. Solids. 10 (1959) 333.

[3] Mathew M., Jayakrishnan R., Kumar P.M.R., Kartha C.S., Vijayakumar K.P., Kashiwaba Y., Abe T., J. Appl. Phys. 100 (2006) 33504.

[4] L. Bhira, H. Essaidi, S. Belgacem, G. Couturier, J. Salardenne, N. Barreaux, J.C. Bernede, Physica Status Solidi (A). 181 (2000) 427.

[5] R.S. Becker, T. Zheng, J. Elton, M. Saeki, Sol. Energy Mater. 13 (1986) 97.

[6] M. Rehwald , G. Harbeke, J. Phys. Chem. Solids. 26 (1965) 1309.

[7] Kambas K., Anagnospopoulos A., Ves S., Ploss B., Spyridelis J., Phys. Stat. Sol. 127 (1985) 201.

[8] EL Shazly A.A., Abdelkady D., Metoually H.S., Segmam M.A.M., J. Phys. Condens. Matter. 10 (1998) 5943.

[9] Hariskos D. et al., Proceedings of 19th European Photovoltaic Solar Energy Conference, Paris, France (2004).

[10] Asikainen T., Ritala M., Leskela M., Appl. Surf. Sci. 82/83 (1994) 122.

[11] Bessergenev V.G., Ivanova E.N., Kovalevskaya Y.A., Gromilov S.A., Kirichenko V.N., Larionov S.V., Inorg. Mater. 32 (1996) 592.

[12] Teny Theresa John, Ph.D Thesis, Cochin University of Science and Technology, India (2004).

[13] Allsop N.A., Schonmann A., Belaidi A., Muffler H.J, Mertesacker B., Bohne W., Strub E., Rohrich J., Lux-Steiner M.C., Fischer C.H., Thin Solid Films. 513 (2006) 52.

[14] Yasaki Y., Sonoyama N., Sakata T., J. Electroanal. Chem. 469 (1999) 116.

[15] Kessler J. et al., Proceedings of 23rd IEEE Photovoltaic Specialists Conference (1993).

[16] Meril Mathew, Ph.D Thesis, Cochin University of Science and Technology, India (2009).

[17] Bayon R., Herrero J., Thin Solid Films. 387 (2001) 111.

[18] Hariskos D., Ruckh M., Ruhle U., Walter T., Schock H.W., Hedstrom J., Stolt L., Sol. Energy. Mater. Sol. Cells. 41-42 (1996) 345.

[19] Sterner J., Malmstrom J., Stolt L., Prog. Photovolt.: Res. Appl.13 (2005) 179.

[20]Yoshida T., Yamaguchi K., Toyoda H., Akao K., Sugiura T., Minoura H., Nosaka Y., Electrochem. Soc. Proc. 97–20 (1997) 37.

[21] Kaufmann C. et al., Proceedings of 28th IEEE Photovoltaic Specialists Conference, Alaska, United States of America (2000).

[22] Teny Theresa John, S. Bini, Y. Kashiwaba, T. Abe, Y. Yasuhiro, C. Sudha Kartha, K.P. Vijayakumar, Semicond. Sci.and Tech. 18 (2003) 491.

[23] Teny Theresa John, C. Sudha Kartha, K.P. Vijayakumar, T. Abe, Y. Kashiwaba, Appl. Surf. Sci. 252 (2005) 1360.

[24] M. Calixto-Rodriguez, A. Tiburcio-Silver, A. Ortis, A. Sanchez-Juarez, Thin Solid Films. 480-481 (2005) 133.

[25] Bouguila N., Bouzouita H., Lacaze E., Belhadj Amara A., Bouchriha H., Dhouib A., J. Phys. III 7 (1997) 1647.

[26] Kim W.T., Kim C.D., J. Appl. Phys. 60 (1986) 2631.

[27] Teny Theresa John, C. Sudha Kartha, K.P. Vijayakumar, T. Abe, Y. Kashiwaba, Vacuum. 80(8) (2006) 870.

[28] P.M. Ratheesh Kumar, Teny Theresa John, C. Sudha Kartha, K.P. Vijayakumar, Nucl. Instr. and Meth. (B). 244(1) (2006) 171.

[29] K.C. Wilson, Tina Sebastian, Teny Theresa John, C. Sudha Kartha, K.P. Vijayakumar, P. Magudapathi, K.G.M. Nair, Appl. Phys. Lett. 89 (2006) 013510.

[30] Meril Mathew et al., Proceedings of Mater. Res. Soc. Symposium, Mexico (2007).

[31] W.T. Kim, W.S. Lee, C.S. Chung, C.D. Kim, J. Appl.Phys. 63(11) (1988) 5472.

[32] L. Bhira, S. Belgacem, J. C. Bernede, J. Appl. Phys. 92(9) (2002) 5327.

[33] L. Bhira, T. Ben Nasrallah, J. C. Bernede, S. Belgacem, Mater. Chem. Phys. 72 (2000) 320.

[34] Angel Susan Cherian et al., Proceedings of MRSI-AGM, NPL, New Delhi (2007).

[35] R.R. Pai, T.T. John, Y. Kashiwabe, T. Abe, K.P. Vijayakumar, C.S. Kartha, J. Mater. Sci. 40 (2005) 741.

[36] R.Jayakrishnan, Teny Theresa John, C. Sudha Kartha, K.P.Vijayakumar, T.Abe, Y. Kashiwaba, Semicond. Sci. and Tech. 20 (2005).

CHAPTER 5

$CuInS_2/In_2S_3$ Junction Fabrication and Analysis

5.1.Introduction

Current emphasis in photovoltaics is directed towards the development of high performance as well as inexpensive solar cells that can serve in the long term as viable alternatives to silicon technology. Foremost among those materials that have emerged as leading candidates are the chalcopyrite type Cu-ternaries. Devices using various Cu ternaries have evolved into cells better than 10% conversion values. Chalcopyrite structured ternary semiconductors were initially investigated for nonlinear optical applications [1] and later for pn junction devices [2]. Interest in Cu-ternary semiconductors for solar cell applications began in early 1970's [3]. The performance potential of Cu-ternary semiconductors is associated with their desirable and exceptional properties for terrestrial photovoltaic (PV) applications.

Solar cells based on thin film $CuInS_2$ homojunction were first described in 1977 and an electrochemical cell using n-type $CuInS_2$ claimed efficiency close to 10% in 1986 [4]. Following these proofs, work on this material continued with focus on thin film heterojunctions. The device performance has improved in recent years and cells with total area efficiencies in the range 11.4% to 12.5% have been achieved [5, 6]. Although this value is still far away from that obtained for other materials, other considerations must be taken into account. One should keep in mind that the difference in efficiency between different materials is much less important when dealing with modules. Although $CuInS_2$ submodule technology has started only recently, efficiencies upto 9.2 % has already been reported [7]. This is comparable with submodule efficiencies of other materials like $CuInGaSe_2$ (14.7%), CdTe (10.6%), unstabilized a-Si (12%) etc. [8]. Moreover, $CuInS_2$ based devices show excellent stability and can be fabricated in a much more reproducible way than its selenide counterpart.

In the case of $CuInS_2$ cells, the basic cell structure, processes and materials used for back contact, buffer layer or window layer were the same as that developed for the standard $CuInGaSe_2$ cells. The most successful techniques for absorber preparation were the multi-source evaporation and two step (sulfurization of metal precursor films) processes [9, 10]. The latter process has superior potential for industrial production. Rapid thermal processing was introduced later to reduce annealing time from one hour to 3 minutes. Cells based on RTP absorbers have reached a confirmed total area efficiency of 11.4% [5].

Presently, work on this material is focused on developing cells using cost-effective methods as well as novel cell structures. It is observed that CSP grown $CuInS_2$ films have the potential for PV applications. Highest reported efficiency of sprayed $CuInS_2$ thin film solar cell which used In_2S_3 as buffer layer, was 9.5 % on lab scale [11]. Recently, nano-structured three dimensional solar cells have been developed which uses spray deposited extremely thin $CuInS_2$ as absorber and In_2S_3 as buffer layer [12].

Through the present work, we have tried to develop sprayed $CuInS_2/In_2S_3$ solar cells using an automated spray unit developed in our lab. In the earlier works done, though cells with good efficiencies were obtained, it was observed that the results could not be extended to areas larger than few mm^2. More over, the problems of uniformity and repeatability were there as these were prepared manually. In the cells deposited using automated system we hoped to have better control over the uniformity of the cell, repeatability and standardization of the process. Above all it was possible to control parameters like spray rate and speed of the movement which are never possible in manual process. Also, through this one can modify the film properties very much.

5.2.Solar cell characterization using I-V measurement

PV cells can be modeled as a current source in parallel with a diode. When there is no light to generate current, the PV cell behaves like a diode. As light is incident on the cell, current is generated, as illustrated in Figure.5.1. Performance

parameters of the cell can be determined from this data, as described in the sections below.

5.2.1.Short circuit current (I_{SC})

The short circuit current corresponds to the short circuit condition when the impedance is low and the voltage is zero.

$$I\ (\text{at}\ V=0)=I_{SC} \tag{5.1}$$

I_{SC} occurs at the beginning of the forward-bias sweep and is the maximum current value in the power quadrant. For comparison of devices with different dimensions, current density (J) is used instead of current (I).

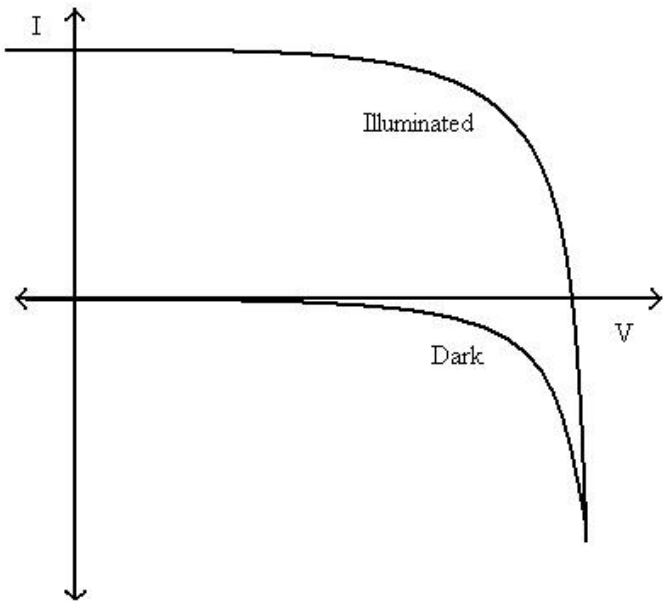

Figure.5.1.Current-Voltage characteristic of solar cell under dark and illuminated conditions.

5.2.2.Open circuit voltage (V_{OC})

The open circuit voltage occurs when no current is passing through the cell.

$$V\ (\text{at}\ I=0)=V_{OC} \tag{5.2}$$

V_{OC} is also the maximum voltage difference across the terminals of the cell for a forward-bias sweep in the power quadrant.

5.2.3.Maximum Power (P_{MAX}), Current at P_{MAX} (I_{MP}) and Voltage at P_{MAX} (V_{MP})

The power produced by the cell in Watts can be easily calculated along the I-V sweep using the equation, $P=IV$. At the I_{SC} and V_{OC} points, the power will be zero and the maximum value for power will occur between the two. The voltage and current at this maximum power point (P_{MAX}) are denoted as V_{MP} and I_{MP} respectively (Figure 5.2).

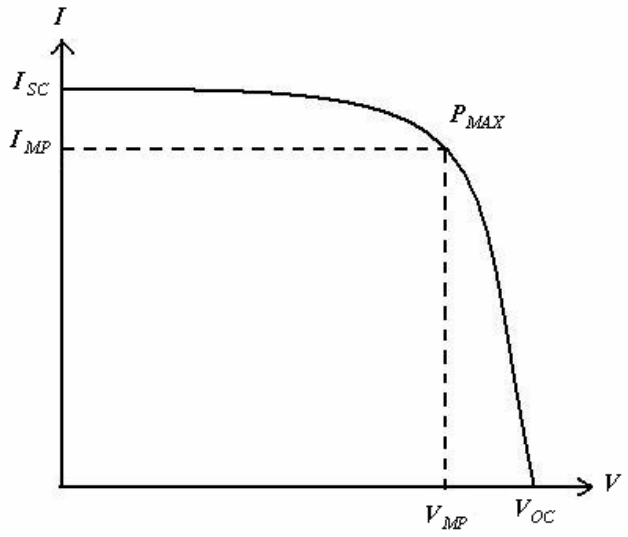

Figure.5.2.Illustration of P_{MAX}, I_{MP} and V_{MP}.

5.2.4.Fill Factor (FF)

The Fill Factor is essentially a measure of quality of the solar cell. It is calculated as the ratio of the maximum power to the theoretical power (P_T). P_T is the product of open circuit voltage and short circuit current. FF can also be interpreted graphically as the ratio of rectangular areas depicted in Figure.5.3.

$$FF = \frac{V_M \cdot J_M}{V_{OC} \cdot J_{SC}} \tag{5.3}$$

A larger fill factor is desirable, and corresponds to an I-V sweep that is more square-like. Typical fill factors range from 0.5 to 0.82. Fill factor is often represented in percentage.

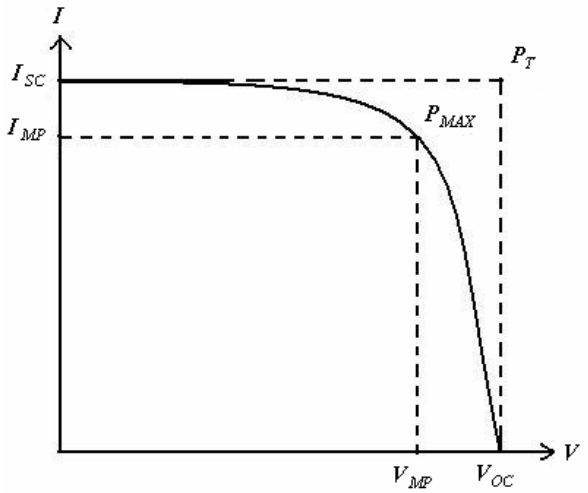

Figure.5.3.Obtaining Fill Factor from I-V sweep.

5.2.5.Efficiency (η)

Efficiency is the ratio of the electrical power output (P_{out}), compared to the solar power input (P_{in}), given to the PV cell. P_{out} can be taken to be P_{MAX} since the solar cell can be operated up to its maximum power output to get the maximum efficiency.

$$\eta = \frac{P_{out}}{P_{in}} \times 100\ \% \Rightarrow \eta_{MAX} = \frac{P_{MAX}}{P_{in}} \times 100\ \% \tag{5.4}$$

P_{in} is taken as the product of the irradiance of incident light, measured in W/m^2 or in suns (1000 W/m^2), with the surface area of the solar cell in m^2. The maximum efficiency (η_{MAX}) found from a light test is not only an indication of the performance of the device under test, but, like all of the I-V parameters, can also be affected by

ambient conditions such as temperature and intensity and spectral distribution of the incident light.

5.2.6.Shunt Resistance (R_{SH}) and Series Resistance (R_S)

During operation, the efficiency of solar cells get reduced by the dissipation of power across internal resistances. These parasitic resistances can be modeled as a parallel shunt resistance (R_{SH}) and series resistance (R_S).

For an ideal cell, R_{SH} would be infinite and would not provide an alternate path for current to flow, while R_S would be zero, resulting in no further voltage drop before the load. Decreasing R_{SH} and increasing R_s will lower the fill factor (FF) and P_{MAX} as shown in Figure.5.4. If R_{SH} is decreased too much, V_{OC} will drop, while increasing R_S excessively can cause I_{SC} to drop instead.

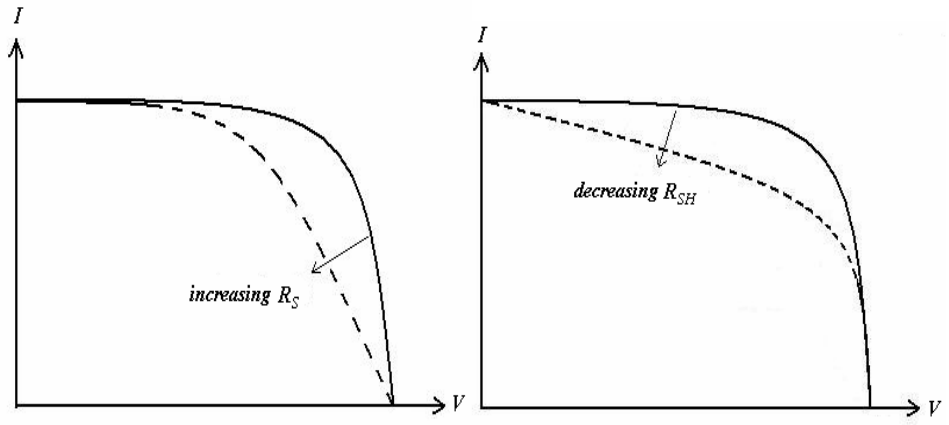

Figure.5.4.Effect of series and shunt resistance on I-V characteristic.

It is possible to approximate the series and shunt resistances, R_S and R_{SH}, from the slopes of the I-V curve at V_{OC} and I_{SC}, respectively. Typically, the resistances at I_{SC} and V_{OC} will be measured as shown in Figure 5.5.

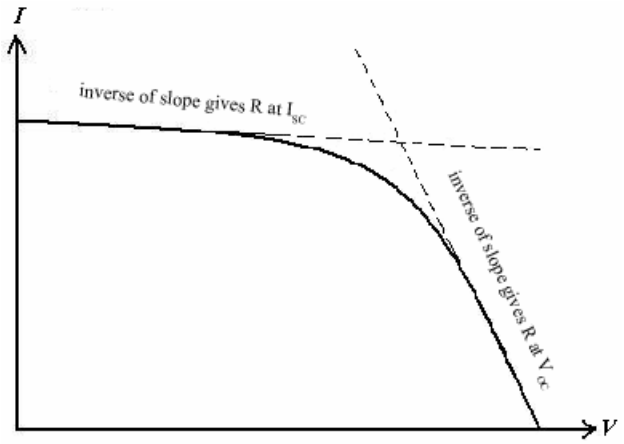

Figure.5.5.Obtaining R_{SH} and R_S from I-V curve.

If incident light is prevented from exciting the solar cell, the I-V curve shown in Figure.5.6 can be obtained. The slope of the linear region of the curve in the third quadrant (reverse-bias) is a continuation of the linear region in the first quadrant, which is same as the linear region used to calculate R_{SH} in Figure.5.5. It follows that R_{SH} can be derived from the I-V plot obtained with or without providing light excitation. Similarly, slope of the linear region of far forward characteristic in first quadrant can be used to calculate R_s.

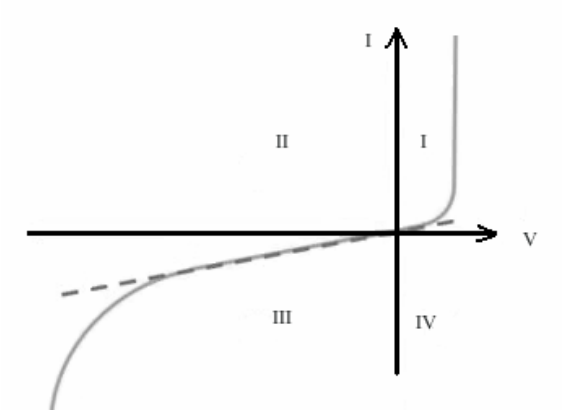

Figure.5.6.Obtaining R_{SH} from dark I-V.

5.3.Junction fabrication and characterization

In the present work, superstrate structure was used in cell fabrication i.e., light was incident on the cell from substrate side which imposed the condition that the substrate must be transparent. Hence, ITO coated glass was used as the substrate. Cell was illuminated from the side of the absorber i.e., in front wall mode. Similar to the case of Cu_xS/CdS junction, front wall mode of illumination was found to be more suitable for $CuInS_2$/ In_2S_3 devices that we fabricated [13].

Junction was fabricated by depositing $CuInS_2$ layer first and In_2S_3 layer over that by CSP method on ITO coated glass. Silver electrodes were then coated using vacuum evaporation. Different parameters like thickness, composition and spray rate were varied and devices were fabricated. The cell structure is illustrated in Figure.5.7.

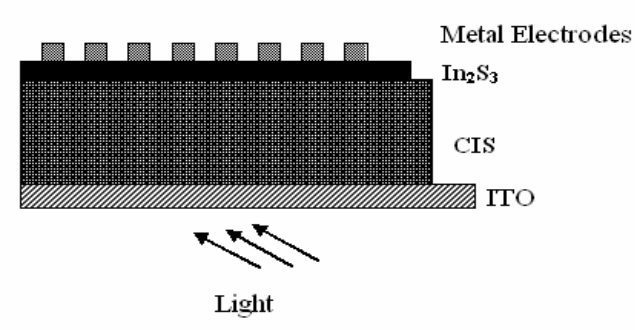

Figure.5.7.Structure of the cell.

5.3.1.Cell fabrication using optimized $CuInS_2$ sample

Near stoichiometric $CuInS_2$ samples were prepared at 623 K, using spray rate 1 ml/min. These samples showed favourable opto-electronic properties and was therefore used for device fabrication. Volume of the solution sprayed was 30 ml and thickness obtained was 0.30 microns. In_2S_3 layer with In/S ratio 2/8 (double molarity i.e., 0.05 M $InCl_3$ and 0.2 M Thiourea), substrate temperature 573 K and spray rate 8 ml/min was deposited over the $CuInS_2$ layer. In_2S_3 layer was made thick so that,

inspite of diffusion of copper from $CuInS_2$ side, a layer of pure In_2S_3 remained on the top surface. This was verified by taking XPS of the junction (Figure.5.8).

XPS analysis showed that there was a copper free layer at the surface of the cell and that the intensity of binding energy (BE) peaks increased inside the cell. There was substitution of sulfur by oxygen at the surface, as indicated by the decrease in peak height of sulfur and corresponding increase in peak height of oxygen.

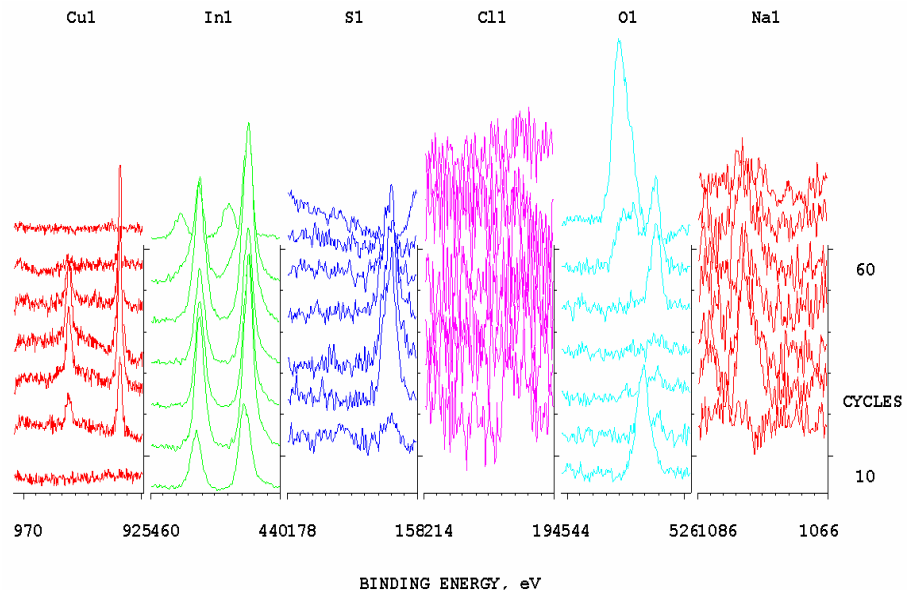

Figure.5.8.XPS depth profile of the cell.

Silver electrodes of area 0.25 mm^2 were deposited by vacuum evaporation over the In_2S_3 layer. This cell was named C1. From the I-V characteristic, it was seen that the junction behaved as a diode under dark condition and showed photo activity when illuminated. Illumination was given using a tungsten halogen lamp and the intensity of illumination was 100 mW/cm^2.

The illuminated I-V characteristic of the junction is given below (Figure.5.9). From the curve, cell parameters such as V_{oc}, J_{sc}, FF and η were calculated and listed

in Table.5.1. The barrier height of the junction was also calculated from the plot of temperature dependent V_{oc}, as shown in Figure.5.10. The plot of V_{oc} against temperature T, extrapolated to 0 K gives the barrier height ($V_{oc}(0)$) of the junction. Barrier height was obtained as 0.93 eV. This low value of barrier height may be due to interface recombination [14].

V_{oc}	0.24 V
J_{sc}	3.3 mA
η	0.16%
FF	20.2%

Table.5.1.Voc, Jsc, η and FF of the cell C1.

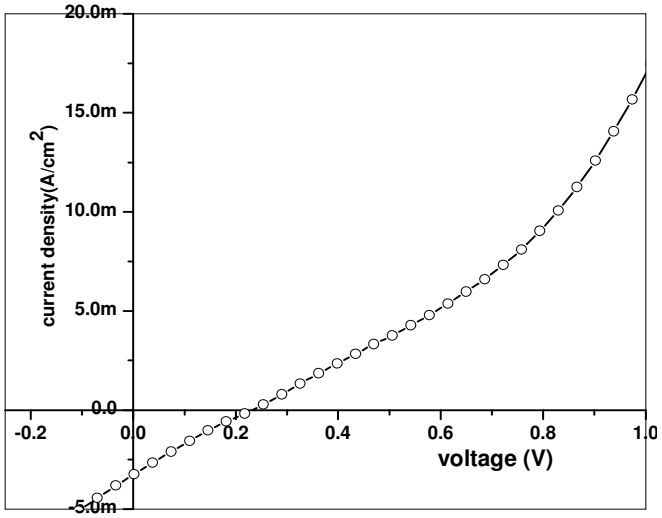

Figure.5.9.Illuminated I-V characteristic of the cell C1.

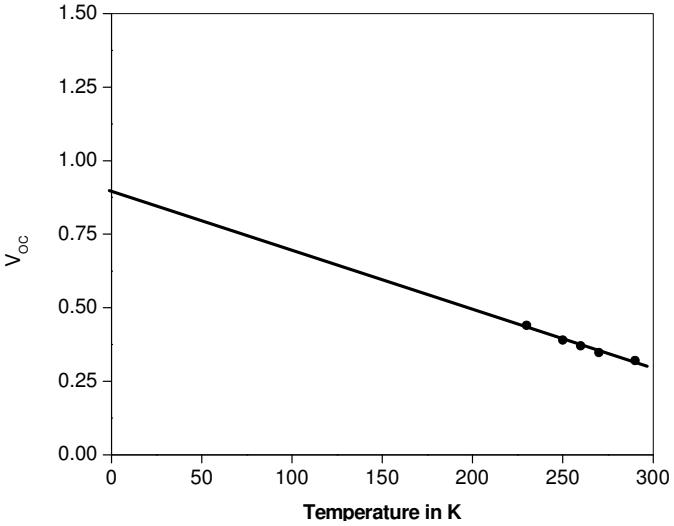

Figure.5.10.Obtaining barrier height from temperature dependent V_{oc}.

5.3.2.Effect of thickness variation of absorber and buffer layer

Thickness of the absorber layer was varied with an intention to improve the performance of the cell. A method to increase the thickness was the multiple spray technique. Thinner layer of $CuInS_2$ than that used for C1 did not yield any photocurrent. Thicker layer of $CuInS_2$ was deposited using 60 ml (30 ml + 30 ml) of $CuInS_2$, sprayed in 2 steps. Above the In_2S_3 layer, silver electrode was deposited using vacuum evaporation (cell C2). In_2S_3 films were deposited with In/S ratio 2/8 (double molarity) at substrate temperature 573 K and spray rate 8 ml/min. The cell was illuminated using light with intensity 50 mW/cm^2. Best current was obtained when 30 ml of In_2S_3 was sprayed over $CuInS_2$ films deposited through multiple spray technique. From the I-V characteristics, the cell parameters were obtained (Figure.5.11) and the values are given in Table.5.2.

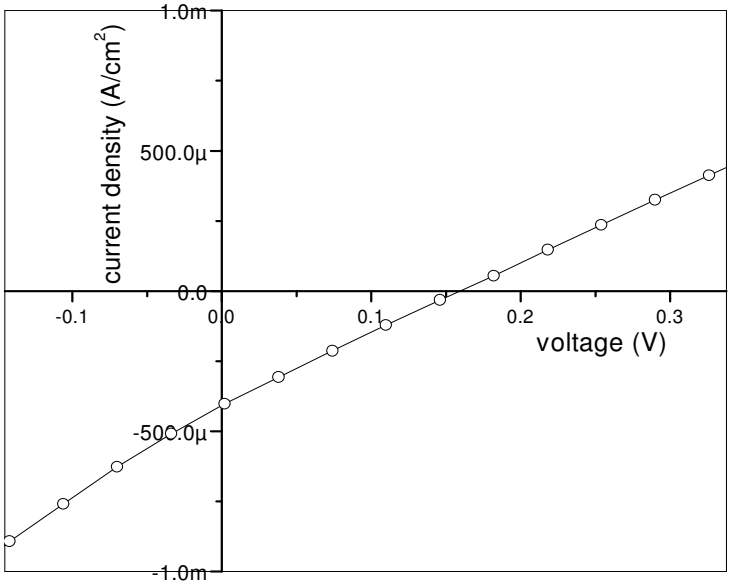

Figure.5.11.Illuminated I-V characteristic of the cell C2.

V_{oc}	0.16V
J_{sc}	0.41 mA
η	0.03%
FF	23.15%

Table.5.2.Voc, Jsc , η and FF of the cell C2.

Another method of increasing the thickness was by increasing the spray rate and spray head movement simultaneously, thus spraying larger volumes in a single spray. Under this condition, near stoichiometric films with good opto-electronic properties were obtained at 573 K. For ~0.4 microns thick $CuInS_2$ films (45 ml sprayed at the rate 8 ml/min and 573 K), we could obtain better values of V_{oc} and J_{sc}

(Table.5.3). In_2S_3 layer used in this was the same as that of cell C2. The I-V characteristic of this cell (cell C3) is given in Figure.5.12.

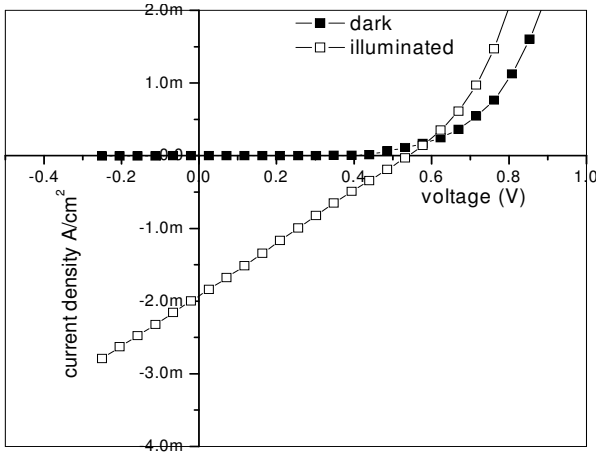

Figure 5.12.Illuminated I-V characteristic of the cell C3.

V_{oc}	0.54V
J_{sc}	1.9 mA
η	0.52 %
FF	25.3 %

Table.5.3.Parameters of the cell C3.

Thickness of In_2S_3 layer in the above cell was changed by varying the volume of spray. It was observed that when lesser volume (25 ml) was sprayed, better characteristics were obtained (Figure.5.13). Under illumination intensity of 50 mW/cm^2, the cell (cell C4) gave an efficiency of ~1%. The cell parameters are given in Table.5.4. In addition to V_{OC}, J_{SC}, FF and η, R_S and R_{SH}, were also calculated. Efficiency of ~1% was obtained for cells having area 1 mm^2 as well as 25 mm^2. Here we have taken electrode area as the cell area and this has been verified by isolating the electrode area by mechanical scribing. We obtained ~1% efficiency for cells with and without scribing.

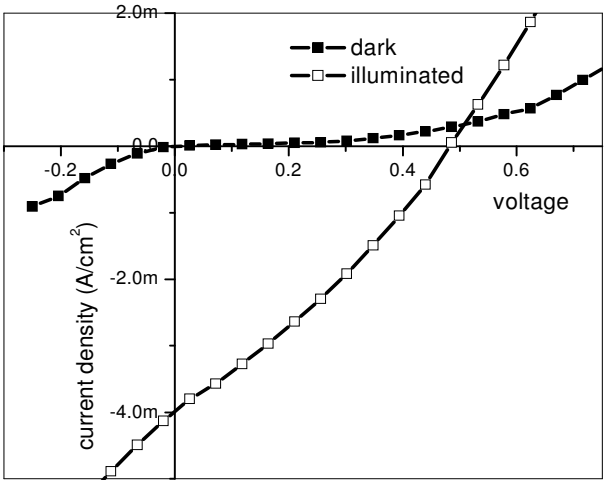

Figure.5.13.Illuminated I-V characteristic of the cell C4.

V_{oc}	0.49 V
J_{sc}	4 mA/cm2
η	1.15 %
FF	30 %
R_S	9.7 Ω
R_{SH}	250 Ω

Table.5.4.Parameters of the cell C4.

5.3.3.Effect of Cu/In ratio variation of $CuInS_2$ layer

$CuInS_2$ with Cu/In ratio 0.5, 1, 2 and with constant S/Cu ratio (= 5) were deposited on ITO coated glass substrates. In each case, 45ml solution was used for spray and deposition was carried out at 573 K. The spray rate was maintained at 8 ml/min during deposition. 25 ml of In_2S_3 having In/S ratio 2/8 was deposited in all the three cases. Silver electrodes of area 1 mm^2 were deposited over In_2S_3. The cells were named as CIS-0.5, CIS-1 and CIS-2 respectively. In all the cases, it was

observed that the dark I-V characteristic showed diode nature. The cells were illuminated with tungsten halogen lamp with intensity 50 mW/cm^2. The illuminated I-V characteristics of the three cells are given in Figure.5.14 and their current and voltage values are given in Table.5.5. From the comparison, it is clear that cell CIS-1 has better efficiency than the other two.

Cell Name	Jsc mA/cm^2	Voc V	η %
CIS-0.5	1.06	0.503	0.26
CIS-1	3.8	0.437	1.012
CIS-2	2.5	0.425	0.50

Table.5.5.Comparison of cell parameters: CIS-0.5, CIS-1 and CIS-2.

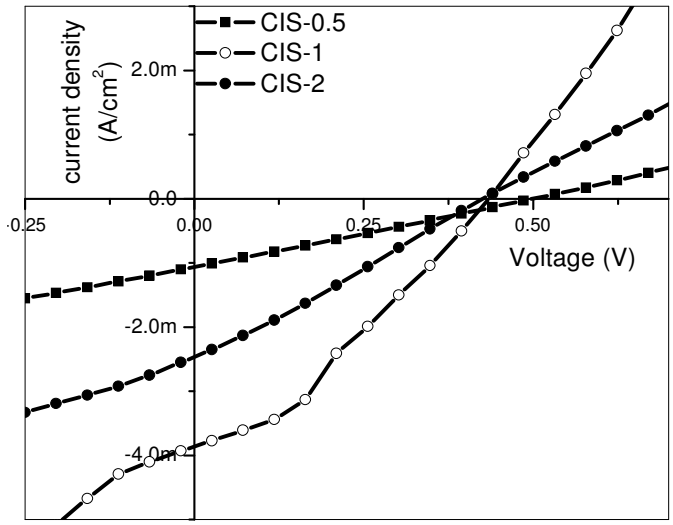

Figure.5.14.Illuminated I-V characteristic of the cells CIS-0.5, CIS-1 and CIS-2.

5.3.4.Effect of post deposition treatments

The cell showing 1% efficiency was annealed in air and vacuum for 30 minutes to study the effect of post deposition treatments on the junction parameters. The cells were named C-A and C-V respectively. It was seen that the junction characteristics deteriorated on air and vacuum annealing as seen from Figure 5.15 and 5.16.

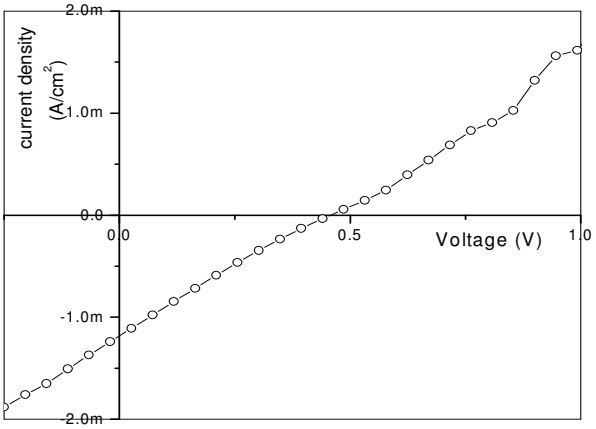

Figure.5.15.Illuminated I-V characteristic of the cell C-A.

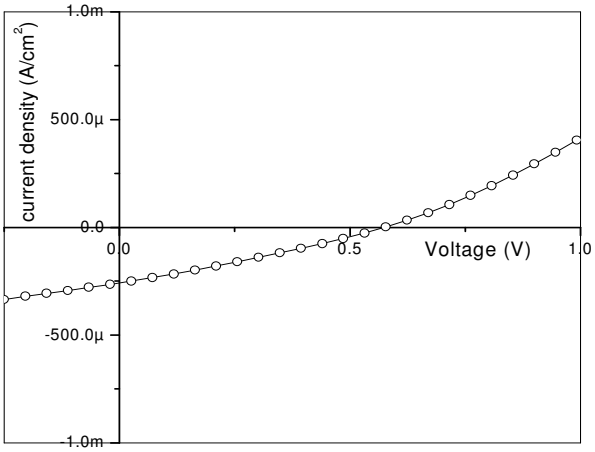

Figure.5.16.Illuminated I-V characteristic of the cell C-V.

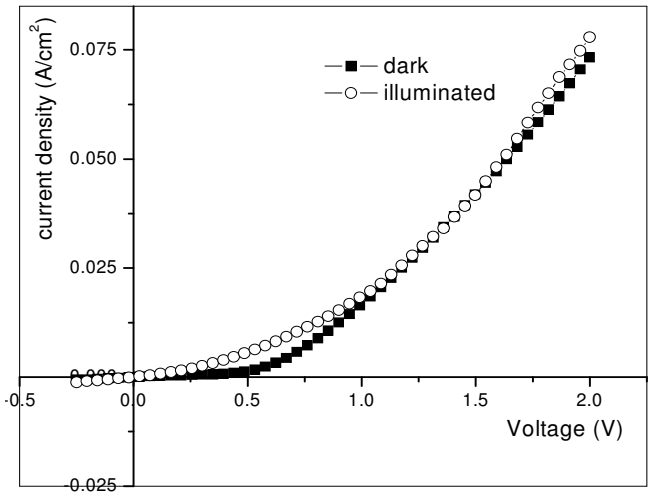

Figure 5.17.Illuminated I-V characteristic of the cell C-S.

Also, $CuInS_2$ samples were given H_2S treatment and then used for device fabrication (cell C-S). From our earlier studies, we have observed that even though the sulfurization improved structural and optical properties, this had a detrimental effect on conductivity and mobility. When device was fabricated using this, no photo activity was observed. I-V characteristics in dark and under illumination are given in Figure.5.17. Hence, from the present study, we could observe that post deposition treatments did not improve the device properties.

5.3.5.Effect of silver diffusion

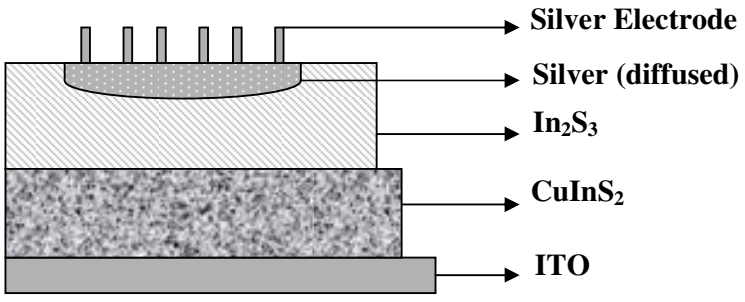

Figure 5.18. Structure of the cell C-Ag.

It has been observed from the works of Mathew et al. that silver diffusion resulted in the improvement of properties of sprayed In_2S_3 films [15]. Hence in the present work, we purposefully diffused a layer of silver over the 1% efficient cell and studied the IV characteristic. 13 mg of silver was evaporated on the cell over an area

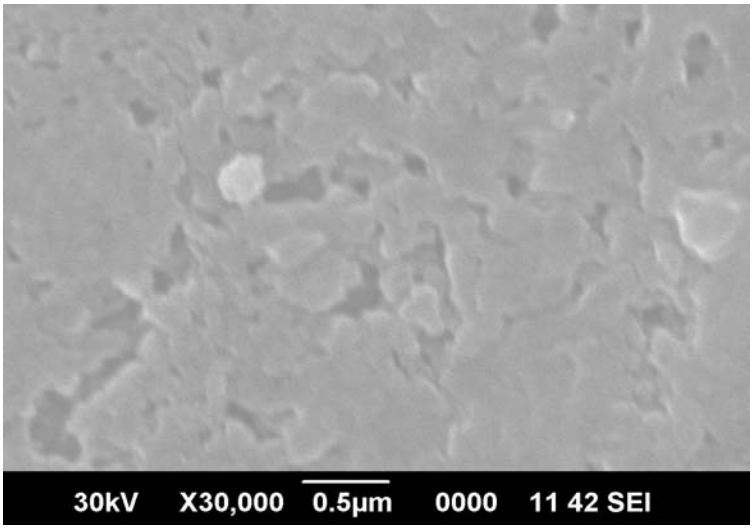

Figure.5.19.SEM image of surface of the cell before silver diffusion.

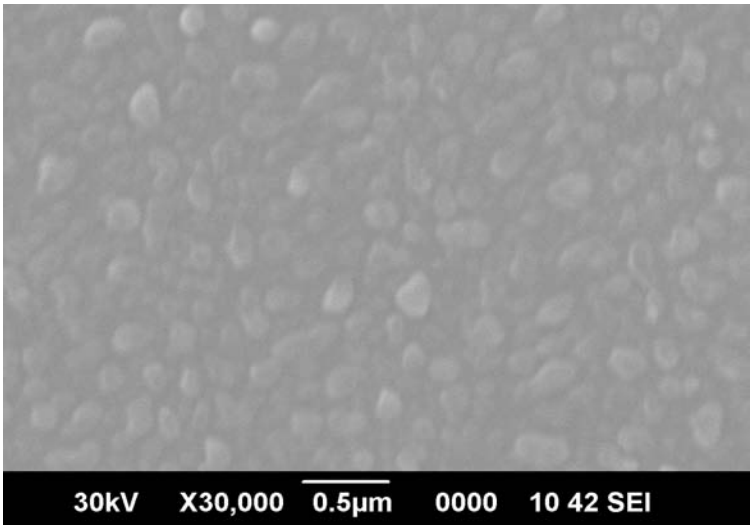

Figure.5.20.SEM image of surface of the cell after silver diffusion.

of 1.0 cm^2 and was annealed at 373 K for 30 minutes in vacuum. Initially, different amounts of silver (8 mg, 10 mg, 13 mg, 15 mg, 18 mg) were evaporated over the $CuInS_2/In_2S_3$ junction and annealed. For quantities of silver higher than 13 mg, the cells were shorted and for lesser quantities, diffusion had no effect on the properties of cell. But when 13 mg silver was evaporated the I-V characteristic showed dramatic increase in current. Figure.5.18 illustrates the structure of silver diffused cell (13 mg silver). Figures.5.19 and 5.20 show the SEM images of the cell surface before and after silver diffusion. As evident from the micrographs, there is a clear increase in grain size of the films after silver diffusion.

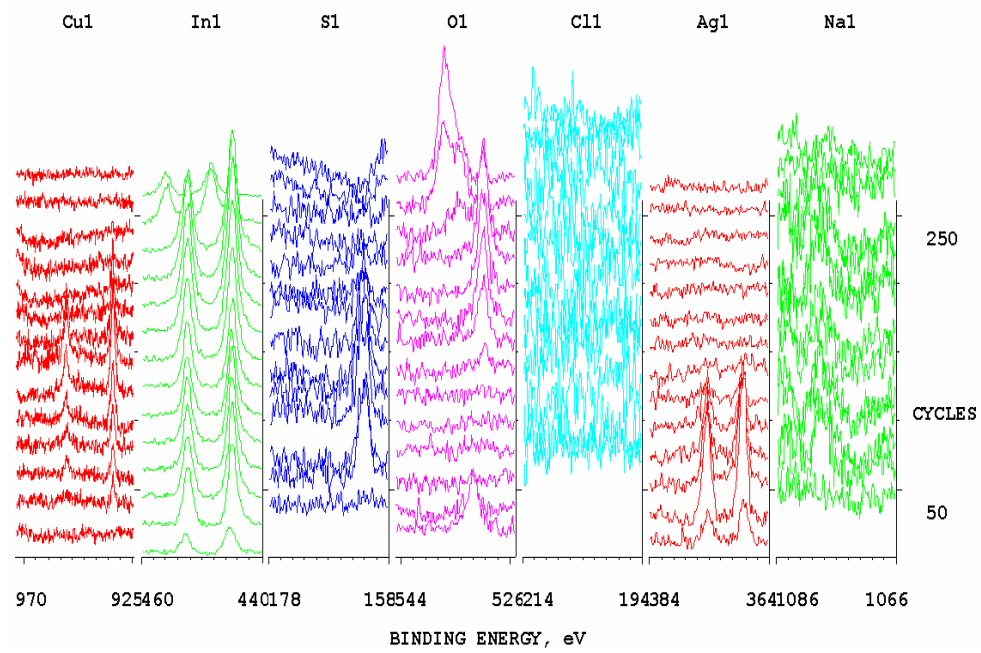

Figure.5.21.XPS depth profile of the cell C-Ag.

From XPS depth profile, it was seen that there is a Cu-free layer at the surface of the cell and that the intensity of BE peaks of copper increased away from the cell surface (Figure.5.21). Substitution of sulfur by oxygen at the surface was indicated by the decrease in peak height of sulfur and increase in peak height of oxygen. Silver in its elemental form was present in the top few layers of the cell.

Silver electrodes of area 1mm^2 were deposited over the diffused area and the I-V characteristic of the cell under illumination of 50 mW/cm^2 was measured (Figure.5.22). A drastic increase in current density was observed in this case when the device area was taken to be 1 mm^2. Other parameters like V_{OC}, R_S and R_{SH} were also found to be better for C-Ag (Table.5.6). This can be either due to the improvement in the properties (like crystallinity and conductivity) of the In_2S_3 layer which can enhance the carrier generation and transport in the cell or, there is possibility of collection of carriers from the metal diffused region other than the area just beneath the electrode i.e., the active cell area may be larger than the cell area used for calculation. Mechanical scribing done to verify this was unsuccessful as it resulted in the damage of device.

V_{oc}	0.55 V
J_{sc}	55.9 mA/cm2
η	16.5%
FF	26.4%
R_S	5.1 ohms
R_{SH}	318 ohms

Table.5.6.Parameters of the cell C-Ag (device area taken as 1 mm^2).

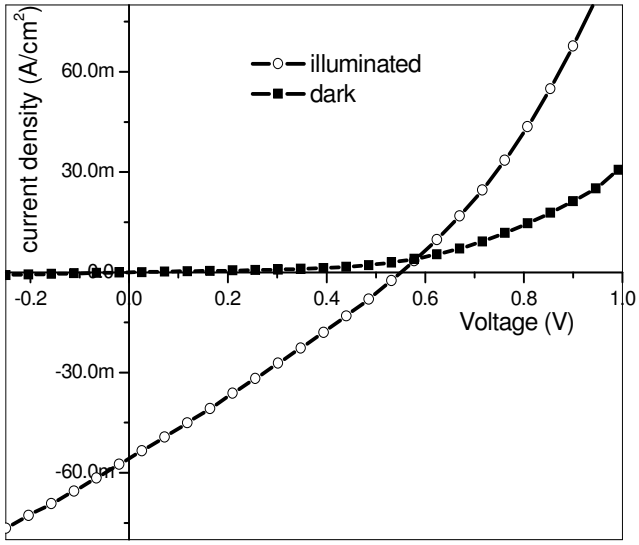

Figure.5.22.Dark and illuminated I-V characteristic of the cell C-Ag.

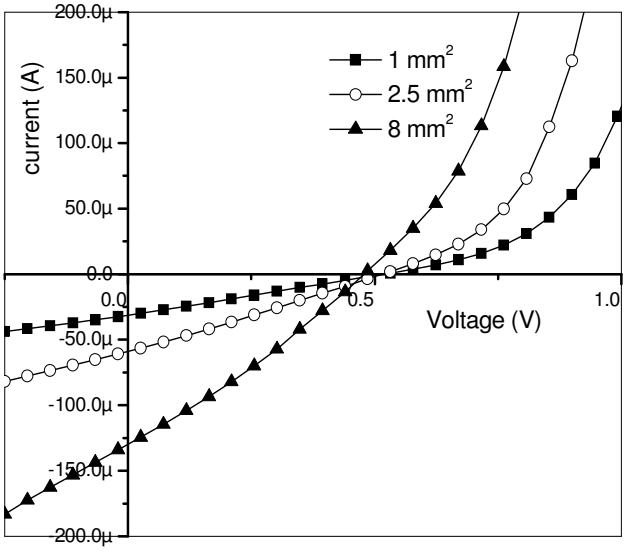

Figure.5.23.Comparison of short circuit current values for different electrode areas.

In the cell C-Ag, if collection was from total diffused area, increasing the electrode area should not change the current collection. But here, increasing the area of electrode resulted in shorting of the device. Area of electrode over the diffused area could be successfully increased only when the thickness of buffer layer was increased (30 ml) i.e., when silver diffusion was done on cell C2. In this case, we diffused 13 mg silver over an area of 0.25 cm^2 and electrodes with areas 1 mm^2, 2.5 mm^2 and 8 mm^2 were deposited over it. It was observed that, when the area of electrode was increased, there was increase in short circuit current (Figure.5.23). Also, this increase was not directly propotional to the increase in area of electrode. Thus, there remains an ambiguity regarding the device area which needs to be investigated further. Also, the cell was very unstable and the high values of current density did not last beyond 12 hours. Further experiments need to be pursued to understand the different processes affecting the parameters and lifetime of silver diffused cells.

5.4.Conclusions

$CuInS_2/In_2S_3$ cells could be successfully fabricated using the automated spray system. Different spray parameters were varied and composition as well as thickness of absorber and buffer layer was changed so as to improve the device performance. Also, effects of post deposition treatments and silver doping on cell parameters were studied. We could fabricate device through a simple three step process i.e., deposition of $CuInS_2$ layer over ITO coated glass, deposition of In_2S_3 layer on it and finally evaporating silver electrodes. Unlike in the case of device fabricated manually, same efficiency was obtained over small and large area electrodes and the device had stable lifetime above one month.

Though air and vacuum annealing did not yield any improvement in efficiency, a dramatic increase in J_{SC} was observed for silver diffused cells. If electrode area was taken as cell area, the efficiency of this device was as high as 16.5%. But, further experiments need to be done for understanding the reason behind this drastic increase in current and works are being pursued in this direction.

References

[1] R.C. Smith, Journal de Physique, 36 (1975) C3-89.

[2] L.L. Kazmerski, S Wagner, Current Topics in Photovoltaics, Academic Press (1985).

[3] Shay J.L., Wernick J.H., Ternary Chalcopyrite Semiconductors: Growth, Electronic Properties and Applications, Pergamon Press, New York, (1975).

[4] R. Klenk, J. Klaer, R. Scheer, M. Ch. Lux-Steiner, I. Luck, N. Meyer, U. Rühle, Thin Solid Films. 480-481(2005) 509.

[5] K. Siemer, J. Klaer, L. Luck, J. Bruns, R. Klenk, D. Braunig, Sol. Energy Mater. Sol. Cells. 67 (2001) 159.

[6] J. Klaer, J. Bruns, R. Henninger, K. Siemer, R. Klenk, K. Ellmer, D. Braunig, Semicond. Sci. Tec. 13 (1998) 1456.

[7] J. Klaer, K. Siemer, L. Luck, D. Braunig, Thin Solid Films. 378 (2001) 169.

[8] Jacabo Álvarez García, PhD Thesis, Universitat de Barcelona, Barcelona (2002).

[9] R. Scheer, M. Alt, I. Luck, H.J. Lewerenz, Sol. Energy Mater. Sol. Cells. 49 (1997) 423.

[10] R. Klenk, U. Blieske, V. Dieterle, K. Ellmer, S. Fiechter, I. Hengel, A. Jäger-Waldau, T. Kampschulte, Ch. Kaufmann, J. Klaer, M. Ch. Lux-Steiner, D. Braunger, D. Hariskos, M. Ruckh, H.W. Schock, Sol. Energy Mater. Sol. Cells. 49 (1997) 349.

[11] Teny Theresa John, Meril Mathew, C. Sudha Kartha, K.P. Vijayakumar, T. Abe, Y. Kashiwaba, Sol. Energy Mater. Sol. Cells. 89 (2005) 27.

[12] Marian Nanu, Joop Schoonman, Albert Goosens, Nano Letters. 5(9) (2005) 1716.

[13] Allen L. Fahrenbruch, Richard H. Bube, Fundamentals of Solar Cells, Academic Press, Newyork (1983).

[14] A. Mere, O.Kijatkina, H. Rebane, J. Krustok, M. Krunks, J. Phys. Chem. Solids. 64 (2003) 2025.

[15] Meril Mathew, R. Jayakrishnan, P.M. Ratheesh Kumar, C. Sudha Kartha, K.P. Vijayakumar, Y. Kashiwaba, T. Abe, J. Appl. Phys. 100 (2006) 033504.

CHAPTER 6

Concluding Remarks and Future Prospects

6.1.Summary and general conclusions

Solar power is hailed as a possible cure to worlds growing energy crisis. Thin film photovoltaic devices have the potential to meet or exceed the performance of traditional cells with a better possibility for power production at reduced cost. Among the various thin film deposition techniques, chemical spray pyrolysis (CSP) is a cost-effective method by which uniform polycrystalline thin films can be deposited over large area. This is specifically important for thin film photovoltaic device fabrication. But so far, there have not been much works in developing this technique, so as to make it a full-fledged thin film deposition technique like sputtering or vacuum evaporation. To ensure repeatability of results and to extend the device area, automation of this technique is essential.

Aim of the present work was to automate CSP process, to deposit and characterize $CuInS_2/In_2S_3$ layers using this system and to fabricate devices using these films. An automated spray system for the deposition of compound semiconductor thin films was designed and developed so as to eliminate the manual labour involved in spraying and facilitate standardization of the method. The system was designed such that parameters like spray rate, movement of spray head, duration of spray, temperature of substrate, pressure of carrier gas and height of the spray head from the substrate could be varied. Using this system, binary, ternary as well as quaternary films could be successfully deposited.

The second part of the work deal with deposition and characterization of $CuInS_2$ and In_2S_3 layers respectively. In the case of $CuInS_2$ absorbers, the effects of different preparation conditions and post deposition treatments on the opto-electronic, morphological and structural properties were investigated. It was observed that preparation conditions and post deposition treatments played crucial role in

controlling the properties of the films. The studies in this direction were useful in understanding how the variation in spray parameters tailored the properties of the absorber layer. These results were subsequently made use of in device fabrication process.

In the case of In_2S_3 layers also, different spray parameters were varied and their effects on properties of films were studied. Effects of copper incorporation in In_2S_3 films were investigated to find how the diffusion of Cu from $CuInS_2$ to In_2S_3 will affect the properties at the junction. It was noticed that there was a regular variation in the opto-electronic properties with increase in copper concentration.

Devices were fabricated on ITO coated glass using $CuInS_2$ as absorber and In_2S_3 as buffer layer with silver as the top electrode. Stable devices could be deposited over an area of 0.25 cm^2, even though the efficiency obtained was not high. Using manual spray system, we could achieve devices of area 0.01 cm^2 only. Thus automation helped in obtaining repeatable results over larger areas than those obtained while using the manual unit. Silver diffusion on the cells before coating the electrodes resulted in better collection of carriers.

From this work it was seen $CuInS_2/In_2S_3$ junction deposited through automated spray process has potential to achieve high efficiencies. Works in this direction need to be pursued further to achieve better results.

6.2.Future prospects

Though automation of CSP process has been achieved, there is enough room for further modifications in the automated system. For example, instead of the temperature controller used, proportional integral derivative (PID) controller may be used to achieve better control of temperature at higher spray rates. Also, in the present system, temperature and pressure control has not been interfaced to the computer. If such modifications could be incorporated, better uniformity and repeatability could be achieved. In addition, methods to improve the throughput of the process so as to minimize wastage of chemicals and reduce deposition time need to be taken up.

One major limitation of sprayed $CuInS_2$ is its small grain size and high resistivity at near stoichiometric compositions which is generally used for cell fabrication. Doping the material will help in overcoming this limitation. Not much work has been done in this direction.

Doping of In_2S_3 has been extensively studied by our group and the results indicated that the properties of In_2S_3 can be suitably tailored through this method. Thus, we can skillfully engineer the properties of buffer layer of the cell. But in the present work, only silver doping has been attempted. Doping using tin, chlorine, sodium etc. in In_2S_3 has to be applied to devices and their effects should also be studied.

Though $CuInS_2/In_2S_3$ cells are promising, the hiking cost of indium prompts one to look for possible alternatives of this material. Materials like SnS, SnS_2, $CuZnSnS_4$ etc. gain attention in this aspect. Deposition, characterization and cell fabrication using these materials need to be pursued.

In the present work, we have used imported ITO coated glass for cell fabrication. Indigenous development of transparent conducting oxide layer like ZnO or SnO_2 will help in the development of cost-effective all sprayed solar cells.

Present work is only a small step towards achieving a greater goal: *development of an efficient and cost-effective all sprayed solar cell*. Lots of effort has yet to be put forth for the fulfillment of such a vision. Only focused and determined efforts in this direction will make this initiative a reality.